PROCESSING OF PROSPECTIVE AND RETROSPECTIVE DURATION ESTIMATES IN MEDIAL PREFRONTAL CORTEX

JOSEPHINE HENKE

Graduate School of
Systemic Neurosciences
LMU Munich

Dissertation der Graduate School of Systemic Neurosciences der Ludwig-Maximilians-Universität München

November 11, 2019

Josephine Henke: *Processing of prospective and retrospective duration estimates in medial prefrontal cortex*

Supervisor: Dr. Virginia Flanagin
2nd reviewer: Prof. Dr. Christian Leibold
3rd reviewer: Prof. Virginie van Wassenhove, PhD

Defense date: March 27, 2020

To Brot & Zucker, with love.

CONTENTS

LIST OF FIGURES

LIST OF TABLES

LIST OF ABBREVIATIONS

ACC anterior cingulate cortex

AFN Atipamezol/Flumazenil/Naloxon

AMPA α - amino - 3-hydroxy - 5-methyl - 4 - isoxazolepropionic acid (Aminomethylphosphonic Acid)

ANOVA analysis of variance

AP anterior-posterior

BG basal ganglia

BSA Bovin serum albumin

CA cornus ammonis

Cg cingulate cortex

CI confidence interval

CV coefficient of variation

dACC dorsal anterior cingulate cortex

DiI 1,1′ - dioctadecyl - 3,3,3′,3′ - Tetramethylindocarbocyanine perchlorate

dlPFC dorsolateral prefrontal cortex

dmPFC dorsomedial prefrontal cortex

DV dorsoventral

EEG electroencephalography

EIB electrode interface board

ERP event-related potential

FI fixed-interval

FR2 frontal area 2

GABA γ-aminobutyric acid

IL infralimbic cortex

IntN interneurons

ip intraperitoneal

IPL inferior parietal lobe

ITI inter-trial-interval

KDE kernel density estimate

LFP local field potential

LO lateral orbitofrontal cortex

lPFC lateral prefrontal cortex

LPM liters per minute

MD thalamic nucleus medialis dorsalis

MI modulation index

ML mediolateral MEGmagnetoencephalography

MMF Medetomidine/Midazolam/Fentanyl

MO medial orbitofrontal cortex

MP measurement phase

mPFC medial prefrontal cortex

MSE mean-squared error

NaCl sodium chloride

NAcc nucleus accumbens

NMDA N - Methyl - D-aspartate

OFC orbitofrontal cortex

PBS phosphate buffered saline

PC pyramidal cells

PFA paraformaldehyde

PFC prefrontal cortex

PI peak-interval

PPC posterior parietal cortex

PrL prelimbic cortex

PSTH peri-stimulus time histogram

RMSE root-mean-square error

RP reproduction phase

rpm rounds per minute

RT room temperature

sc subcutaneous

SCN nucleus suprachiasmaticus

SD standard deviation

SDN state-dependent network

SET scalar expectancy theory

SMA supplementary motor area

SNR signal-to-noise ratio

TTC time to contact

vACC ventral anterior cingulate cortex

VE virtual environment

VLO ventrolateral orbitofrontal cortex

vmPFC ventromedial prefrontal cortex

VO ventral orbitofrontal cortex

VR virtual reality

VRML virtual reality modeling language

VTA ventral tegmentum

ABSTRACT

We, humans, created clocks to measure time and invented maps to navigate to locations. However, these tools only assist our natural capabilities for processing temporal and spatial information as we guide our lives through time and space – capabilities, that we share with other species. However, our bodies are not equipped with a sensory organ for the passage of time. Time is ultimately not a material object of the world for which we have a unique receptor system as we have ears for sound or eyes for light, with respective processing stages in the brain. The perception of duration – the interval between two successive time points of events – is essential for survival. Animals must integrate durations to reach sources of food or find mating partners or adapt fundamental cognitive processes such as decision-making and planning of action.

The perception of time is not associated with specific sensory pathways but uses a highly distributed system in the brain. The medial prefrontal cortex appears to be one prominent member for time perception and duration processing. Cells in the frontal cortex exhibit climbing neural activation as a potential neural mechanism for the representation of duration. Climbing activity has been widely associated with mnemonic functions in temporal information processing.

To get a better understanding of how duration estimation as a temporal integration process in the supra-second range is represented in the rodent brain, I performed in-vivo extracellular recordings in the medial prefrontal cortex of behaving Mongolian gerbils (*Meriones unguiculatus*). Specifically, I sought to find out if characteristic effects of magnitude estimation, like range effect, regression effect, and scalar variability, are captured by the encoding system. I designed and established a time estimation task, which required subjects to judge duration in a retrospective and prospective manner: First,

subjects had to measure the experience of an unexpected time stimulus in hindsight and second reproduce this duration of experience in time passing. Experiments were performed in a virtual reality behavioral setup in which subjects traveled along a virtual linear corridor. Locomotion was tracked with an optical sensor-equipped treadmill.

I showed that the behavioral paradigm I used is effective in reproducing known behavioral effects, such as range effect, regression effect, and scalar variability in experiments with humans. I succeeded in using the timing task paradigm with gerbils and gained comparable results to humans. My experiments demonstrate that gerbils can learn and perform complex time estimation experiments that are more intense in cognitive processing than time discrimination tasks or experiments based on peak procedure paradigms.

With recordings in gerbil medial prefrontal cortex, I showed that prefrontal neurons respond with various patterns of neural activity to the passage of time. However, relevant patterns were mostly observed for prospective time estimation while reproducing a known time stimulus until a future point in time than for retrospective time estimation, where duration had to be judged for past events. The majority of prefrontal neurons responded by ramping neuronal activity. In doing so, the size of the time stimulus was encoded in gradually adapted total discharge rate, or by gradually adapted ramping speed in a generalized activity pattern until reaching a unified threshold. The adaptation of ramping speed was put into effect by temporally scaling the response pattern, notably towards the end of time reproduction. The applied scaling followed the prediction of stimulus sizes, yet with minor oversizing. Hence, a key discovery was that no matter the neurons' response, the rate at which they adjusted their activity depended on the time interval required. I also investigated whether cells encoded the accuracy and precision of the duration estimate after the end of a trial, where animals were informed about their performance via visual feedback and appetitive reinforcement. On a populational level, the adaptation of firing rates to the level of accuracy demonstrated that regression effects, resulting from strategies to cope with uncertainty about sensory information,

are represented by neuronal activity. Precision of duration estimates was represented by the magnitude of firing as well, although to an internal reference instead of an absolute external value. Using higher firing rates to provide higher information content for less regression and low variance corroborates the fact that the objective of timed behavior is maximal accuracy and minimal variance.

Therefore, my results demonstrate that the medial prefrontal cortex in rodents profoundly provides timer functions at an internal clock stage. However, the prefrontal cortex does not exclusively code for time but also fulfills mnemonic functions by integrating the outcome and interaction of the decision with the environment. This integration might serve to compare the present outcome with previously stored values in memory. Activity during delay phase supports the idea that the prefrontal cortex concurrently acts as a memory stage integrating prior knowledge and updating posterior knowledge about the stimulus duration in accordance with Bayesian inference.

1

INTRODUCTION

Our daily lives provide us with a vast number of sensory cues. These sensory cues can be integrated and processed and thereby will give information on how to adapt our behavior and actions to the environment of continuously changing situations. In the past decades, researchers have put much effort into deciphering and identifying the brain's sensory systems, which enable us to navigate through life. While it is to date well known how we perceive and process auditory (Hudspeth, 1997), visual (Kuffler, 1953; Baylor, 1987) or tactile (Johnson and Hsiao, 1992) stimuli, we still try to identify and locate the respective sensory system - analogously to the sensory systems of sight, smell, sound or touch - devoted to the sense of time and space. Many percepts and our actions in response to these percepts are acutely dependent on the precise representation of time and space dimensions. The terms "time" and "temporal processing" encompass a broad range of phenomena, including simultaneity, temporal order, and the perception of duration. Nevertheless, no specific receptor for temporal and spatial stimuli per se has been identified and localized, although their integration and processing in the brain has already been intensively investigated. Spatial information, for example, is well represented in the subregions 1 and 3 of the cornus ammonis (CA) of the hippocampus. The neurons in this formation of the brain, so-called place cells (O'Keefe and Dostrovsky, 1971) encode position in space or distance from one location (Etienne and Jeffery, 2004). This internal representation of space is nevertheless influenced by multisensory inputs, such as proprioceptive (Terrazas et al., 2005; Haas et al., 2019), visual (Frenz and Lappe, 2005) or vestibular (Sharp et al., 1995) cues and hence might strongly depend on the inclusion of multiple senses. However, the hippocampus is not only known for encoding spatial but rather spatiotemporal information

(Pastalkova et al., 2008; Macdonald et al., 2011; Kraus et al., 2013; Howard and Eichenbaum, 2015; Salz et al., 2016). Apart from the hippocampus, prefrontal (Kim et al., 2013; Xu et al., 2014), parietal (Leon and Shadlen, 2003; Janssen and Shadlen, 2005) and motor (Lebedev et al., 2008) cortices, the cerebellum (Mauk and Buonomano, 2004), and the striatum (Matell et al., 2003; Jin et al., 2009; Adler et al., 2012; Mello et al., 2015) have also been shown to encode temporal information during testing of different timing tasks. The integration and processing of temporal information are not as clear-cut defined as it is for spatial information. Therefore the brain areas involved in timing are variously reported, and also their possible neuronal responsiveness.

1.1 TIME IN THE BRAIN

The passage of time is an objective measure. A minute is 60 seconds, an hour is 60 minutes, and so on. However, the brain processes time in the realm of memories and experiences, so it is not always as clear-cut as minutes and seconds. Numerous studies show evidence for specific networks of cells in dedicated brain areas that express our sense of time and fold it into memories and experiences. Whereas the number of time estimation studies has increased in recent years (Wiener et al., 2010), the underlying mechanisms remain unclear. Time information has to be used flexibly, adjusting our behavior to changing temporal adjustments. Thus, humans and other animals continuously have to judge intervals between our actions and their effects. Organisms have developed multiple systems to deal with time. Circadian timing, interval timing, and millisecond timing are active over more than ten orders of magnitude and deal with various degrees of precision.

1.1.1 *Time scales*

Circadian timing. Circadian rhythms are most recognizable in nature. They operate in the range of the 24-h dark-light cycle, control our sleep-wake cycle, wakefulness, physical activity, body temperature, and the secretion of hormones (Reppert and Weaver, 2001, 2002). The rhythm strongly relies on light input and other cues that guide a molecular network of regulatory feedback loops controlling gene transcription and translation. One of the significant neural structures controlling this rhythm - the "clock" - is located in the nucleus suprachiasmaticus (SCN) of the hypothalamus (Darlington et al., 1998). The SCN receives direct input from specialized retinal ganglion cells, which contain melanopsin as a photopigment. Hence, light resets the internal clock to start a new cycle. Single neurons in the SCN are responsible for the ticking. Each tick is approximately 24 hours long (Aton and Herzog, 2005). It has been suggested that the use of a circadian rhythm is the requirement for successful time-space learning. This ability allows animals to represent event-stimulus properties in memory together with the place and the time of the event and thus to form an episode (Gallistel, 1990; Petruso et al., 2007).

Millisecond timing. The shortest interval to estimate is an interval of only a few milliseconds. Millisecond timing is thought to be associated with the motor system (Perbal-Hatif, 2012) and thereby is crucial for motor control, speech generation, and cognition (Mauk and Buonomano, 2004), playing music and fine-tuned movements (Ivry and Spencer, 2004). Lesion studies revealed an inability of patients to perform tasks requiring precise motor timing like repetitive pecking. Furthermore, patients show impairments in tasks requiring perceptual, non-motor timing, such as discriminating the duration of two different intervals (Ivry et al., 1988). Thus, it is suggested that millisecond timing is controlled by the cerebellum (Church, 1984; Gibbon et al., 1984), more precisely, by cerebellar long-term-potentiation and long-term-depression (Ivry, 1996).

Interval timing. Time estimation in the seconds-to-minutes range is called "interval timing". It is a continuous event, a cognitively controlled system (Lewis and Miall, 2006; Ivry and Spencer, 2004), which requires attention and is associated with the basal ganglia and involving related cortical structures, such as prefrontal and parietal cortices (Duncan, 2001; Kumar et al., 2013). It is fundamental for survival and goal-reaching. As my interest is accurate time estimation for actions on a timescale of daily activities, I focused on the biological substrates and cognitive systems of time estimation in the range of seconds.

Time estimation experiments. The literature offers countless methods for investigating the nature of time perception and time estimation. The classic interval timing paradigm is the fixed-interval (FI) procedure in which the subject's first response is rewarded only after a specified amount of time has elapsed. A widely used discrete-trial variant of FI procedure is the peak-interval (PI) procedure (Catania, 1970; Roberts, 1981). Using a modified FI procedure, Mello et al. (2015) could show, that response times of striatal neurons rescaled with the interval being timed. Furthermore, duration categorization was reported in striatum (Gouvêa et al., 2015), and it was found that parietal neurons represent an estimate of elapsed time on a trial-by-trial basis and that time intervals are measured prospectively to the desired motor plan to reproduce a specific interval (Jazayeri and Shadlen, 2015). Various forms of temporal information processing have also been observed in the prefrontal cortex (Niki and Watanabe, 1979; Brody et al., 2003; Sakurai et al., 2004; Tsujimoto and Sawaguchi, 2005b; Genovesio et al., 2006; Oshio et al., 2006; Lebedev et al., 2008), along with the motor and premotor cortex (Lucchetti and Bon, 2001; Renoult et al., 2006; Mita et al., 2009) including scaling of firing patterns (Xu et al., 2014) and diverse neuronal activity temporally correlated with phases during a duration discrimination task (Kim et al., 2013). Time interval processing is essential for sensorimotor and cognitive functions (Mauk and Buonomano, 2004; Buhusi and Meck, 2005), and often comes along with a high degree of context-dependency in prefrontal time processing (Tsujimoto and Sawaguchi, 2005a; Genovesio et al., 2016). To investigate how internal timing mechanisms adapt to statistics

of temporal stimuli, Jazayeri and Shadlen (2010) asked human subjects to reproduce time intervals drawn from different underlying distributions. They found that humans can exploit the uncertainty associated with measurements of elapsed time to optimize their timed responses to the statistics of the intervals that they encounter. Several recent reviews and meta-analyses of neuroimaging studies have shown that many parts of the brain contribute to time estimation. Macar et al. (2002) defined the dorsolateral prefrontal cortex (dlPFC), anterior cingulate cortex (ACC), right inferior parietal lobe (IPL), supplementary motor area (SMA), cerebellum and basal ganglia (BG) as the core time estimation network. Lewis and Miall (2003b) reviewed many neuroimaging studies of timing and concluded that supra second timing tasks most commonly activated the bilateral prefrontal cortex, bilateral parietal cortex, and cerebellum. In their studies, the right dlPFC was the most frequently activated area. In contrast, a relatively recent meta-analysis reported that the SMA and right inferior frontal gyrus were part of the core network mediating time estimation in the brain. In contrast, the dlPFC was less important for time estimation (Wiener et al., 2010). Thus, there have been inconsistencies regarding the neural correlates of time estimation in previous studies, probably because different brain structures are activated depending on the paradigm, temporal task and duration range used (Wiener et al., 2010; Perbal-Hatif, 2012). However, neuroimaging studies revealing areas of activity while subjects estimate duration or time their movements, suggest that a core temporal-processing mechanism is located in the right prefrontal cortex for both sub- and supra-second intervals (Rubia et al., 1998; Brunia et al., 2000; Lewis and Miall, 2003a).

1.1.2 *Prospective vs. retrospective time estimation*

Time estimation offers two different but fundamental distinguishable perspectives: prospective and retrospective time estimation (James et al., 1890; Zakay and Block, 2004):

Prospective time estimation. In this cognitive model, an observer judges the duration of an interval that is being presently experienced. Prospective time estimates are those that people expect to make and are used in situations where it is important to keep track of time in passing, such as for instance the routine-life event of cooking pasta. The chef has to keep track of time after pasta has been put to boiling water and determine that time point in future, when cooking time has reached to drain the noodles and have them al dente. In literature, experimental tasks on prospective time estimation involve that subjects are informed that they would be asked to judge the duration of the task interval after its completion and that they should monitor the time going by (Brown, 1985). Prospective time estimation assumes an internal clock model (see subsection 1.3.2) with a pacemaker producing a sequence of time units that are fed into an accumulator (Church, 1984; Treisman et al., 1990). As a variant of the pacemaker-accumulator model, time units can only be registered when attention is directed to time. Thus, prospective timing is always a dual task since an observer has to divide attention between temporal and non-temporal processes (Taatgen et al., 2007; Macar et al., 2013). In addition to the pacemaker, several cognitive processes such as working memory, long-term memory, attention and decisions are involved in prospective time perception. Pure prospective duration judgments are only conceivable over a limited and shorter time range where an observer attends to time for a period of seconds to minutes (Pouthas and Perbal, 2004).

Retrospective time estimation. In retrospective time estimation, by contrast, an observer estimates a timespan that has already been passed and to which he is only now paying attention. For instance, to answer the question: “How

long was your drive?" one must make a retrospective time estimate – that is, an unexpected time estimate of a past interval. Usually, in experiments on retrospective time estimates, subjects are given no information about the timing, in contrast to a prospective paradigm (Brown, 1985). In retrospective time estimation, the duration of a time interval that has already elapsed is to be judged. Then, an observer has to estimate a given time in retrospect from the amount of processed and stored memory contents; that is, the duration must be reconstructed from memory (Ornstein, 1997; Flaherty et al., 2005; Noulhiane et al., 2007). The more changing experiences we have during a specific timespan — which are stored in memory and later retrieved — the longer the duration is subjectively experienced (Bailey and Areni, 2006). In retrospect, routine activity, when compared with novel activity, leads to the perception of shorter time intervals (Avni-Babad and Ritov, 2003). Thus, the subjective impression of a long time interval depends on the actions of the subject with diverse experiences and recruits the activation of areas involved in episodic memory (Noulhiane et al., 2007). Retrospective duration judgments are based on temporal intervals spanning short durations where short-term memory is required, e.g., a few seconds to ranges incorporating long-term memory, which can, in principle, be a whole lifetime (Wittmann and Lehnhoff, 2005).

There is a comprehensive report about the relative duration of time intervals judged prospectively versus retrospectively: Intervals judged prospectively are most often reported to be perceived as longer than intervals judged retrospectively (Block and Zakay, 1997; Tobin et al., 2010). Moreover, retrospective judgments are reported to be much more variable than prospective ones (Block and Zakay, 1997).

1.2 THE MAMMALIAN PREFRONTAL CORTEX

In the mammalian brain, the prefrontal cortex (PFC) is the anterior part of the cerebral cortex, which covers the front part of the frontal lobe. The PFC is more or less pronounced amongst all mammals. However, it has undergone a process of extraordinary enlargement in all mammalian species, most in primates and especially in humans (Fuster, 2008). By representing approximately one-third of the entire neocortex (Figure 1.1a), it plays an essential role as a close link to the limbic system as well as being considered the highest association center of the mammalian brain (Fuster, 2001, 2002, 2008). This brain region has been assigned to play a role in planning complex cognitive behavior, decision making, and inhibition (Fuster, 2011; Coutlee and Huettel, 2012). Opinions about functional differentiation of the PFC are diverse, whether there are operational subregions or if PFC shows single-operation performance (Goldman-Rakic, 2011). The PFC has been hypothesized to exert top-down modulatory influences on subcortical and posterior cortical areas (O'Reilly et al., 2002).

The cortex contains excitatory and inhibitory neurons. Pyramidal and fusiform neurons are the cortex's principal cells, which are glutamatergic – excitatory at their synaptic terminals. Excitation occurs through the release of glutamate, opening α - amino - 3-hydroxy - 5-methyl - 4 - isoxazolepropionic acid (Aminomethylphosphonic Acid) (AMPA), kainate, and N - Methyl - D-aspartate (NMDA) types of receptors, resulting in neuronal firing. Most types of interneurons are gabaergic-inhibitory, except for stellate cells in layer IV, which are excitatory (see Figure 1.2). γ-aminobutyric acid (GABA), the inhibitory neurotransmitter, opens GABA receptors, causing hyperpolarisation and thereby increasing the threshold for neuronal firing (Petersen, 2014). Generally, in the neocortex, the ratio of inhibitory and excitatory neurons varies between cortical areas and layers. Layer-specific modulations caused by a layer-specific ratio between the opposing conductances were observed in different brain areas, such as the somatosensory, visual, or auditory cortex (Adesnik and Scanziani, 2010; Isaacson and Scanziani, 2011; Dehghani et al., 2016).

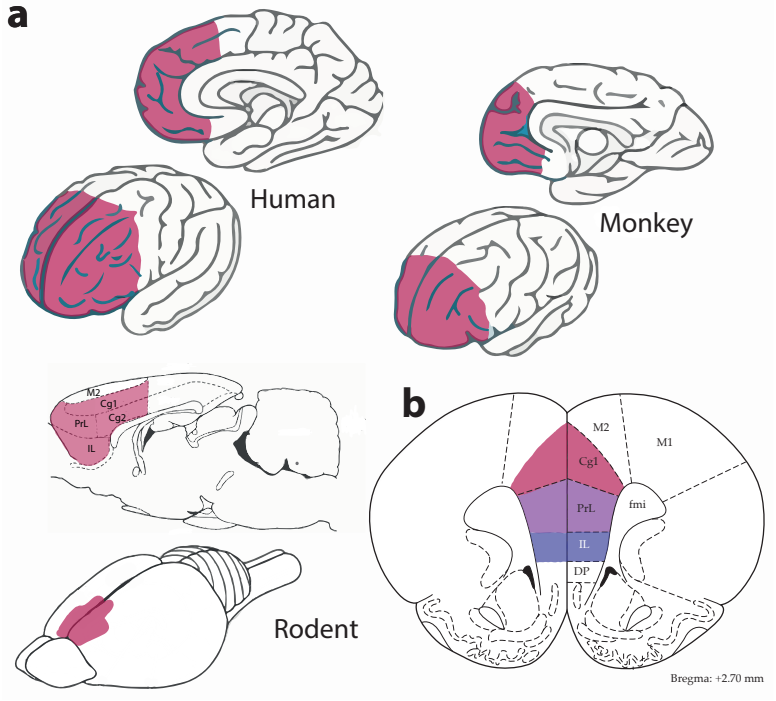

Figure 1.1: The prefrontal cortex in mammalian species. (a) Location and dimensions of prefrontal cortex (magenta) in human, monkey (chimp) and rodent species, after Fuster (2002). (b) Coronal slice of a rat brain at bregma +2.70 mm. The prefrontal cortex begins below the motor cortex M2. Its subdivisions are aligned medially on the dorsoventral axis: The cingulate cortex Cg1 (magenta) is followed by the prelimbic cortex (PrL) (lavender), which is on the above infralimbic cortex (IL) (violet), after Radtke-Schuller et al. (2016).

1.2.1 *Neuroanatomical organization of the prefrontal cortex*

The mammalian cortex can be subdivided by its neuroanatomical organization into neocortex and allocortex. The term isocortex or neocortex, which shows lamination in six layers, describes a region of the cerebral cortex. The human neocortex shows an extensive folding pattern. In contrast, the rodent brain has a smooth appearance without

sulci and gyri (Sun and Hevner, 2014), which is in line with the differences between rodents and humans in their higher cognitive functioning. The allocortex, however, is assigned to cerebral regions with heterogeneous laminar structures (Palomero-Gallagher and Zilles, 2015). The transitional zone between these two cortical regions shows a gradual change in the architectonical lamination pattern. Starting with a typically isocortical structure, it turns into the characteristic allocortical structural organization. The prefrontal cortex is represented by the rostral part of this transition area around the frontal pole of the hemisphere (Uylings and van Eden, 1990). The anatomical definition of the PFC in rats is not as clear as in monkeys (Preuss, 1995; Uylings et al., 2003). In rodents, in both of the two prefrontal subdivisions, a clear internal granular layer IV is absent, unlike its equivalents in higher primates and humans, which have a distinctly developed internal granular cell layer IV. This finding has been used to discuss the commonly assumed homology between the rat's medial prefrontal cortex and the monkey's lateral prefrontal cortex (Preuss, 1995). A more sensible criterion for the definition of the prefrontal cortex might be a hodological approach, considering the connective fibers' distribution of the cortical projections. A definition based on the reciprocal projections existing between the PFC and the thalamic nucleus medialis dorsalis (MD) represents the PFC extending medially and ventrally in the anterior part of the cerebral cortex. Thus, the PFC can be subdivided into a medial prefrontal cortex (mPFC), a lateral prefrontal cortex (lPFC) and an orbitofrontal cortex (OFC) (Fuster, 2001, 2002) which serves as a transitional area between the lPFC and mPFC, represented by the dorsal and ventral agranular insular cortex. The OFC includes areas such as the medial, ventral, ventrolateral, and lateral orbitofrontal cortices (MO, VO, VLO, and VL, respectively).

1.2.2 *The medial prefrontal cortex*

The mPFC is made up of cytoarchitectonical different portions: the frontal area 2 (FR2), the cingulate cortex (Cg), prelimbic cortex (PrL), which are the most rostral components of the ACC and the adjacent infralimbic cortex (IL) (Vogt, 2015). The cingular cortex consists of the Cg 1-3 subareas. The subdivisions Cg1, Cg2 and Cg3 are also known as dorsal anterior cingulate cortex (dACC), ventral anterior cingulate cortex (vACC) and prelimbic area (Ongur and Price, 2000; Heidbreder and Groenewegen, 2003; Steketee, 2003; Uylings et al., 2003). Based on various anatomical criteria, the mPFC is divided into a dorsal (dmPFC) and a ventral (vmPFC) component. The dmPFC component includes the FR2 and the ACC, while the vmPFC component is represented by the PrL and IL (Figure 1.1b). Despite the heterogeneity in the classification, the medial PFC of the rat is equivalent to the dlPFC of humans (Uylings and van Eden, 1990; Uylings et al., 2003). Although the IL was shown to have a primitive lamination pattern compared to other medial prefrontal areas and additionally has no reciprocal association with the MD, it is considered as a portion of the PFC (Tzschentke, 2001). This finding is supported by the topography of the corticocortical afferents, which also applies to the frontal area of the PFC (Heidbreder and Groenewegen, 2003; Uylings et al., 2003).

1.2.3 *Neuropsychological functions of the prefrontal cortex*

The prefrontal cortex, with its rich cortical and subcortical connections, is often classified as a multimodal association cortex that integrates extremely processed information from various sensory modalities in a precise fashion. It mediates prominent actions, i.e., executive functions, which can be defined as the ability to organize a sequence of actions towards a goal. The strong connective properties of this brain region suggest that the PFC is involved in integrating or combining

different types of information according to the task goal. As a highly developed information-processing stage, the PFC plays a crucial role in elaborating and controlling voluntary and goal-directed behaviors, expanding behavior far beyond the sole repertoire of automatic and reflexive actions. These executive functions, which can be seen as the principal, the most general function of the PFC, encompass physiologic constructs of memory, i.e., short-term memory tasks (Chao and Knight, 1998) or working memory (Fuster et al., 2000), decision making as well as inhibitory control of interference and planning complex cognitive behavior such as language, i.e., regulating spontaneous speech, narrative expressions or verbal fluency. Furthermore, the PFC is involved in initiating and carrying out sustained attention (Luria, 1962), motor attention, i.e., attention directed to events in the motor or executive sector (Stuss, 1992), filtering or gating mechanism for information processing (Shimamura et al., 1990), perception and intricate action, stimulus detection and sequencing tasks (Lepage and Richer, 1996), set-shifting, flexibility, delayed responding, and active problem-solving (Romine and Reynolds, 2004).

The retrospective and prospective aspects of executive function complement each other to serve the more general purpose of temporal integration, which finds use in working memory and planning. Logical reasoning considered under the aspects of intelligence as a complex construct is mediated by the PFC as well. Prominent among these are memory, abstraction, and the ability to formulate plans of goal-directed behavior as well as strategies to pursue them (Drewe, 1974). The PFC plays a significant role in the encoding and retrieval of memory. Neuroimaging studies found involvement of the PFC with memory encoding and retrieval of episodic memory (Fletcher et al., 1998a,b; Nolde et al., 1998). Lesion studies, in contrast, reported of the PFC playing an important role in recent memory (Luria, 1962), source memory, i.e., memory involving contextual factors associated with learning, and sequential memory, i.e., encoding and representation of temporal information (Stuss and Knight, 2013). Working memory is the ability to retain an item of information for the prospective execution of action dependent on that information. It is an essential cognitive function for

the mediation of cross-temporal contingencies in the temporal integration of all the above-mentioned functions.

The PFC is connected with the sensory systems involved in perception, enabling access to information about the current environment. It receives information about past events and knowledge though connections to long-term memory circuits. Consequently, the PFC serves as a processing stage to integrate new informational input with already existing information content. Linked to that, the PFC is also involved in information processing concerning the relation of the environment and one's self e.g., spatial or temporal relationships or to perform tasks that require the guidance of one's actions by visual information, spatial, or otherwise (McFie and Thompson, 1972). Executive functions are also closely linked to emotional regulation. As a part of the limbic system, the PFC receives information on individual needs, emotions, and motivations (Schoenbaum et al., 2009; Burgess and Fellows, 2013) to guide decisions.

The PFC interacts with motor systems that program, perform, and monitor the plan of actions (Catani and de Schotten, 2012; Yeterian et al., 2012; Cole et al., 2013). Thus, the PFC can be considered a convergence hub that enables the integration of multimodal information from different sources to create mental representational formations of both the external and inner worlds (Ramnani and Owen, 2004; Reynolds et al., 2006; Nee et al., 2014) to guide more sophisticated patterns of behavior. The diverse functions of the PFC can individually be mapped onto separate subareas of the frontal region. Specifically, the mPFC appears to be involved in coordination, attention to demanding cognitive tasks, modulation of body states, spatial memory, self-initiated movement, or and conflict resolution. The ACC is assigned to be involved in the perception of pain and possibly in mediating the emotional response behind it. Reward and goal-related activity correspond to the unique patterns of connections that link the rostral cingulate motor cortex with the prefrontal and limbic cortices (Ramachandran, 2002). The ventromedial region plays a role in decision-making (Spinella et al., 2004) and the retrieval of information from long-term memory and metacognitive processes (Schnyer et al., 2005).

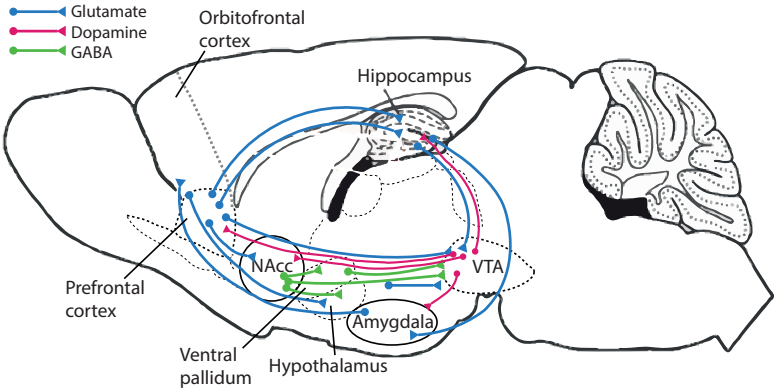

Figure 1.2: Main neuronal circuits for the mesolimbic system of the neurotransmitters. Sagittal section through a rat brain showing key nuclei in the limbic system. Main neuronal circuits for mesolimbic dopamine system, showing dopamine neurons ascending from ventral tegmentum (VTA) (red), glutaminergic pathways (blue) linking prefrontal cortex, hippocampus, and basal ganglia (NAcc), and GABAergic inhibitory neurons (green), after Kelley and Berridge (2002).

1.2.4 *Prefrontal interconnections*

The prefrontal cortex is highly interconnected with much of the brain. It receives influencing afferents from numerous cortical and subcortical brain structures. The medial-dorsal subdivisions of the PFC can not only be structurally assigned by the cytoarchitectonically organization but also according to the inter-regional connectivity. Practically all the prefrontal connections are reciprocal: structures sending fibers to the prefrontal cortex are also the recipients of fibers from it. Concerning the thalamocortical connectivity, the dorsal mPFC is reciprocally connected to the lateral part of the MD, whereas the ventral mPFC is reciprocally connected to the medial part of the MD (Cummings, 1993). Concerning the cortico-cortical connectivity, the dorsal mPFC is reciprocally connected to the occipital, parietal and retrosplenial cortices, whereas the

ventral mPFC is reciprocally connected to the rhinal cortex and amygdala (Ongur and Price, 2000; Steketee, 2003; Uylings et al., 2003).
The ventral mPFC can also be characterized as a medial prefrontal area that receives a heavy innervation from the CA1 field of the hippocampus (Jay and Witter, 1991; Cenquizca and Swanson, 2007; Hoover and Vertes, 2007) (see Figure 1.2). Additionally, the PFC also receives input from lower levels of the brainstem (Alvarez and Emory, 2006). These converging efferents from the diencephalon, mesencephalon, and limbic system play a prominent role in the involved functions of the prefrontal cortex (see subsection 1.2.3).

All stages of the frontal motor hierarchy (prefrontal, premotor, and primary motor) are connected with posterior neocortical areas of sensory and mnemonic functions (Cummings, 1993). They are also connected with the BG by reentrant connective loops that course through the lateral thalamus and the cerebellum. The three stages of that frontal hierarchy constitute the upper stages of the perception-action cycle. These anatomical observations suggest that the dorsal mPFC is the most likely candidate for the rodent brain region comparable to the ventral dlPFC in the monkey brain, whereas the ventral mPFC in rodents may be comparable to the mPFC in monkeys. Anatomical studies indicate that the ventral dlPFC in monkeys and the dorsal mPFC in rodents have much in common, such as that they are both the major targets of parieto-frontal projections. Empirically, both the monkey ventral dlPFC (Petrides and Pandya, 1984, 1999, 2006; Cavada and Goldman-Rakic, 1989) and rodent dorsal mPFC (Ongur and Price, 2000; Uylings et al., 2003) are reciprocally connected to the posterior parietal cortex (PPC). They also form thalamo-cortical and cortico-striato-thalamo-cortical circuits, as the other frontal regions do (Alexander et al., 1986). The closed-loop reverberating circuit may be included in those inter-regional projections.

1.3 MECHANISTIC MODELS OF TIME PROCESSING

A large number of competing models exist for how the brain creates a representation of time (Meck, 2005; Grondin, 2010). Prominent theories suggest a neurobiological internal clock (Ivry, 1996; Ivry and Spencer, 2004; Buhusi and Meck, 2005), centrally managing the temporal processing on different time scales, organized in different areas of the brain. Other models propose several synchronous timekeepers distributed throughout the brain, acting as a network codifying time in a linear or non-linear fashion, being state-dependent, or depending on the task to be timed.

1.3.1 *Scalar expectancy theory*

Of these, perhaps the best known and most prominent theoretical accounts of animal and human timing (Church and Gibbon, 1982; Gallistel and Gibbon, 2000; Machado and Arantes, 2006) is the one of the internal clock, which is based on scalar expectancy theory (SET) (Gibbon, 1977; Gibbon et al., 1997). SET is a quantitative model and deals with three principle psychophysical properties of timing data: flexible accuracy, multiplicative variance, and ratio comparisons. Therefore, the model consists of three components: an internal clock, that is a timer or pacemaker-accumulator, a memory stage, and a decision process, e.g., a comparator. It differs from many other timing theories in its emphasis on scalar variability, a term that refers to the linear increase in the standard deviation of timing errors as a task's criterion time increases, explained in detail in subsection 1.4.3. SET describes a theory of temporal control that uses a scalar-timing process, which rescales estimates for different values of the interval being timed. According to Gibbon (1977), scalar-timing implies a constant coefficient of variation. Expectancies of reward based on these estimates are formed, and discrimination between response alternatives is made by taking a ratio of their expectancies. As applied in psychophysical

studies of duration discrimination, the expectancy ratio reduces the likelihood ratio, and in conjunction with the scalar property, results in a general form of Weber's law:

$$\frac{\Delta I}{I} = K \tag{1.1}$$

The Weber Fraction K captures the relationship between physical and psychological quantities: as the stimulus intensity ΔI increases, it takes greater and more significant changes in intensity I to change the perceived magnitude by some constant amount.

1.3.2 *Pacemaker accumulator model – Oscillator model*

The SET incorporates a pacemaker-switch-accumulator mechanism. Based on some periodic neural process, a hypothetical internal pacemaker emits isochronous pulses gated by a switch during the current to-be-timed interval and collected by an accumulator (Gibbon et al., 1997). When attention is directed to time passing, the switch closes, allowing the impulses from the pacemaker to flow into the accumulator (Kornbrot et al., 2013). At the end of the timed duration, the switch reopens and interrupts the flow of impulses (Effron et al., 2006). The output from the pacemaker is assumed to be Poisson-distributed pulses. The accumulator's content is further transferred and stored in the working memory, which is compared with previous exposure to the time interval stored in the reference memory. The comparison between these accumulated pulses in working memory and learned temporal representations in reference memory determines the time estimation response. If the difference between the value from reference memory and the current accumulator value is below a given threshold, the decision is made that the time interval is equal to the memory for a standard (see Fig. 1.3). Thus, time is estimated according to the numbers of impulses accumulated during the interval of time (Kaneko and Murakami, 2009).

According to this model, individual differences in time estimation may be attributable to alterations in pacemaker speed, memory efficiency, and comparator function (Meck, 2005). Despite the effectiveness of the SET in explaining various behavioral and physiological results, its relevance to the neural substrates involved in accurate time estimation is not entirely clear (Buhusi and Meck, 2005). Many lines of evidence suggest that separate brain mechanisms are responsible for different stages of the SET (Buhusi and Meck, 2005). In this framework, a memory stage is functionally separated from other processing stages (Caselli et al., 2009), and accurate time estimation capacity is heavily dependent on working memory efficiency.
The second class of models relies on multiple neuronal oscillators with coincidence detectors associating particular patterns of firing with given time intervals, effectively time-stamping when an event occurs (Miall, 1989; Church and Broadbent, 1990; Matell and Meck, 2000). Brown et al. (2000) suggest an alternative type of oscillator-based timing model, which assumes that some representation of the state of an already-running set of oscillators is associated with each event in memory, in essence, as one of the features of the event.

Most organisms provide psychological and behavioral evidence for biological oscillators driving repetitive motor patterns like flapping, walking, licking, and rhythmic functions, i.e., heartbeat or breathing, and thus, it seems reasonable that they include concurrently oscillators involved in interval timing (Buhusi and Meck, 2005). Instead of counting pulses, each state of a set of oscillators of different periodicities is recorded. The oscillators have different frequencies, and thus, the periods can be longer than a day, or months or years, or even as long as the animal's lifetime. Instead of counting pulses, this model of interval timing records the times of a signal's on- and offset in terms of oscillator status indicators and computes the duration from this information. Accordingly, Buhusi and Meck (2005) suggested that interval timing might involve coincident detection activity in multiple areas of the brain.

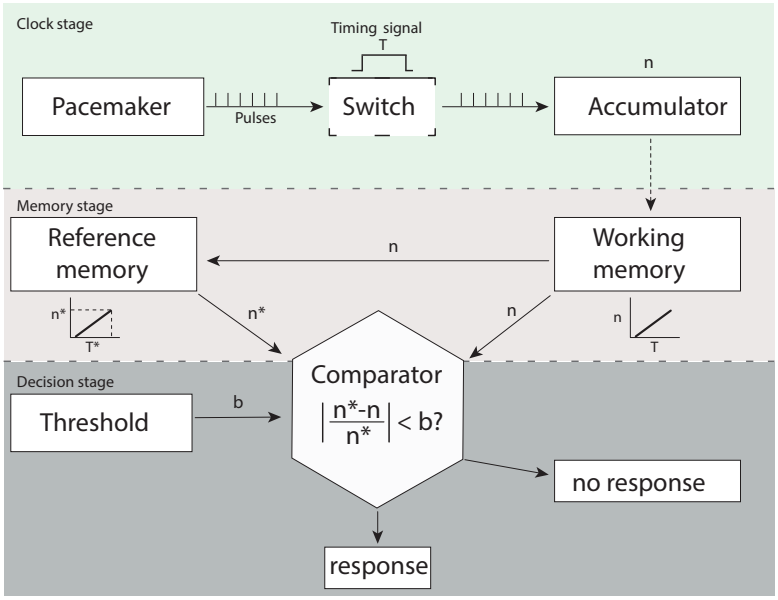

Figure 1.3: Schematic representation of the three-stage internal clock model. Clock stage: pulses emitted from a pacemaker are passed via an attention-modulated switch into an accumulator during a to-be-timed interval. Memory stage: a subjective time estimate of the present duration is held in working memory and passed to reference memory to be evaluated. Decision stage: Comparing the ratio of the value from the accumulator to the value of reinforced time in reference time memory yields a decision about whether the current time is acceptably close to the remembered time.

1.3.3 *Neural networks*

Besides the theoretical approaches incorporating an internal clock, such as the pacemaker accumulator model or its extension to the attentional gate model (Treisman, 1963; Gibbon et al., 1984; Zakay and Block, 1995), there are other timing models different from the neurophysiological mechanisms proposed for time processing, which do not suggest any internal clock components but share the idea of multiple timing mechanisms distributed across the brain.

Additionally, another dichotomy can be made to the central versus local timing debate, issuing the neural mechanisms which, independent of their location, ultimately perform the temporal computations that are specialized for timing (Ivry and Schlerf, 2008). This specialized representation of time is sought to be achieved in terms of neural-network states (Karmarkar and Buonomano, 2007a) or neural circuits e.g., corticostriatal, responsible for timing (Coull et al., 2004) in dedicated brain areas. In this theoretical approach, the psychophysical task, sensory modality, and lengths of time intervals determine the engagement of each single mechanism (Ivry and Richardson, 2002; Durstewitz, 2003; Matell and Meck, 2004; Buonomano and Maass, 2009).

Single-cell activity varying with time, which might influence psychophysical judgments (Brody et al., 2003; Leon and Shadlen, 2003; Janssen and Shadlen, 2005) has intensely been studied. A question that to date bothered many scientists is, how these cells might reliably encode temporal patterns if they communicate with each other and exchange dynamics in the scope of a neural network (Durstewitz, 2003; Matell and Meck, 2004; Mauk and Buonomano, 2004; Reutimann et al., 2004; **?**). One idea hypothesizes the existence of spectral models of timing, constituting a modular process. The phasic interactions of a bank of oscillators (Miall, 1989; Matell and Meck, 2004) or the exploitation of differential activity patterns in a set of delay lines (Fiala et al., 1996; Ivry, 1996) can define different intervals.
In dedicated models, these representations are viewed as specializations, unique to particular neural structures, that provide a functional chronotopy that is recruited across diverse task domains. Previous studies have reported that several specialized brain areas are responsible for time perception. The basal ganglia have been assigned to play a central, content−free and supramodal role in time perception (Coull et al., 2011). Likewise, the cerebellum has been considered to play a significant role in this function. Besides the subcortical activations in the cerebellum and BG, wide-ranging cortical network activations have been shown during timing tasks.

Itskov et al. (2011) reported a network that generates long-lasting, reliable sequences that may be used for time-keeping in the hippocampus on the scale of tens of seconds. Ferrandez et al. (2003) showed that a stimulus duration comparison task activated the BG, SMA, ventrolateral prefrontal cortex, inferior parietal cortex, and temporal cortex. This study suggested that the BG and SMA are related to the time-keeping mechanisms, while the frontoparietal network might be related to the attention and memory processes required for time perception.

Karmarkar and Buonomano (2007b) proposed a model without a centralized focus on timing and instead conceptualizes a state-dependent network (SDN). On a time scale of tens to hundreds of milliseconds, time may be represented as specific states of a neural network. Temporal information is encoded in the context of the entire pattern, not as conjunctions of the component intervals, and can be explained by a complex nonlinear function of the stimulus interaction (Buonomano et al., 2009). This alternate model presents cortical networks that are inherently able to tell time as a result of time-dependent changes in a network state. Intrinsic models give a more generic and radically different perspective on the perception of time. These models assume that there is no specialized brain system for representing temporal information, asserting that time is a general feature of neural circuits and is inherent in neural dynamics. Consequently, these same circuits process both spatial and temporal information in a multiplexed fashion. This property might be limited to neural regions capable of sustaining their activity in the absence of sensory input (Brody et al., 2003; Reutimann et al., 2004). For example, in delayed response tasks, the duration can be encoded in the ramped activity of neurons that provide a working memory representation of the stimulus or the time until the response (Lebedev et al., 2008). The model represents interacting neuronal populations that generate an event-based representation of time by slowly increasing activity, experimentally, demonstrated in striatum (Matell et al., 2003) or PPC (Leon and Shadlen, 2003). Most importantly, this event-based representation of time is consistent with Weber's law in interval timing, i.e., demonstrates the scalar property (Reutimann et al., 2004).

1.4 PSYCHOPHYSICS OF MAGNITUDE ESTIMATION

The estimation of different sensory stimuli, such as distance or brightness, follows specific psychophysical laws. Several attempts tried to capture and develop mathematical relationships between the physical dimensions of a stimulus and its perception in history. As one of the first, Wagner (1844) and Fechner (1860), suggested a logarithmic relationship between the intensity of a physical stimulus I and its perceived sensation S, described by the Weber-Fechner law

$$S = c \cdot \log \frac{I}{I_0} \tag{1.2}$$

with I_0 and c depicting the detection threshold of the respective stimulus magnitude. Almost one century later, Stevens extended the equation because the perception of each stimulus has a characteristic relationship to its physical value. He captured the growing magnitude as a power function of the stimulus magnitude in Stevens' psychophysical power-law (Stevens, 1957) with c referring to another constant and the exponent n depending on the respective modality tested.

$$S = c \cdot I^n \tag{1.3}$$

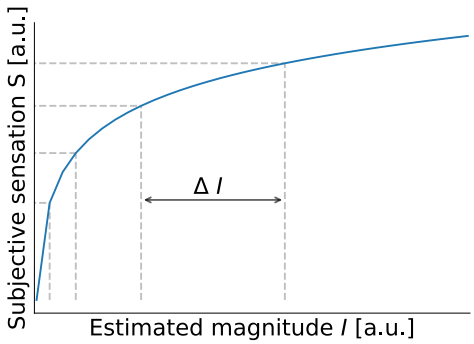

Figure 1.4: Logarithmic relationship between subjective sensation and stimulus intensity. A linear increase in stimulus magnitude causes a logarithmic increase in subjective sensation intensity as proposed by the Weber-Fechner law.

Emerging from Stevens' power-law, interpretations of Teghtsoonian and Teghtsoonian (1978) indicated that the

exponent in Stevens' power-law is not a fixed entity but could reflect the subjective sensitivity range of observers. Poulton (1968), in contrast, interpreted that the exponent in Stevens' power-law does not contain any information about the observer's subjective sensation range, but purely reflects variability in the experimental stimulus range. These interpretations reflect two major influencing aspects of magnitude estimation. In detail, these are that the estimation process is strongly dependent on internal as well as external factors. These factors have been intensively studied in the past and result in psychophysical principles describing specific biases known as range effect, regression effect and scalar variability (Poulton, 1968; Teghtsoonian and Teghtsoonian, 1978; Zeiler and Hoyert, 1989; Jazayeri and Shadlen, 2010; Petzschner and Glasauer, 2011; Thurley and Schild, 2018).

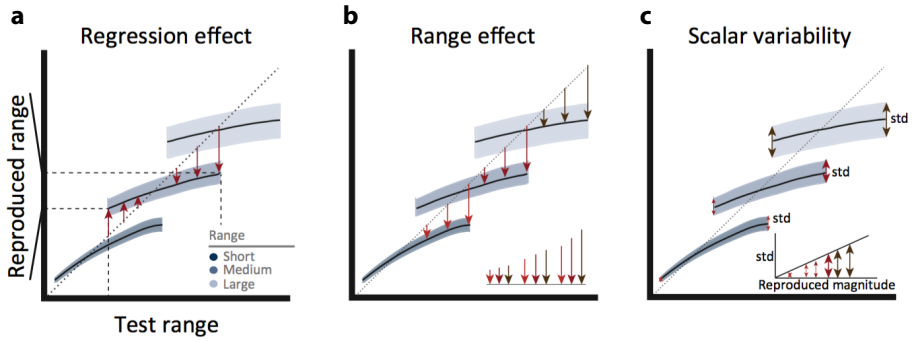

Figure 1.5: Schematic overview of psychophysical effects in magnitude estimation. a) Regression effect: estimated magnitudes tend to be biased towards the center of the full stimulus range. As a consequence, large magnitudes are underestimated, and small ones are overestimated. b) Range effect: the slope, representing the relationship between estimated magnitude and stimulus magnitude, decreases with increasing stimulus range. c) Scalar variability: the standard deviation of estimated magnitude increases linearly with corresponding mean estimated magnitude. Adapted and reprinted from *A Bayesian perspective on magnitude estimation*, Vol 19, Petzschner FH, Glasauer S, Stephan KE, No.52, 285-293., Copyright (2015), with permission from Elsevier.

These biases indicate that the estimation of magnitude is not purely a scalar measurement of a sensory stimulus but reflects a perceptual estimate processed at different stages involved.

1.4.1 *Regression effect*

The central tendency of judgment (Hollingworth, 1910), or better known as the regression effect, describes the tendency of estimates of magnitudes such as time, distance, or weight to be gravitationally biased towards the center of the full range of stimulus magnitude. This bias results in a systematic underestimation of magnitudes above the mean, an overestimation of magnitudes below the mean, and a correct estimation of the mean magnitude in the tested distribution (Jazayeri and Shadlen, 2010; Petzschner and Glasauer, 2011; Thurley and Schild, 2018). The strength of the regression seems to be subject-specific and modality-dependent (Stevens, 1960; Stevens and Greenbaum, 1966).

1.4.2 *Range effect*

The range effect can be interpreted as a correlation between the range of stimuli tested and the reciprocal exponent of the power function. This effect describes a decrease in the relationship between estimated magnitude and magnitude of the stimulus with increasing stimulus range (Petzschner and Glasauer, 2011; Thurley and Schild, 2018). It can be summarized as an enhanced regression effect for larger stimulus distributions, which becomes apparent as a decreased slope of the stimulus-response relationship for stimulus ranges that contain larger magnitudes (King, 1986).

1.4.3 *Scalar variability*

Scalar variability is the linear increase of the standard deviation of a repeatedly reproduced stimulus. As denoted by Weber's law (see 1.3.1), responses of subjects become more variable with increasing stimulus magnitude. This linear relationship implies a constant coefficient of variation (Gibbon, 1977). It is still not clear whether this relationship is based on the fact that subjects become increasingly noisier in their response to larger magnitudes (i.e., there is an actual scalar increase in variability), or if magnitudes are represented on a logarithmic scale and this compression of the scale for larger magnitudes causes the increase in variability (Dehaene, 2003; Cantlon et al., 2009).
Besides these most common psychophysical effects which appear more or less pronounced in subjects, there are considerable variabilities which play an important role in comparing data sets from different subjects or, which should at least be taken into consideration when data is pooled across subjects. On the one hand, this additional variability consists of subject-specific variability and, on the other hand, of experience-dependent variability.

Subject-specific variability. Individual subjects are more or less successful and accurate when estimating a stimulus. These differences can be due to strong individual sensitivity to a given magnitude or be dependent on the modality to be estimated (Thurley and Schild, 2018). The individual response characteristics might cancel out when only population data is reported. Therefore, it is necessary to evaluate individual subject's data.

Experience-dependent variability. Learning and experience can influence the decision about responses made in magnitude estimation. The experience can encompass the same modality (Marks and Algom, 1998; Marks and Gescheider, 2002), i.e., across consecutive experimental sessions or even different

modalities (Jones and Woskow, 1962; Ekman et al., 1968). A correlation could also be observed for responses on subsequent trials (Taylor and Lupker, 2007; Jones et al., 2013). Stimuli presented after a large stimulus tended to be overestimated, whereas responses to stimuli with a preceding small stimulus tended to be underestimated. This correlation is referred to as sequential effect. This effect was suggested to be the basis of the stimulus regression effect, as trials with very high stimulus magnitudes are more likely preceded by a smaller stimulus magnitude in a fixed test range and vice versa. Thus, estimates should tend to be biased towards the center of the full stimulus range (Ward, 1979). Both experience-dependent correlations suggest that there might be a memory component in the behavior as previous stimuli influence the estimation of the current stimulus. There is also evidence that the session-to-session correlations are only influenced by short-term experience because they are not persistent over long time scales (Teghtsoonian and Teghtsoonian, 1971). The influence of experience-based information on responses was intensively discussed by Petzschner et al. (2015). They describe a Bayesian inference rooted process in a probabilistic framework for perception, which determines the estimation behavior based on the incorporation of a-priori knowledge in the broadest sense. They argue that the a-priori knowledge is combined with sensory information to yield an estimate of the magnitude.

1.4.4 *Bayesian modeling*

In contrast to the most common models which try to explain the representation of magnitudes in estimation processes, Bayesian approaches do not solely focus on modality-specific or effect-specific explanations (Lappe et al., 2007) but rather provide a more general explanation that applies to various of the behavioral characteristics and overcomes modality-dependency. According to the Bayesian model, observed characteristic biases during magnitude estimation result from integrating noisy sensory information while incorporating prior experience

(Roach et al., 2017). Hence, estimation errors are not the product of sensory limitations of the receptor channels nor deficient representations in the cortex. Instead, the Bayesian framework suggests an optimization process on the resulting behavior as a consequence of principles underlying perceptual inference by accounting for noisy information (Acerbi et al., 2012). A critical aspect of a Bayesian model is that it is based on a generative model of concrete sensory observations. To recognize a presented stimulus, a Bayesian model compares predictions based on a generative model to the observed sensory input. This comparison leads to belief values through Bayesian inference, indicating how probable it is that the stimulus caused the sensory observations (Griffiths and Tenenbaum, 2011; Vilares and Kording, 2011; Zhang and Zhou, 2017). Whenever the prior differs from the current physical stimulus, the combination of prior knowledge and sensory input produces biased magnitude judgments under optimality constraints. This bias increases with the precision, represented by the strength of the prior belief and decreases with the signal to noise ratio of the sensory input (Figure 1.6a$_1$ and Figure 1.6a$_2$).

According to Bayes' rule, an observer process combines the prior knowledge $P(\pi)$ about the environment's statistics with noisy sensory inputs represented by the likelihood function $P(s|\pi)$

$$P(\pi|s) \propto P(s|\pi) \cdot P(\pi) \tag{1.4}$$

The resulting estimate is known as the posterior $P(\pi|s)$, which is more accurate than either of the two information sources individually. Assuming that both, the prior and the likelihood are Gaussian distributed, the resulting posterior will be Gaussian as well, with the mean of the posterior representing the uncertainty-weighted average of the sensory input about the physical magnitude and the prior mean μ_π (1.6b).

$$\mu_{\pi|s} = w_s \cdot \pi_s + w_\pi \cdot \mu_\pi \tag{1.5}$$

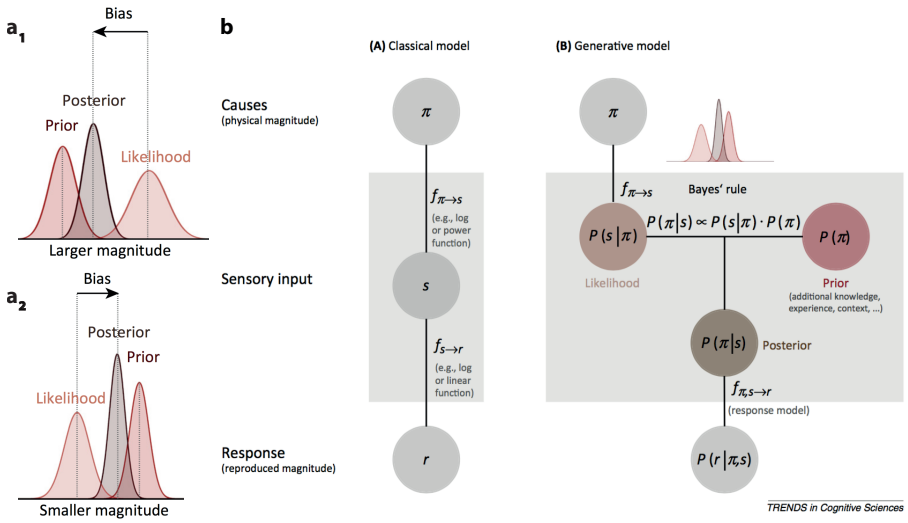

Figure 1.6: Bayesian modeling of magnitude estimation. According to Bayes' theorem, the posterior is a proportional product of likelihood and prior. The strength of the bias correlates with the relative uncertainty of likelihood and prior. The standard deviation of the likelihood increases with the size of the magnitude and thereby causes an increased bias towards the prior for larger magnitudes (a_1) in contrast to smaller magnitudes (a_2). b) The generative model of the Bayesian framework, combines a-priori information, the so-called prior with noisy sensory input representing the likelihood, and weighs the two information sources by their relative uncertainty. The resulting posterior estimate is computed by inferring the external cause (physical stimulus) on current sensory input and a-priori knowledge (e.g., experience or context) and translates it into a resulting response via an appropriate response model. Adapted and reprinted from *A Bayesian perspective on magnitude estimation*, Vol 19, Petzschner FH, Glasauer S, Stephan KE, No.52, 285-293., Copyright (2015), with permission from Elsevier.

The precision of the estimates is represented by the respective weights w_s and w_π, which are inversely proportional to the variance of sensory input and prior depicting the uncertainty.

$$w_s = 1 - w_\pi = \frac{\frac{1}{\sigma_s^2}}{\frac{1}{\sigma_s^2} + \frac{1}{\sigma_\pi^2}} \tag{1.6}$$

Interval timing, as the basis for perception and action, is consistent with Bayesian inference in various tasks, such as sensorimotor coincidence timing (Miyazaki et al., 2005), temporal order judgment (Miyazaki et al., 2006; Yamamoto et al., 2012), and time estimation (Jazayeri and Shadlen, 2010; Ahrens and Sahani, 2011; Acerbi et al., 2012; Cicchini et al., 2012). Exposed to either simple uniform distributions (Jazayeri and Shadlen, 2010; Cicchini et al., 2012), or complex temporal contexts (Acerbi et al., 2012), timing performance can be optimized by making use of the internally represented temporal statistics of the interval to be timed.

1.5 THE PREFRONTAL CORTEX AND PERCEPTUAL CATEGORIES

PFC neurons have a crucial ability for cognitive control. With the ability to develop abstract representations, the prefrontal cortex plays an essential rule in generalizing and developing concepts and principles (Miller et al., 2002). The ability to transform raw sensory inputs into distinct categories optimizes reproductive behavior while minimizing fatal mistakes. Categorizing sensory inputs might be essential for survival as the perceptual categories of crickets show: a specific range of pure tones is divided into 'mate'-tones, which will cause the cricket to turn towards the sound source for potential mating versus 'bat'-tones of a predator which will make the cricket turn away from the sound source as it could mean death. Until a certain point (16 kHz) (Wyttenbach et al., 1996), there is virtually no distinction between frequencies over a wide range on either side of the boundary. However, at the boundary, the sensory input is sharply divided into perceptual categories. This example illustrates that even though the input varies along a continuum, the output is a binary behavior. Further, it shows that the physical appearance of a stimulus might vary or gradually change. To categorize efficiently, sharp boundaries without gradual transitions are necessary. Can we thereby

assume that the neuronal representation does gradually adapt to changes, and neural activity encodes certain attributes? The acquired behavioral and neurophysiological data recorded from prefrontal cortex might help address the question of whether there is a fixed or adaptive boundary for perceptual categories of over- and underestimation of time intervals, analogously to the boundary of 16 kHz in the example of the crickets. The analysis of data sets on time estimation where specific time stimuli were embedded in different stimulus distributions might give an insight if the same procedural concept is applied when the same specific sensory information is tested in different contexts. These hypotheses could give rise to the question if perceptual categories can be linked to the Bayesian model and central tendency effect, with the mean of the stimulus distribution as the crux of the matter and how perceptual categories can be mapped onto under- and overestimation of time intervals.

1.6 THE MONGOLIAN GERBIL AS MODEL ORGANISM

The Mongolian gerbil (*Meriones unguiculatus*) is widely used as a model organism in laboratory experiments. For more than 30 years now, there exist numerous studies in diverse fields of research using gerbils as their animal model of choice, notably in hearing research (Kraus et al., 1987). Its popularity is due to its auditory properties which – unlike in mice and rats - include most of the human low-frequency hearing range (Ryan, 1976) and its predominantly use in the investigation of the circuitry underlying sound source localization in vitro and in vivo (Pecka et al., 2008; Kandler et al., 2009; Lingner et al., 2012; Grothe and Pecka, 2014). Besides auditory research, gerbils are frequently used in studies investigating learning and memory (Reichenbach et al., 2015; Jarvers et al., 2016; Caras and Sanes, 2019), navigation in space (Haas et al., 2019; Mankin et al., 2019), in-vivo pharmatoxicology (Lachau-Durand et al., 2019), or social and cognitive-behavioral strategies compared to other rodents

(Varty et al., 2002; Deng et al., 2017; Wang et al., 2018). Further, the gerbil is commonly used to approach medical-biological issues such as aging (Cheal, 1986), epilepsy (Fujisawa et al., 2003), parasites (Conchedda et al., 2006), and viral infections (Watanabe et al., 2001). As it allows for modeling human disease, it offers the possibility to study types of cancer (Liu et al., 2016) or the mechanisms of brain ischemia (Chen et al., 2017).

The taxonomic classification of the genera is not consistent. Following the classification of Wilson and Reeder (1993), the subfamily of *Gerbillinae* belongs to the family of *Muridae*. In contrast, according to the taxonomic classification after Grzimek (1960), the animals are assigned to the family of *Cricetidae*, which agrees with the classification of other authors (Kornerup Hansen, 1990; Schmidt, 1996; Sambraus and Steiger, 1997). Most of today's laboratory gerbil colonies used in Europe and America descend from 20 breeding pairs of the Mongolian gerbil, captured in the basin of the river Amur, China, in 1935 (Stuermer et al., 2003). These animals were brought to Japan, bred, and the offspring transferred to Tumblebrook Farm, America. Nine specimens were bred in a closed commercial colony and have been shipped worldwide for scientific purposes since 1954 (Stuermer et al., 2003). However, the laboratory strain bred in captivity revealed significant morphological and behavioral differences, such as reduced body weight and size, increased litter size, reduced brain size (Stuermer et al., 2003), improved reproductive fitness (Stuermer et al., 2006), or readiness to learn and motivation (Stuermer and Wetzel, 2006) when compared to the wild-type strain. Due to their diurnal activity cycle (Pietrewicz et al., 1982), peak activity levels are observed around the hours of dawn and dusk. This activity cycle influences the basal metabolic rate of the animals and nutritional requirements, modulated by ambient temperature conditions (Ding et al., 2018). Unlike other diurnal rodents, gerbils are currently available from commercial suppliers and appropriate for research that requires a model with human-like diurnal activity rhythms (Refinetti and Kenagy, 2018). Gerbils proved to be suitable for behavioral and neurophysiological experiments due to their strong exploratory behavior (Ehrat et al., 1973), and because they showed less fear and anxiousness when traversing an open field in comparison to other rodents

like rats (Wang et al., 2018). In accordance with other studies, I previously could demonstrate, that gerbils show no thigmotaxis while exploring unfamiliar environments and have the ability to use complex cognitive-behavioral strategies (Ingle, 1981; Thurley et al., 2014). Additionally, as a visual alert rodent (Ingle, 1981) with extraordinary visual properties regarding color vision and vision under twilight conditions (Jacobs and Neitz, 1989; Applebury et al., 2000), it could be shown, that gerbils have a unique receptor configuration which even allows for UV-vision (Jacobs and Deegan, 1994; Garbers et al., 2015). In a recent study, I could show that the virtual reality setup I used can address these specific visual properties and use them with a behavioral paradigm testing for color discrimination in gerbils (Garbers et al., 2015). With their behavioral and visual abilities, gerbils have proven to be a suitable model organism that ideally can be used to approach scientific issues using behavioral tasks implemented in virtual reality. (Thurley et al., 2014; Garbers et al., 2015; Kautzky and Thurley, 2016; Haas et al., 2019).

1.7 FOCUS OF THE THESIS

We heavily rely on external timekeepers and temporal organizers like clocks to keep track of the temporal properties of events, but we are also adept at keeping track of time on our own given the appropriate circumstances (Nobre et al., 2010). As in other animals, our ability to time external events in the seconds to minutes range (interval timing) allows us to experience the passage of physical time subjectively. It allows us to integrate action sequences, thoughts, and behavior as well as to detect emerging trends and anticipate future outcomes (Bechara et al., 1996; Nussbaum et al., 2006; Kotz et al., 2009). The present thesis employed a retrospective and prospective time estimation task to quantify time estimation; this methodology is widely used in human studies (Fortin and Breton, 1995). This is reasoned by the fact that the participants' load is minimal, and the experimental procedure is easy. However, this methodology

has rarely been used in animal studies where interval duration must be estimated retrospectively and prospectively in the same experiment.

In the first phase of the timing task, the animal is required to measure a stimulus' duration while the animal is sitting still and passively participating in the present task event. As the animal can not know how long the time interval will be, it has to judge the duration of the presented stimulus time in a backward fashion: 'How long was the presented stimulus?'. Thus it estimates the unexpected time of the past interval, which I interpret to represent retrospective time estimation. In the task event phase following this first measurement phase, the animal then has to reproduce the previously estimated time with a running response actively. Here the animal knows about the stimulus interval and has to keep track of time while running until that time point in the future when the end of the stimulus duration has reached. Therefore, I claim that the reproduction of the stimulus interval complies with prospective time estimation. This task is suitable for the aimed research objective because it relies on the scaling of subjective time by units used in daily life.

Questions to be solved are about generic principles about the behavior of time estimation in accordance with present theories, such as Bayesian optimization, the role of context, and species-specificity of these parameters. Further, I aim to contribute to the overall knowledge of neuronal mechanisms underlying this time estimation behaviors. I divided my research into two major parts:

1. I implemented a time estimation task incorporating retrospective and prospective time perspective with humans. After standard principles of magnitude estimation were met by using this duration estimation task, the behavioral paradigm was implemented for rodents using a virtual reality setup. The obtained results were evaluated in comparison to human results.

2. The behavioral paradigm for rodents was then extended with electrophysiological recordings to get a better

understanding of what the neuronal activity during time estimation tells us about the processing of time in the brain. By means of the data, I tried to find evidence if the prefrontal cortex can be seen as a dedicated brain area for interval timing, considering reward expectation and motor planning. Activity in measurement phase and reproduction phase was compared to investigate if retrospective (measurement) and prospective (reproduction) interval timing do have a shared timer. Further, behavioral outputs were related to neuronal activity and tested if the data represented Bayesian principles.

2

MATERIALS AND METHODS

2.1 SUBJECTS

Animals. For the behavior study (see section 3.1), experiments were performed with a total of seven female adult Mongolian gerbils (*Meriones unguiculatus*) genetically originating from a wild-type culture colonized at the local animal facility of Ludwig-Maximilians-Universität München. Animals were kept in small family groups with a maximum of 4 animals per cage. The box-shaped housing had dimensions of 71x46x31 cm^3 and contained bedding of wooden chips, a sleeping house made of solid rigid plastic, and social enrichment, such as treat sticks for gnawing and paper towels for nesting. Animals were held under constantly controlled laboratory conditions at room temperature (RT) (23 °C) with 55% humidity on an artificially created 12-hour day/night cycle. Experiments were performed in the light phase of the cycle. Unrestricted water access was ensured at any time, whereas animals were put on a diet throughout the time of experiments. Daily dry food (ssniff Gerbil; ssniff Spezialdiäten GmbH; Soest, Germany) was rationed to maintain the gerbils at about 85-95% of their free-feeding weight to allow for conditioning by reward motivation. During the experiments' active phases, animals were rewarded with rodent enrichment chocolate- and banana-flavored pellets (20 mg Purified Rodent Tablet, TestDiet, Sandown Scientific, UK). Gerbils were at a minimum age of three months when training sessions started at which the animals weighed between 70 and 80 g. All experiments were approved according to national and European guidelines on animal welfare (Regierung von Oberbayern, AZ. 55.2-1-54-2532-10-11, and AZ. 55.2-1-54-2532-70-2016).

To track the neuronal activity while executing the behavioral task, I trained a new subset of a total of 3 animals on time estimation on a continuous scale. Gerbils contributing to electrophysiological experiments (see section 3.2) were separated and housed individually before surgery of the chronic brain implant.

Humans. Experiments with humans were conducted with six participants, aged between 21 and 32 years old. All participants had a normal or corrected-to-normal vision and were naive to the purpose of the experiments. All participants gave written informed consent to participate in the study, which was approved by the ethics committee of the medical faculty of the Ludwig-Maximilians-Universität München and performed in accordance with The Code of Ethics of the World Medical Association (Declaration of Helsinki) for experiments involving humans.

2.2 EXPERIMENTAL SETUP

Animal experiments. A virtual reality (VR) setup customized for rodents (Figure 2.1b) designed after Hoelscher et al. (2005) and Harvey et al. (2009) was built up at Ludwig-Maximilians-Universität München. The VR setup has already been content to previous studies (Thurley et al., 2014; Garbers et al., 2015; Kautzky and Thurley, 2016; Haas et al., 2019) with gerbils and was used for experiments presented in this thesis.

Human experiments. Participants were placed in front of an LCD computer monitor (resolution, 1280 800; frame rate, 59 Hz) driven by an ATI Mobility Radeon HD 3400 graphics card. Experiments were conducted in complete darkness

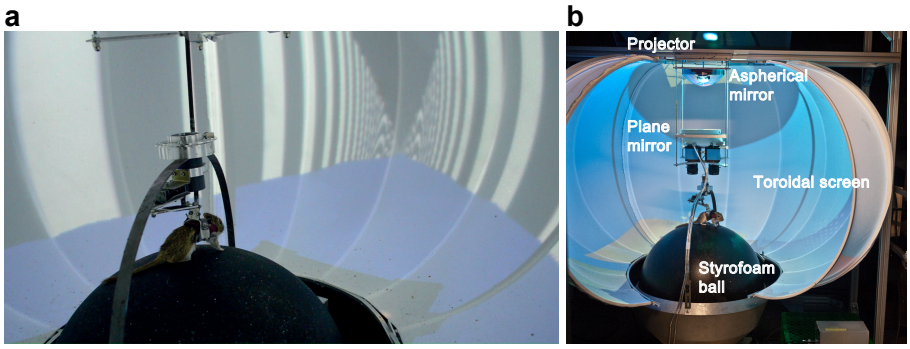

Figure 2.1: Virtual reality setup. (a) Example training session with infinite track projection. (b) Overview of the VR setup.

except for the illumination by the monitor. The eye height in VR was adjusted individually to the eye height of each participant. Humans performed virtual movement with the help of a multidirectional joystick (Speedlink Competition Pro). Also, pink noise was played to the subjects via headphones (RaidSonic ICY Box IB-HPh2) to hinder counting or equivalent strategies. The volume was adjusted to acceptable levels for each individual.

2.2.1 *Movement system of the VR*

A hollow styrofoam sphere with a diameter of 50.0 cm made up the central component of the VR setup acting as a treadmill (Figure 2.1b and 2.2a$_1$). The styrofoam ball sat in an aluminium bowl with a diameter of 50.4 cm which itself had a connection port of 8 cm width for pressured air at the bottom. An air stream was directed to the aluminium bowl from below and allowed the styrofoam sphere to float by generating a laminar air flow. To inhibit the treadmill's rotation in the azimuthal plane, two directional wheels allowing for the ball's movement in X- and Y- but not Z-coordinates were installed (Figure 2.2a$_1$). These directional wheels were placed perpendicular to the sphere's surface at the equator of the aluminium bowl. The animal was positioned on the north pole of the sphere with the help of a multi-component animal fixation. The fixation consisted of a custom-fitted harness, made of artificial leather which

covered the full upper body with leaving the head and legs freely movable. The harness was further attached to a magnetic setup handle which enabled unrestricted body movements and rotation around the animal's vertical body axis. Animal's legs movement induced rotations of the sphere while the animal was safely fixated in place. The treadmill's movement was detected by two optical infrared sensors with a minimum throughput of 16 bit per axis to ensure sufficient sampling during high speed running of the animal. With a timely resolution of 2^{16} pixels between successive USB messages, signals were fed into a personal computer at a rate of 1000 Hz and updated the virtual position of the gerbil with a sampling rate of 20 Hz (Δt = 0.05 seconds). This computer generated and updated a virtual visual scene in real-time that was displayed via the optical component of the VR setup.

2.2.2 *Optical system*

The virtual visual scene was displayed with a video projector (Sanyo PLC-ET30L with custom-mounted Sanyo LNS-T11 objective) via a multi-level mirror system, consisting of a planar (LINOS Photonics) and a rotational symmetric aspherical mirror (Kugler GmbH, Salem, Germany) onto a 360° toroidal projection screen surrounding the treadmill and thereby created a full 360° image. The geometry of the VR setup was adapted according to the optical model proposed by Chahl and Srinivasan (1997). The appropriate distance of the toroidal projection screen from the image center in relationship to the position of the optical transmission system and the resulting height of the projected image on the screen was calculated with an angular magnification of $\alpha = 11$ following the law of reflection by Snell. For real-time rendering and simulation of the visual properties of the environment, Vizard Virtual Reality Toolkit (v5, WorldViz, `https://www.worldviz.com`), acting as an interpreter of 3D data written in virtual reality modeling language (VRML) was used. The virtual environment, hereinafter named "maze", was designed and generated with the open-source software

Blender (v2.49, http://www.blender.org) from which 3D data was exported in VRML format. For details see Thurley et al. (2014).

Whenever the animal succeeded in terms of the behavioral paradigm (see section 2.3), a reward was delivered via the automatic reward system controlled by the VR software. As Vizard triggered the reward release, a food pellet was delivered from a pellet dispenser (20 mg pellet dispenser, model 80209-20M, http://lafayetteneuroscience.com) located next to the projector, outside of the image field. The pellet was guided through a vertical tubing system to stop in a customized 3D-printed collecting tray adjacent to the animal's snout when facing the maze's direction.

2.3 BEHAVIORAL PARADIGM

2.3.1 *Maze design*

The behavioral procedure was a modified version of a "ready-set-go" timing task (Jazayeri and Shadlen, 2010; Petzschner and Glasauer, 2011) in which performance depends on accurate reproduction of time intervals. By implementing the task in a VR, it was possible to prevent landmark-based strategies for task-solving and additionally decouple time from a distance during responding. Subjects had to estimate the duration of a visual stimulus (black screen) and reproduce it by running along a virtual hallway. The task was implemented in a virtual environment (Thurley et al., 2014) to ensure time estimation. The hallway was presented as an infinite linear track of 0.5 m width. A repetitive pattern of black and white stripes, each with a height to width ratio of 1:5, covered the walls of 0.5 m height (Figure 2.2a$_1$ and Figure 2.2b). The floor was presented in a homogeneous medium light-blue color, and the sky was black (Figure 2.1a). Object colors were chosen to

be within the detectable color spectrum of gerbils (Garbers et al., 2015). No distal cues were provided. By randomly changing the corresponding “gear ratio”, ranging from 0.25 to 2.25 for animals and ranging from 1.0 to 7.0 for humans, uniformly distributed, movement speed and optic flow were decorrelated.

2.3.2 *Time estimation task*

The timing task followed a basic procedure, adapted from Jazayeri and Shadlen (2010). The behavioral paradigm applied for gerbils and humans alike is depicted in Figure 2.2a$_1$. Subjects had to estimate the duration of a visual stimulus (black screen) and reproduce it by moving in a virtual environment (VE). Each trial started with the subject's estimation of a randomly drawn time stimulus presented as a black screen at rest (measurement phase (MP)). Afterward, the reproduction phase (RP) started with the visual scene switching automatically to the virtual hallway. During RP, the subject had to reproduce the previously estimated passed time stimulus with a movement response. Gerbils were running on the treadmill, and humans moved the joystick forward. Response initiation was self-paced by the animal and not forced by the experimenter or a motorized treadmill. The running must fulfill the following criteria to be included in the analysis: (1) Continuous running of minimum 1 second and (2) minimum 0.5 seconds of rest to terminate the trial. The trial aborted automatically if the criterion of continuous running was not met. In addition, gerbils but not humans were provided with feedback on their reproduction before initiating a new trial. Following the RP, an evaluation screen, called inter-trial-interval (ITI), appeared. The ITI's duration was 3.0 seconds $\pm$ up to 0.5 seconds. The evaluation screen represented an accuracy tolerance that scaled with the tested stimulus. If the given response fell "in"-side the applied tolerance range, the feedback was presented as a homogeneous green screen, whereas responses "out"-side the tolerance range were presented as a white screen (Figure 2.2a$_1$). Supplementary, the animal was rewarded for “in”-trials with one automatically

delivered food pellet (see section 2.1 and subsection 2.2.2 last paragraph). At the beginning of training, the relative tolerance ranged from -60% to +60% of the tested time stimulus. Over the time course of the session, this accuracy tolerance decreased by three percentage points (-3%) for responses being "in" the previous tolerance range and increased by three percentage points (+3%) for responses "out"-side the tolerance range (Figure 2.2a$_2$). The adaptation modality of the tolerance range was visible for the animal and was represented during ITI by the response's feedback screen. During training, animals constantly could minimize the tolerance to about 15 percentage points ($\pm$15%). This performance quality was further stabilized during test sessions (see Figure 6.3). After ITI, a new trial started.

Animal experiments. Gerbils were tested on time intervals between 3.0 seconds and 13.5 seconds, randomly chosen from three different overlapping distributions (Figure 2.2c, filled circles). Time stimuli included in the tested distributions were: 3.0 s, 3.75 s, 4.5 s, 5.25 s, 6.0 s, 6.75 s, 7.5 s (test set A), 6.0 s, 6.75 s, 7.5 s, 8.25 s, 9.0 s, 9.75 s, 10.5 s (test set B), and 9.0 s, 9.75 s, 10.5 s, 11.25 s, 12.0 s, 12.75 s, 13.5 s (test set C). Animals were tested for one distribution per day. Stimulus distributions were tested for 3-5 days en bloc but presented across distributions in a mixed fashion.

Human experiments. Analogously to gerbils, humans were tested on time intervals randomly chosen from three different overlapping distributions. The stimulus distributions covered durations between 3.0 seconds and 16.0 seconds (Figure 2.2c, filled squares). Time stimuli included in the tested distributions were: 3.0 s, 4.0, s 5.0 s, 6.0 s, 7.0 s, 8.0 s, 9.0 s, 10.0 s (test set A), 6.0 s, 7.0 s, 8.0 s, 9.0 s, 10.0 s, 11.0 s, 12.0 s, 13.0 s (test set B), and 9.0 s, 10.0 s, 11.0 s, 12.0 s, 13.0 s, 14.0 s, 15.0 s, 16.0 s (test set C).

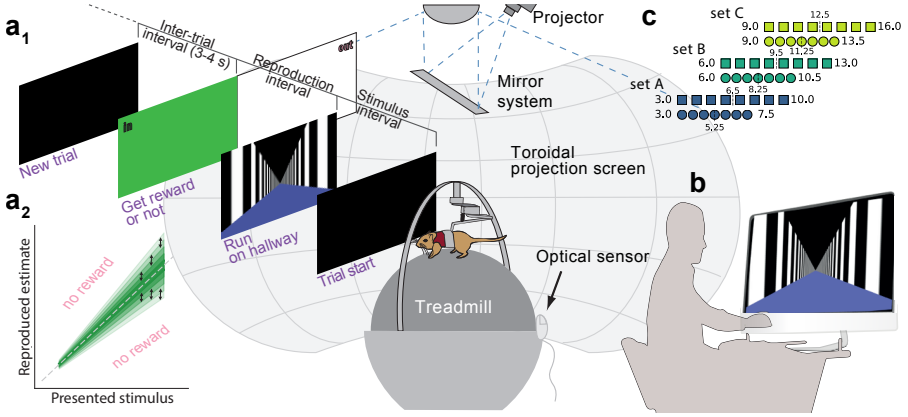

Figure 2.2: The interval duration estimation task. Experimental apparatus and task design for (a_1) gerbils and (b) humans. A gerbil was placed on top of a spherical treadmill that was surrounded by a toroidal projection screen. Participants were placed in front of an LCD computer monitor and performed virtual movement with a multi-directional joystick. At the beginning of a trial, a timed stimulus was presented (black screen). The subjects had to estimate its duration and, upon presentation of a virtual linear corridor, reproduce the duration by running or pushing the joystick. If the response fell into a feedback interval close to the stimulus ("in") a food reward was delivered for the animals. The feedback range increased/reduced after each "out"/"in" response (a_2). Additional feedback was given visually by setting the entire screen to either green ("in"), or white ("out") for 3-4 seconds. Finally, another trial was initiated. (c) Sample intervals were drawn from a discrete uniform distribution with seven values for gerbils (circles) and eight values for humans (squares). The sample intervals were tested in 3 overlapping separate distributions, set A (dark blue) ranging from 3.0 s to 7.5 s for gerbils, 3.0 s to 10.0 s for humans; set B (sea green) ranging from 6.0 s to 10.5 s for gerbils and 6.0 s to 13.0 s for humans and set C (light yellow) ranging from 9.0 s to 13.5 s for gerbils and 9.0 s to 16.0 s for humans respectively.

2.3.3 *Experimental schedule and training*

Behavioral training and experimental sessions for gerbils. During training, one session lasted until 20 - 25 minutes had passed. During test sessions, animals had to perform at least 45-60 responses to finish the session. Before the test sessions, animals needed to familiarize with the experimenter, the VR setup, and learn the behavioral task. This habituation comprised several steps that were based on each other. First, gerbils were familiarized with the laboratory environment where the VR setup is located and get used to the experimenter by playful handling, i.e., by being stroked and free running over the experimenter's hands. As animals did no longer show restraint or shyness, they were familiarized with the harness. Therefore gerbils were allowed to run through the loosely closed harness, which thereby formed a kind of short tube. After gerbils got familiar with the general appearance of the harness, the animals had to acclimate to wear the harness in a separate cage. To softly introduce the animals to wearing the harness, it was firstly loose-fitted with the Velcro-closure in the back and later tightened step-by-step. To facilitate harness acclimatization and to enhance reward habituation, animals were given flavored pellets during this habituation period. This general adaptation took 5-10 days. Following, the animals were familiarized with the VR setup itself. Therefore, the animal was placed on the north pole of the treadmill while wearing the harness, which was further connected via torso-lateral Velcro patches to the magnetic setup handle, holding the animal in place. During training, the toroidal screen was used in a 270° closed configuration to allow for any time possible guidance and assistance by the experimenter. When animals showed natural running behavior in the VR setup, the timing task with its consecutive phases was trained with only two time stimuli (3.0 seconds and 6.0 seconds), which were easy to distinguish. During this initial training phase, which took 2-4 weeks, the animals were assisted by the experimenter by blocking the ball during the presentation of the time stimulus to inhibit movement and take action during RP by start rolling and stopping the ball. To proceed with further testing, the animal's behavior was required to show a stable coefficient of variation

and root-mean-square error (RMSE) (Figure 2.3). After the task structure was understood and all task criteria were met, all animals were tested on stimulus distribution A, to introduce the animals to time stimuli on a continuous scale. The collected data were evaluated daily. Two measures were considered to decide whether to proceed with the remaining test distributions or if further data collection was needed: The RMSE which is a frequently used measure of the differences between values predicted by an estimator and the values observed, calculated as

$$\mathrm{RMSE} = \sqrt{\frac{\sum_{i=1}^{N} (\mathrm{Predicted}_i - \mathrm{Actual}_i)^2}{N}} \tag{2.1}$$

must be stable. A positive linear correlation of stimulus time and reproduction time must be visible (Figure 3.1a) to proceed. When the criteria mentioned above were met, testing continued on the other two test distributions B and C, randomly shuffled across the animals.

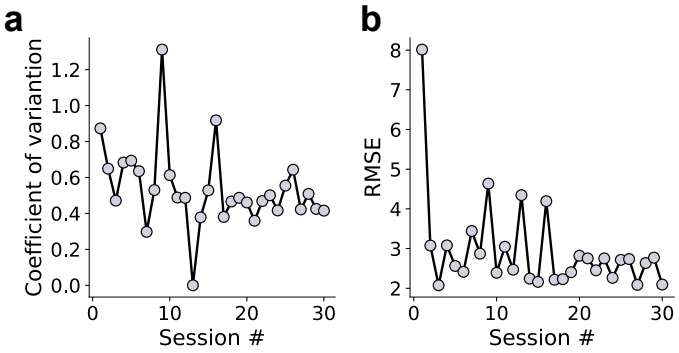

Figure 2.3: Coefficient of variation and root-mean-square error during training. The subject had to show a stable coefficient of variation (a) and stable root-mean-square error (b) over sessions to proceed after initial training on two well distinguishable time stimuli (training phase). Both parameters stabilized after approximately 20 training sessions. Data is shown for one example animal.

Behavioral training and experimental sessions for humans. Before each experimental session, humans were instructed to their tasks. At the beginning of each session, participants could perform 20 training trials to familiarize themselves with the

task and VR. Most participants chose to do the training only before the first session. During these trials, visual feedback on the performance was given after the reproduction with a text message saying how far off the participants were. Afterward, testing began, which consisted of approximately 100 test trials. No feedback was given. Only test trials were used for data analysis. Similar to animal experiments, the trial order for presented time intervals was randomly shuffled. Additionally, the experimental stimulus distributions set A, set B, and set C were performed in a randomized order.

2.4 ELECTROPHYSIOLOGICAL RECORDINGS

The subset of 3 animals provided data from electrophysiological recordings with correlated behavioral data. A reusable microdrive with eight tetrodes, which allowed movement of all tetrodes together only, was implanted after gerbils showed stable performance in behavior.

2.4.1 *Electrodes and recording device*

The electrodes loaded onto the microdrive were prepared as tetrode bundles. To obtain tetrodes, a 17 µm diameter platinum-iridium wire (Platinum 10% iridium HML (Heavy Polyimide) insulation, 1, California Fine Wire company, 17.8 microns, Size: 0.0007, Length: 100 Ft, Tare: 38.295, http://www.calfinewire.com/) was cut to a length of 23 cm. The wire ends were closed with a soft-sticking tape and thereby created a loop that was further folded such, that two loops parallel to each other were formed. The four aligned wire segments were twisted together with 90 clockwise turns until approximately two-thirds of the tetrode segment were organized in a tight bundle. Another 20 turns were applied

counter-clockwise to release tension and keep the four wires in the upper third of the tetrode segment well separated. To tighten and intensify the bonds of the single electrodes, the insulation of the wires was heated at $230 - 240°C$ with a heat gun with an attached reflector nozzle for 60 seconds. After a short cooling phase, the tetrodes were trimmed and stored in anti-static boxes until further processing.

The microdrive itself comprised a precision screw with a pitch of 200 µm (Axona Ltd., St. Albans, UK), which served as a movable shuttle for the tetrodes (Figure 2.4e, left pole). It carried the electrode interface board (EIB) (Figure 2.4d) with its connecting wires for each channel. The used Quick Clip EIB (Neuralynx) for eight tetrodes with 36 channels (32 electrode channels and four reference channels) was prepared by applying an acid-based flux (e.g., phosphoric acid) with a 30 Gauge needle into the vias of the single channels and following pre-soldering of the vias. The channels of each tetrode were connected to a quadruplet of contact wires, color-coded for each tetrode (Kynar Wire Wrap Aderleitung 0,05 mm2 Kupfer versilbert, starr, Kynar isoliert, 0,4 A), which was soldered into the respective vias from below. Protruding wire ends on the top of the electrode interface board (EIB) were cut and sealed with epoxy resin.

The contact wire bundles were aligned and bend into banana-shape to fit the geometry of the microdrive's shuttle bone and the final implanting position on the rodent's head (see Figure 2.4a and Figure 2.4b). Air-drying dental cement (Simplex Rapid, Kemdent, UK) was used to glue both components together. When the cement had hardened, a mapping scheme was created to identify the individual wire pins with the output channels of the EIB (Figure 2.4c and Figure 2.4d). This procedure was necessary to check for proper connectivity at the soldered sites and to determine defects which might play a role in the later steps of gold-plating or recording (see subsection 2.4.1 and subsection 2.4.2).
A guide tube was cut from a 19 Gauge needle and glued into a platform of air-drying dental cement placed on the open longitudinal side of the microdrive's skeleton for further holding the loaded tetrodes. From a 17 Gauge needle, a protection tube was cut, approximately the same length as the guide tube

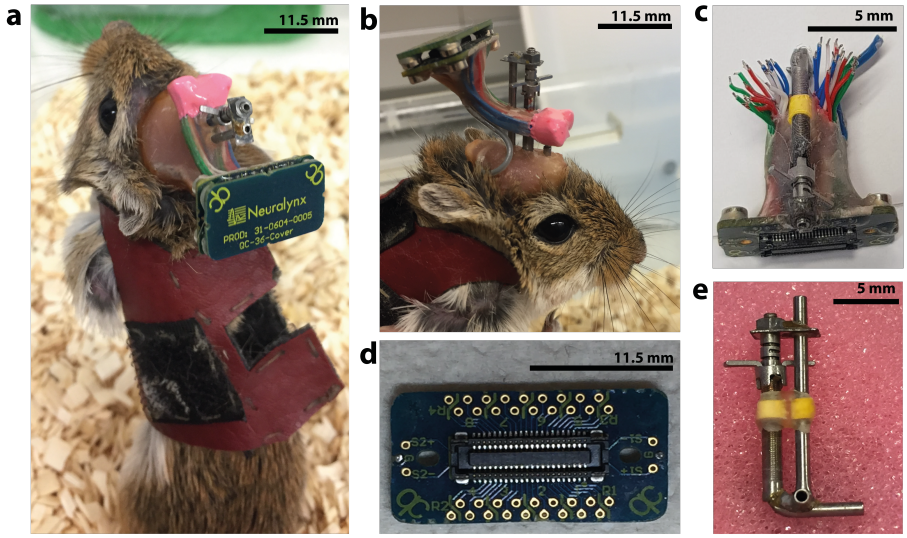

Figure 2.4: Chronic brain implant for electrophysiological recordings. (a) Microdrive with eight tetrodes implanted in a gerbil's brain. The implant was mounted with skull screws molded in dental cement. (b) Implanted microdrive in profile view shows the movement mechanism of the microdrive along the dorso-ventral axis with the help of the precision screw. (c) The reusable microdrive is shown after cleanup for the next use. Arrays of de-insulated pins of the contact wire are color-coded for each tetrode. (d) Electrode interface board (EIB) for 32 Recording channels. (e) The bare bone serving as the skeleton of the microdrive comprising the precision screw, guide track, and foot to be mounted onto the rodent's skull.

extending the cement platform. The tubes were telescoped and reversibly fixated with putty-like pressure-sensitive adhesive (BLU TACK, Bostik) for easy removal during surgery (see subsection 2.4.2). Additionally, a small patch of BLU Tack was applied onto the top of the cement platform and spread with forceps to later embed and arrange the loaded electrodes to the respective contact wire. When the microdrive was fully assembled with the EIB, tetrodes could be loaded into the guide tube. Therefore, the insulation at the tips of the separated electrodes of a tetrode was burned off with an ethanol lamp until the blank wire was visible over a length of minimum 1 cm. One tetrode was loaded at a time, and the single electrodes were carefully arranged and fixated in the BLU TACK top

patch to reach the corresponding contact wire. The blank part of the electrode was tightly wrapped around the contact wire's de-insulated pins with the help of two ceramic-coated fine-tipped forceps (Dumont #5, Fine Science Tools). When all tetrodes were loaded and electrodes connected to the respective channels' pins, the wrapped-around tips were covered with conductive silver paint (SCP03B, Electrolube, `https://uk.farnell.com`) to enhance electrical conductivity. Applied superglue in the entry of the guide tube held the tetrodes in place. The wrapped-around and silver-painted pins were further covered with commercially available nail polish to make them touch-resistant and impact-proof.

As a final step, the tetrode tips to be implanted into the rodent's brain were aligned by applying a drop of pure water and cut to 4-5 mm length to end at the same level with high precision ceramic coated scissors (Cerama-Cut, Fine Science Tools). This crucial step was monitored with binoculars to verify that the cut led to a shiny slice plane and did not indicate that insulation would cover the electrodes and thereby might inhibit the tetrodes' electrical sensitivity. To increase the electrical sensitivity (Buzsáki, 2004), the tetrode tips were gold-plated to reduce resistance manually or with the use of the auto-plating software nanoZ (software v1.4, Neuralynx). For the manual plating, the initial impedance of the several channels was measured in isotonic sodium chloride (NaCl) solution 0.9% (Fresenius Kabi Deutschland GmbH). After the tips had been rinsed with distilled water, an electric pulse of 2% 100 µA was applied for 2 seconds, while tetrode tips were dipped into gold chloride solution (HT1004, Sigma-Aldrich). After this step, the remaining impedance of each electrode was measured again. The procedure was repeated as necessary until a final resistance of 150 - 250 kΩ was reached.

2.4.2 *Surgical implantation of the microdrive*

On the day of surgery, the animal was brought to the operating room in the morning, weighted, and let sit for approximately one hour to calm down. Afterward, the animal was injected with a completely antagonizable three-component anesthetic containing Medetomidine/Midazolam/Fentanyl (MMF) (Schneider, 2000; Erhardt et al., 2011). The initial dose was adjusted to 0.15 mg/kg body weight Domitor®, 7.5 mg/kg body weight Dormicum® and 0.03 mg/kg body weight fentanyl injected subcutaneous (sc). Optional, to reach deep anesthesia, each subsequent injection with a volume of 0.05 ml was given every 30 minutes. To maintain stable anesthesia during surgery, it was refreshed with injections of 2/3 the initial dose every 2 hours. When testing the status of anesthesia by a toe pinch and the resulting withdrawal reflex revealed that the animal was deeply asleep, lidocaine (Xylocain®, Astra Zeneca GmbH) was applied to the scalp. Additionally, Meloxicam (Metacam®, Boehringer Ingelheim) was given at a dosage of 0.2 mg/kg body weight (Henke and Erhardt, 2001; Sotocinal et al., 2011; Matsumiya et al., 2012) as analgetic. The animal was placed on a heating pad to keep body temperature at 37°C and eyes were covered with ointment (Bepanthen® nose and eye ointment, BAYER). The head was carefully shaved with an electric hair trimmer and cleaned with an antiseptic (octenisept® pump spray, SCHÜLKE & MAYR GmbH) and cotton wipes.

The gerbil was placed in a stereotactic frame (Stoelting Co.), the snout was fixated with the jaw holder, and the nose clamp, while the skull was held in place with tapered ear bars. A nose cone was placed in front of the snout, providing the animal with oxygen at a flow rate of 1.0 liters per minute (LPM) throughout the whole surgery. The gerbil's body system was kept hydrated with NaCl injections (10 mg/kg body weight and hour) into either flank. Before surgery started, the animal was covered with surgical incise drape, and the eyes were additionally protected with tin foil covers. All used instruments were autoclaved beforehand or, if needed, sterilized during surgery with a hot bead sterilizer (Fine Science Tools) for a

minimum of 20 seconds at 240-270 °C. All surgical steps were performed using a binocular microscope.

Before opening the skin, it was sufficiently cleaned and antiseptically treated with octenisept®. The incision of the scalp was done with a scalpel to expose the area of the skull, where the sutura coronalis meets the sutura sagittalis, the so-called bregma in the upper third of the scalp opening. It was further extended also to expose the skull where the sutura sagittalis meets the sutura lambdoidea and forms the landmark known as lambda. The skin should show smooth cutting edges to prevent the risk of necrosis. I cleaned the skull from pericranium, fascia, and connective tissue using a bone scraper (Fine Science Tools) across the opened scalp and especially at and below the cutting edges, but being careful not to incise or punctuate the muscles above the ears and eyes. The skull was rinsed with isotonic NaCl and dried with lint-free cotton buds. With the help of applicator sticks, 35% phosphoric acid gel (Etch 35 Gel,iBond®; Heraeus Kulzer GmbH) was spread over the skull and etched the bone for a better bond. The etch was removed after 20-30 seconds with cotton sticks and washed with NaCl. The skull was hydrated with NaCl at regular intervals.

The head of the micro drill was aligned to bregma. The resulting coordinates provided by the stereotaxic instrument were taken as the origin to find the brain region of interest. From this starting point, I navigated above the right medial prefrontal cortex which lies 2.1 mm anterior-posterior (AP) above and 0.7 mm mediolateral (ML) aside bregma (Figure 2.5a). A hole was drilled in the right os frontale with a dental burr of drill head size 9. Another seven holes for mounting screws were drilled with a burr of drill head size 14: 1 into the contralateral os frontale, two into either os parietale and two in os occipitale of which one was used for the electrical ground (Figure 2.5a). The DIN 84 cylindrical screws with 1.6 x 2 mm dimensions were mounted into the drill holes and should serve as anchors or hooks in combination with liquid dental cement to fixate the microdrive on the gerbil's head. The meninges, consisting of dura mater encephali, arachnoidea, and pia mater encephali, needed to be opened by careful punctuation, i.e., with forceps or needle hook. The microdrive was attached to the probe holder of

the stereotaxic instrument and originating from alignment point with bregma, tetrodes were moved to the right medial prefrontal cortex and placed in the cortex just in the motor area M2 (+2.1 mm AP, -0.7 mm ML) at a dorso-ventral (DV) cortical depth of 0.7 mm (Loskota et al., 1974; Radtke-Schuller et al., 2016).

To seal the craniotomy, I used alginate (0.5% sodium alginate and 10% calcium chloride, Sigma-Aldrich), which was further covered with paraffin wax molten with a cauterizer. The reversibly fixated protection tube, telescoped on the tetrodes' guide tube, was now lowered to sit on the hardened paraffin wax. Thereby it was protecting the exposed tetrodes between the exit of the microdrive and entry in the brain. A 2-step etch rinse light-curing adhesive (iBond®, Total etch, Heraeus Kulzer GmbH) was applied around the craniotomy. To further protect the tetrodes, the protection tube was shielded with a light-curing hybrid composite. The composite was applied layer by layer onto the etch & rinse adhesive to end at the upper rim of the protection tube and cured with UV-light in between. Mobility in the dorsal-ventral axis was maintained as the guide tube holding the tetrodes could slide into the protection tube deeper into the brain. The wire of the ground screw was connected to the ground of the EIB. Afterward, the microdrive was anchored to the head by creating a continuum between the skull screws and foot of the microdrive's barebone with dental acrylic cement (iBond® Etch, Heraeus Kulzer GmbH, Germany; Simplex Rapid, Kemdent, UK) (see Figure 2.4a). After successful implantation of the microdrive, the implant was wrapped in soft-adhesive tape to protect it from dust and lint. At the end of the surgery, another dose Metacam for analgesia, glucose solution (500mg/kg body weight), and enrofloxacin antibiosis (Baytril®, 10 mg/kg body weight) were injected sc. Anesthesia was antagonized with Atipamezol/Flumazenil/Naloxon (AFN) (Antisedan, 0.4 mg/kg; Anexate, 0.4 mg/kg; Narcanti, 0.5 mg/kg, sc). Also, analgesia was given postsurgical for three days and antibiotics for five to seven postoperative days. The animals were allowed to recover for two days after surgery before recordings started.

2.4.3 *Electrophysiological recording procedures*

A digital high-density electrophysiology acquisition and experiment control system, allowing for wide-band recording (Digital Lynx, Neuralynx Inc.) was used to record the neuronal activity while animals performed the behavioral task. The EIB of the head-mounted microdrive was connected via a magnetic QuickClip 32 channel headstage pre-amplifier. The recorded analog neural signals were digitized on the headstage and were further passed via a digital tether into the electrophysiology acquisition system connected to a personal computer. As the single-unit activity was recorded as extracellular action potentials, it was necessary to invert the input arriving at the acquisition system. The animal ground, mounted above the occipital lobe, or alternatively, one of the tetrode channels, was used as a reference to denoise the system. The recorded amplified activity was band-pass filtered at 600 Hz to 6 kHz and recorded at a sampling rate of 32 kHz. Additionally, the activity of one channel from each tetrode was recorded as a continuously sampled signal, the so-called local field potential (LFP) at a rate of 2 kHz and band-pass filtered between 1 to 500 Hz. However, the LFP was not used for analysis. By turning the precision screw, I changed the tetrodes' position during the recording period along the dorsoventral axis of the medial prefrontal cortex. To ensure proper movement of the 8-tetrode bundle through the subregions of the mPFC, I lowered the tetrodes 50 μm every second day. The position of the tetrode tips during the recording epoch could only be calculated with the help of the number of turns but not be verified visually.

2.5 HISTOLOGICAL VISUALIZATION OF TETRODE POSITION

The location of the tetrodes was verified by postmortem histological visualization. Animals were euthanized, the brain preserved and prepared for examination by histopathology (Figure 2.6).

2.5.1 *Preservation of the brain*

After 20 weeks of neurophysiology experiments, the animal had to be euthanized according to the guidelines of the animal permit provided by the Animal Welfare. The gerbil was weighed, anesthetized with isoflurane in a gas chamber, and injected intraperitoneal (ip) with a lethal overdose of sodium Pentobarbital (400 - 800 mg/kg body weight, 160 mg/ml Narcoren) (Close et al., 1996, 1997; Demers, 2006). To intracardially perfuse the animal with 4% paraformaldehyde (PFA), the thorax was opened with a 2-3 cm lateral incision through the integument and abdominal wall just beneath the rib cage. The liver was carefully separated in order to prevent perforation while opening the diaphragm with a small incision. The incision was continued along the entire opening of the rib cage to expose the pleural cavity. The rib cage was opened with a caudal-cranial cut up to the collarbone on the lateral thorax. This step was repeated on the contralateral side. The tip of the sternum was clamped with a hemostat, lifted away, and placed over the animal's head. The perfusion pump was started with an even pressure of 80 mm Hg. This pressure was maintained throughout the entire infusion period. A 26 Gauge injection needle was injected into the posterior end of the left ventricle, infusing ringer solution. Immediately afterward, an incision to the animal's superior vena cava and right atrium leading to the right ventricle was made using spring scissors (Dowell, Fine Science Tools) to create as large an outlet as possible without damaging the descending aorta. If needed, the perfusion needle was shifted up into the ascending aorta but did not reach the aortic arch where the brachial and carotid arteries

diverge. At this position, it was fixated and held in place with clay attached to the dissection tray. Once the liver showed visible clearing, which is an indicator of good perfusion, and the fluid ran clear, the valve was switched to pass PFA (200 - 250 ml). Fixation tremors were observed within seconds, also indicating successful perfusion.

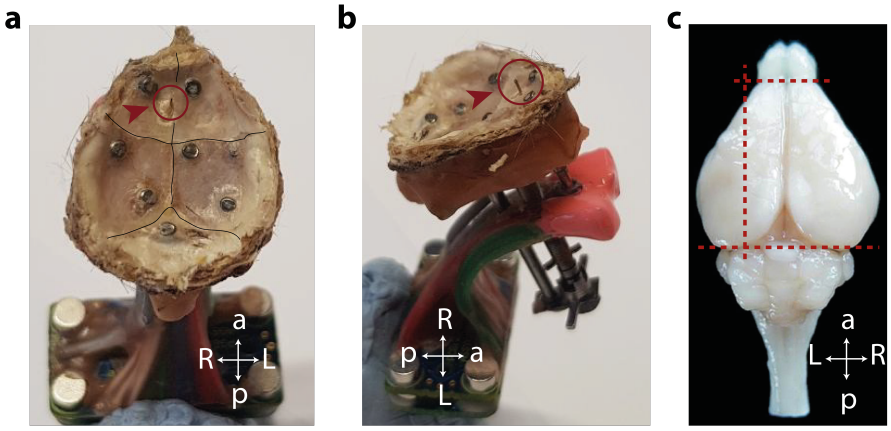

Figure 2.5: Conserved brain and brain implant after neurophysiological recordings. After 20 weeks of neurophysiological recordings, the brain of the animal subjects had to be conserved and removed from the skull. The position of the tetrode placement and position of the skull screws could be verified postmortem relative to bregma and lambda coordinates (a). The conserved brain implant revealed intact movability of the tetrodes along the dorso-ventral axis (b). The explanted brain was fixated in PFA and trimmed (dashed lines) for vibratome slicing to identify the right and left hemisphere (c). Compass at the bottom of each subfigure identifies the anterior-posterior axis and right and left hemisphere of the animal.

Before dissection, the tetrode tips' final position was reinforced with lesion currents of 10 µA, animal-ground vs. channels. The head was removed, and the skull exposed with a midline incision along the integument from the neck towards the nose until reaching the rim of the cement cap holding the implant. The remaining neck muscles were trimmed off so that the base of the skull was exposed. Any residual muscles were removed with scissors. To get access to the cerebellum, a pair of sharp iris scissors was used to cut from the foramen magnum extending to the distal edge of the posterior skull surface along one side

at the inner surface of the skull. This step was repeated on the contralateral side. The skull around the cerebellum was cleared away using blunt-tipped forceps or rongeurs. The cut along the inner surface of the skull was extended from the dorsal distal posterior corner towards the distal frontal edge of the skull on either side, always cutting beneath the rim of the cement in order to separate the microdrive from the animal's head (Figure 2.4b and 2.5b). As the implant was fully released from the skull, it was carefully lifted and removed. With the help of a spatula, the brain was carefully lifted from the ventral skull, and the nervous connections along the ventral surface of the brain were cut with spring scissors. The brain was gently teased from the head, and the remaining dura trimmed and peeled off with forceps. The brain was finally extracted from the head and stored in a vial containing fixative fluid (approx. 80 ml). Brains were incubated overnight in a fridge (5±3°C), placed on a shaker (40 - 60 rpm).

2.5.2 *Histology*

Preparation for slicing and sectioning. After 18-24 hours of incubation time, the brain was washed in 0.02 M phosphate-buffered saline (PBS) three times for 10-15 minutes placed on a shaker (60-80 rpm). As a next step, the brain was trimmed, by slicing off the cerebellum, olfactory bulbs in the coronal plane, and half of the non-implanted hemisphere was removed in the sagittal plane (see Figure 2.5c). The brain was placed in a small Petri dish with natural DV orientation and embedded in 4% molten agar, cooled to RT. When agar had hardened, the agar carrying the brain was cut to obtain a cube-shaped block. The brain was glued to a holding plate with rostral-caudal axis flipped to be vertical and fixated in the bath chamber filled with 0.02 M PBS, and placed in the vibratome to obtain coronal brain slices of 60-80 μm thickness, depending on the chosen staining method.

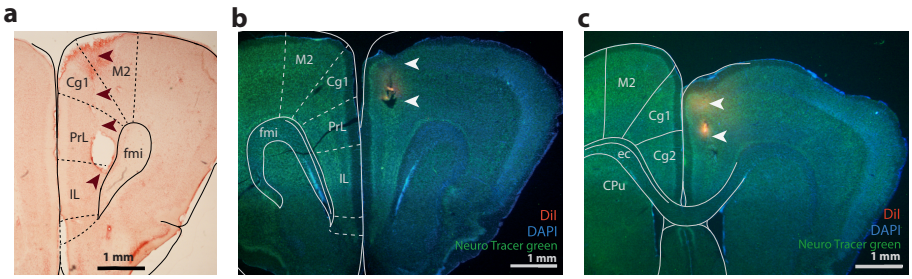

Figure 2.6: Histological visualization of tetrode placement. Slices of animals were stained with Neutralred (a) or DiI with DAPI and NeuroTrace green (b and c). Coronal sections show the tetrode track through PFC subareas of motor area 2 (M2), cingulate cortex (Cg1), prelimbic cortex (PrL) and infralimbic cortex (IL), which lie above and medially to the forceps minor (fmi), depicted by arrowheads (a). In other animals, recording sites were identified in subareas if PFC in M2, Cg1, PrL (b) and M2, Cg1, and Cg2, right above the external capsule (ec) by histopathology (c). Scale bars correspond to 1 mm.

For Neutralred staining, 80 µm slices were used, whereas 60 µm slices were needed for successful staining with DiI (1,1' - dioctadecyl - 3,3,3',3'-Tetramethylindocarbocyanine perchlorate), NeuroTrace green and DAPI (4,6-diamidino-2-phenylindole). Slices were cut with a speed of 60 mm/s and 1.20 mm razor amplitude. One after the other, slices were collected with a brush, transferred to a separate Petri dish filled with PBS, carefully cleaned from agar, and pulled onto gelatin covered slide. Slides were dried overnight under a laboratory fume hood protected from light.
Neutral Red is a eurhodin dye that marks cell bodies by staining lysosomes (Winckler, 1974; Chazotte, 2011) appearing in red color when observed under the light microscope (Figure 2.6a). Neutral Red staining was done following the staining protocol summarized in Table 2.2

Immunohistochemical staining. The immunostaining with DiI stain (DiIC_18(3), D282, Invitrogen^{TM}, Thermo Fischer Scientific), NeuroTrace green (NeuroTrace^{TM} 500/525 Green Fluorescent Nissl Stain, N21480, Invitrogen^{TM}, Thermo Fischer Scientific) and DAPI (DAPI Solution (1 mg/mL), 62248, Thermo Scientific^{TM}, Thermo Fischer Scientific) required thinner slices of 60 µm to obtain a consistent distribution of the fluorochromes within a short blocking interval.

Chemical substance	Duration
Neutral Red	8 - 10 min
Distilled water	rinse until colorless
70% EtOH	~2.5 min
96% EtOH	~2.5 min
96% EtOH	~2.5 min
100% i-PrOH	~2.5 min
100% i-PrOH	~2.5 min
xylene	~2.5 min
xylene	~2.5 min
xylene	~2.5 min

Table 2.2: Staining protocol for Neutral Red staining. Used reagents and corresponding bathing duration for the consecutive steps from top to bottom.

DiI, known as DiI$C_1$8(3), is a fluorescent lipophilic cationic indocarbocyanine dye used for electrode marking. It labels neurons via lateral diffusion in the plasma membrane. The dye has its absorption maximum when excited with green light at a wavelength of 549 nm and an emission maximum at 565 nm wavelength, which appeared as orange light (see Figure 2.6b and Figure 2.6c). The NeuroTrace green fluorescent Nissl stain binds to the Nissl substance, which is present exclusively in the somata of neuronal cells. NeuroTrace green exhibits bright, green fluorescence at 525 nm wavelength (see Figure 2.6b and Figure 2.6c) that is visible with filters appropriate for fluorescein when excited with blue light at 500 nm wavelength.

DAPI is a blue fluorescent dye that fluoresces brightly upon selectively binding to the minor groove of double-stranded DNA. Its selectivity for DNA and high cell permeability allows efficient staining of nuclei with a little background from the cytoplasm. Its excitation maximum lies at 360 nm wavelength, which corresponds to UV in the electromagnetic spectrum and responds with an emission maximum at a wavelength of 460 nm, visible as blue light (see Figure 2.6b and Figure 2.6c).

For the blocking solution, 50 mg of Saponin, which serves as a non-ionic surfactant, was weighed and dissolved in 0.02 M PBS to obtain a final volume of 50 ml. 500 mg of Bovine Serum Albumin (BSA) was weighed and dissolved in the blocking solution. Additionally, 2.5 ml of 10% Triton® X-100, already dissolved in PBS, were added to permeabilize the tissue and facilitate optimal staining. Dilution factors of 1:1000 for DAPI and 1:200 were used for successful staining. For six slides, 900 µl blocking solution was mixed with 0.9 µl DAPI and 4.5 µl NeuroTrace green. Approximately 150 µl of the diluted stain was applied to each slide with a microliter pipette (Eppendorf, single-channel pipette 20-200 µ) until the sections were sufficiently covered. The slides were stored horizontally in a humid staining chamber and incubated overnight at 4°C in the dark. The next day, the staining solution was drained off, and the slides were washed for 10 minutes by applying a blocking solution with a microliter pipette onto the slides. A dipping tray was filled with 0.02 M PBS, and slides were drained off again, loaded into a slide staining rack, and washed three times for 5 minutes. After washing, PBS was blotted off with filter papers, and slices let dry a little. A suitable mounting medium for fluorescence (Vectashield H-1000, Vectorlabs) was applied, and the sections covered with a coverslip, which was cleaned with a lintfree lens cloth. A small line of Vectashield was applied, the short edge of the coverslip was lowered first, and then the coverslip's longitudinal axis was carefully lowered and softly jiggled to avoid the inclusion of air bubbles. The mounting medium was drawn into the seal gap as far as the seal edge through its capillary forces. Excess fluid was removed by wrapping the single slides in laboratory tissues. Seal edges were covered with clear nail polish and slides let dry in the dark. Slices were observed under a fluorescence microscope

(Nikon Eclipse 80i) with a super high-pressure mercury lamp with 2x objective and appropriate filters for the corresponding stains of DAPI, Nissl, and DiI. Images were recorded with Lucia Image software and a selected image size of 640 x 480 'Normal'. Camera settings 'mono camera' and linear contrast was selected. The setting for exposure time and gain had to be adjusted for each filter and slice and are summarized in Table 6.1 and Table 6.2. The single color channels for each slice were later merged with Photoshop CS6 (Adobe) by creating an overlay of the color channels red (R), green (G), and blue (B).

2.6 DATA ANALYSIS

2.6.1 *General analysis*

Data analysis was done with open-source software Python v2.7 using the packages Numpy v1.11, Matplotlib v2.0, Scipy v0.19, Statsmodels v0.8, and Seaborn v0.7.

For review, statistical test results were reported at significance levels of 0.05, 0.005 and 0.001 and depicted in figures with $p \leqslant 0.05$ *, $p \leqslant 0.01$ **, $p \leqslant 0.001$ ***.

2.6.2 *Comparison parameters for behavioral data*

To compare data sets across animals and stimulus distributions, I used the following parameters to describe the accuracy and precision of the time estimate. As described in subsection 2.3.3, the RMSE, which was used to evaluate performance quality, is the square root of mean-squared error (MSE), and measures for the deviation between a given stimulus s and the respective

response r. It is described by the decomposition of variance and squared BIAS of the response r given stimulus s,

$$\mathrm{MSE}(r) = \mathrm{Var}(r) + \mathrm{BIAS}^2(r), \tag{2.2}$$

which are further used as quality parameters to evaluate the subject's performance on time estimation.

The variance describes the average of the squared deviations from the mean for responses r given stimulus s and is defined as

$$\mathrm{Var}(r) = \mathrm{E}[(r - \mathrm{E}[r|s])^2]. \tag{2.3}$$

For evaluation of individual subjects, the standard deviation (SD) was calculated for each subject and each stimulus size presented in one stimulus range, pooled across sessions (Figure 3.2 and Figure 3.4). The point-wise squared deviation of the average response r from the accepted reference stimulus s is called BIAS^2. Estimation bias is a systematic error that leads to an under- or overestimation of the actual value. The direction of the systematic error is expressed in

$$\mathrm{BIAS}(r) = \mathrm{E}[(\mathrm{E}[r|s] - s)]. \tag{2.4}$$

with E being the expected value of the response r given stimulus s. The bias of individual subjects was calculated analogously to SD for analysis. As the estimated quantity provided non squared values, the above mentioned parameters were further reported as square roots, i.e., SD, $\sqrt{\overline{\mathrm{BIAS}}^2}$ and root-mean-square error (RMSE) $\sqrt{\mathrm{MSE}}.\sqrt{\overline{\mathrm{BIAS}}^2}$ for each subject was calculated as the average $\sqrt{\overline{\mathrm{BIAS}}^2}$ for each stimulus size presented in each session. RMSE was calculated session-wise for each subject, using the mean response values of each presented stimulus size.

The coefficient of variation (CV) for the responses r was calculated as the average CV for each stimulus in one stimulus range, i.e.,

$$\mathrm{CV} = \mathrm{E}_s \left[\frac{\mathrm{SD}(r \mid s)}{\mathrm{E}_s [r \mid s]} \right]. \tag{2.5}$$

The slope of the linear regression between stimulus and response was computed to compare data sets. A slope of one would correspond to veridical estimation (i.e., no bias), whereas

smaller slopes indicate stronger regression and thereby biased estimates.

2.6.3 *Spike sorting*

Action potentials recorded from tetrodes were sorted according to their spiking properties as spikes occurred on multiple cells simultaneously. Because spikes occurring on different cells should show different waveform parameters (peak height, total energy, waveform shape, etc.), the spikes from a single cell will form clusters in that high-dimensional space (Fig 2.7 a_1 and a_2). The spike sorting was done offline in a two-stage operation. First, spike data was roughly pre-sorted using the automated spike-separation algorithm *KlustaKwik* (v1.6), which performed an expectation-maximization fit of n Gaussians to the data and created a set of putative clusters (McNaughton et al., 1983). These separate clusters containing spike trains were refined in the multidimensional parameter space with waveform parameters represented in amplitude, peak height and valley, total energy, and waveform shape (Wilson and McNaughton, 1993; Baeg et al., 2003), by using MClust v4.3 ran on MATLAB2015b+ (Matlab^{TM}, The MathWorks Inc., Natick MA). The received output t-files, which contained a list of timestamps in a binary format at a resolution of 10 timestamps/ms, were used for further data analysis. Putative interneurons and putative excitatory cells were included in the analysis alike. Quality of spike-sorted t-files was determined via isolation distance and L-ratio calculated using two spike features, the peak and the valley of the waveform for each cell (Schmitzer-Torbert et al., 2005; Rey et al., 2015) (Figure 2.7b and Figure 2.7c).

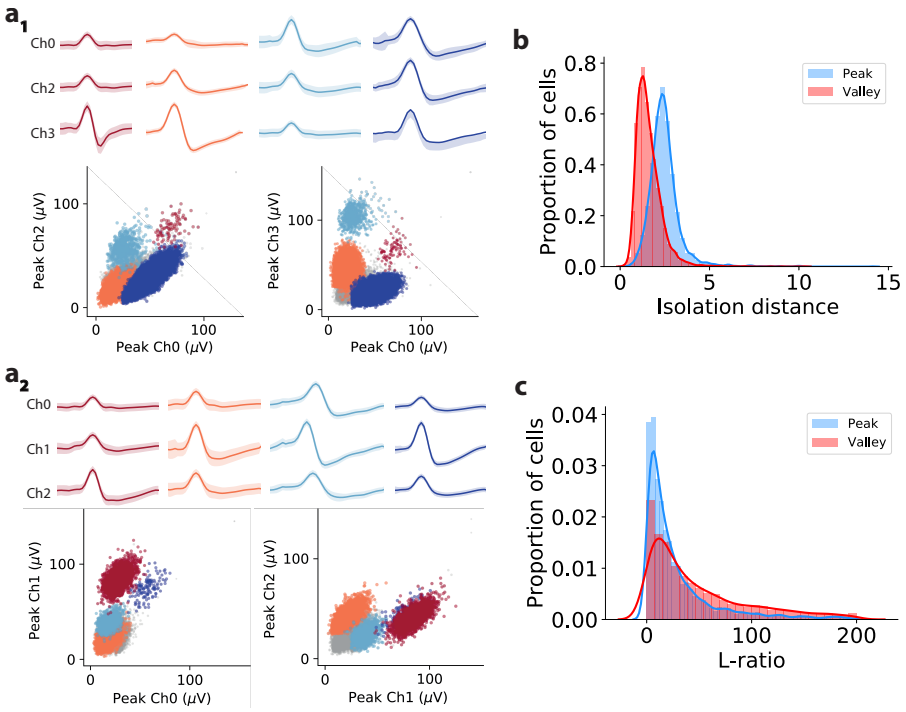

Figure 2.7: Spike clustering and verification of cluster quality. Examples of spike clusters and corresponding waveforms on each electrode channel are shown for two representative tetrode recordings of different sessions (a_1 and a_2). Only waveforms of channels used in the two-dimensional feature plots are shown. Filtered spikes from the same unit are coded by color and accumulated in clusters. Unclustered spikes are depicted in gray. Two projections are shown in the feature space of 'peak' on different channels. Waveform plots display mean waveform and corresponding SD. Distribution of isolation distance (b) and L-ratio (c), calculated for the feature space of 'peak' (light blue) and 'valley' (light red), were used to verify cluster quality.

2.6.4 *Classification of units*

In order to separate putative pyramidal cells and putative interneurons, a unit classification was performed. Therefore, spikes waveforms from each cluster were aligned on each channel. The width was determined by means of the absolute maximum and minimum of the averaged aligned waveform, which was then correlated with the mean firing rate. Based on the resulting correlation, a Gaussian mixture model was used to identify two population clusters in the data, reflecting the two subgroups of cell types.

2.6.5 *Peri-stimulus time histograms*

Spikes of each neuron were sorted according to the tested time stimuli and computed as peri-stimulus time histogram (PSTH). The occurring spikes along the time axis for each stimulus s were binned with a bin-width of 100 ms and smoothed by applying a bin shift using a Gaussian kernel with a window-width of 100 ms.

2.6.6 *Modulation of activity profiles*

The PSTH signals of the two alignments to be compared were separated by stimulus size and first tested for normality with Shapiro-Wilk test and further tested for significance with a paired t-test or Wilcoxon test respectively. If a cell showed significant differences between the two alignments, activity

profiles across event phases measurement and reproduction were evaluated by the modulation index (MI) calculated as

$$\mathrm{MI} = \frac{\overline{\mathrm{R}} - \overline{\mathrm{M}}}{\overline{\mathrm{R}} + \overline{\mathrm{M}}} \tag{2.6}$$

with the incorporation of the mean firing rate of measurement ($\overline{\mathrm{M}}$) and mean firing rate of reproduction ($\overline{\mathrm{R}}$). The modulation index yields values of +1, 0, or -1, thereby giving information about the event phase with higher activity.

3

RESULTS

3.1 TEMPORAL ESTIMATES OF SUPRA-SECOND INTERVALS IN RODENTS AND HUMANS - A BEHAVIOR STUDY

In this section, the focus is on the systematic behavioral characteristics observed in timing, as described in section 1.4. It is investigated whether the systematic errors in timing can be characterized as effects of magnitude estimation behavior and can be observed in different species tested. Evidence already exists that characteristic effects in magnitude estimation can, similar to effects in higher cognitive processes, be caused by the incorporation of a-priori assumptions. These assumptions are likely learned from experience or based on other contextual information sources. The behavioral approach provides the basis for investigations on the neural representation of interval duration of retrospective and prospective estimates.

First, it was assessed whether a behavioral paradigm could effectively be set up and tested analogously for animals and humans. Second, it was examined whether the systematic errors reported in interval timing can comparably be observed in both species and therefore understood as characteristic effects in magnitude estimation. Additionally, I aimed to show whether the use of a-priori knowledge can explain this characteristic behavior. Therefore, I designed two studies on interval timing with rodents and humans that aimed to change the a-priori assumptions of subjects by changing their immediate prior experience. The first study tested human time estimation in a combined retrospective and prospective perspective using a production-reproduction task for three different prior experience conditions by changing the underlying sample distributions. In the second study, the abilities of gerbils to

retrospectively and prospectively estimate durations were tested alike.

To analyze the main characteristics of the time reproduction in my experiments, I started by looking at the relation of the reproduction times and the tested stimulus times for each species group.

3.1.1 *Time estimation in gerbils.*

I conducted experiments with seven gerbils in which they first estimated and following reproduced the duration of a visual time stimulus via self-motion through a visually online-updated virtual environment on a treadmill (Figure 2.2a$_1$). Stimuli in each session were randomly drawn from one of three uniform distributions, comprising seven durations (Figure 2.2a$_2$). All animals performed roughly similar. Reproduced values depended on the stimulus range. Example data of one representative animal is shown in Figure 3.1a. The data of all individual animal subjects is given in Figure 6.1. The representative subject showed regression effects, which increased with the magnitude of the stimulus distribution. In the example of the chosen animal, the standard deviation increased with stimulus size (Figure 3.2b; example animal marked with an asterisk).

Also, for the remaining six gerbil subjects, standard deviation increased with stimulus magnitude (representing scalar variability, i.e., the increase of the variability of an estimate with the magnitude of the stimulus, reflecting a consequence of the Weber-Fechner law). Different comparison parameters were extracted to quantify the results species-specific across all subjects (see subsection 2.6.2). The square root of the mean squared bias $\sqrt{\overline{\text{BIAS}^2}}$ gives an estimate of the deviation between stimulus and reproduction and thereby provides information

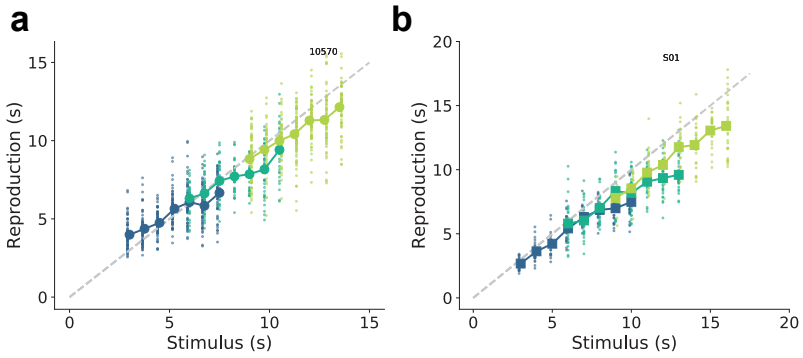

Figure 3.1: Time reproductions of a representative subject for gerbils and humans. Individual reproduced values for tested stimulus intervals for one gerbil subject (a), and one human participant (b) are given as small dots. Averages for each stimulus are depicted as filled circles (gerbils) or squares (humans) connected by a solid line. Colors identify stimulus distributions (cf. Figure 2.2c). Gray dashed lines mark bisecting lines. For both subjects, regression effects were visible, which increased with the magnitude.

about the size of the error. The $\sqrt{\overline{\text{BIAS}^2}}$ increased linearly with the magnitude of the tested stimulus distribution.

The BIAS, which is a good indicator for over- and underestimation, showed to be more differentiated compared to SD and $\sqrt{\overline{\text{BIAS}^2}}$. For smaller magnitudes of time stimuli, the density peaks were slightly right-shifted to zero. The larger the magnitude gets, the stronger the peaks were shifted left, indicating that the absolute bias gets more negative for larger stimulus distributions (Figure 3.2c).

Data were pooled for all subjects and experimental sessions across stimulus distributions to compare the behavioral parameters mentioned above. For the paired data comparison across stimulus ranges, I first tested the individual data sets for normality with Shapiro-Wilk tests. If data followed a Gaussian distribution, differences across stimulus sets were detected with one-way ANOVA. In case data sets were non-normally distributed, differences were detected with non-parametric Kruskal-Wallis test. If differences across stimulus distributions could be detected, an independent 2-sample t-test was used to

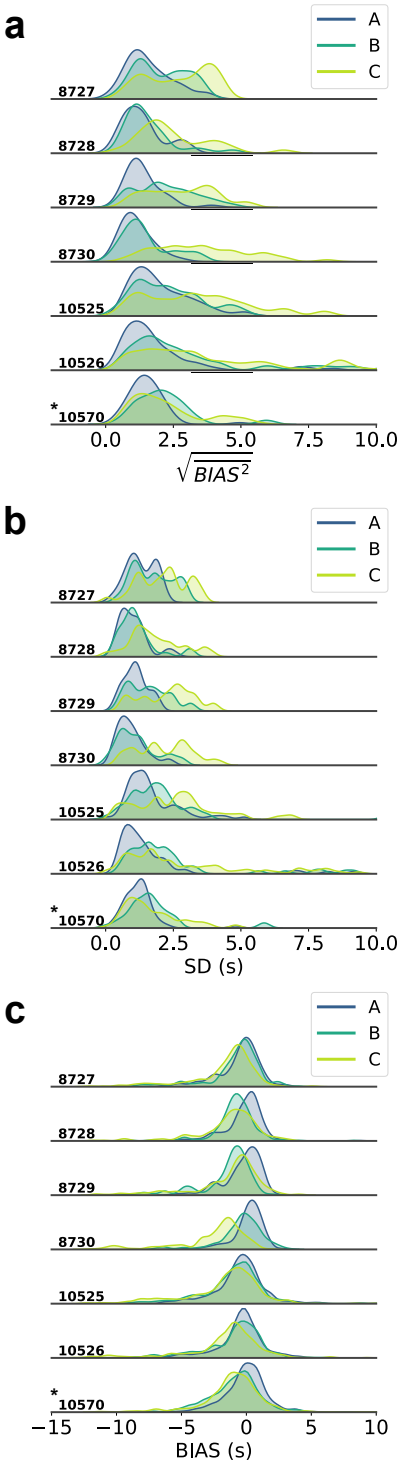

Figure 3.2: Comparison parameters $\sqrt{\overline{BIAS^2}}$, SD, and BIAS of time reproductions of gerbils. Selected parameters are shown for each subject individually as density estimates for $\sqrt{\overline{BIAS^2}}$ (a), standard deviation (b), and BIAS (c). $\sqrt{\overline{BIAS^2}}$ and standard deviation increased with stimulus size (scalar variability). The signed bias decreased with increasing stimulus size. $\sqrt{\overline{BIAS^2}}$ density was calculated as the square root of the mean squared bias for response values per stimulus, presented in each session within each stimulus distribution. The density of the signed bias was calculated as the averaged bias per response of all sessions. Standard deviation density was calculated as the standard deviation of all responses per stimulus, in each stimulus range. The representative subject indicated in Figure 3.1 is marked with an asterisk. Colors identify stimulus distributions (cf. Figure 2.2c).

identify the differences within pairs of stimulus distributions AB, BC, and AC. Due to multiple comparison testing, the p-values were adjusted with the help of Bonferroni correction.

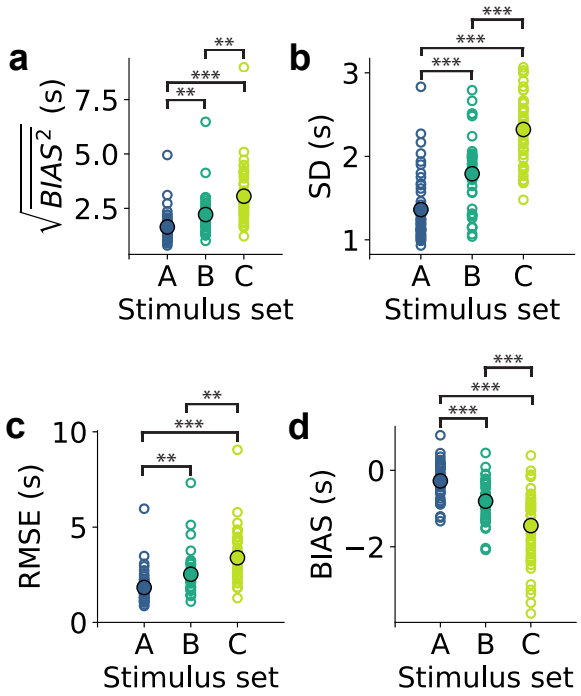

Figure 3.3: Comparison parameters $\sqrt{\overline{BIAS^2}}$, SD, RMSE, and BIAS of time reproductions of gerbils pooled across all subjects. Parameters were pooled across all subjects with values from each experimental session. $\sqrt{\overline{BIAS^2}}$ (a) as well as standard deviation (b) differed significantly between all tested stimulus distributions. The RMSE (c) was significantly different for the tested stimulus magnitudes, and the BIAS (d) showed significant differences between stimulus distributions. Colors identify stimulus distributions (cf. Figure 2.2c). Filled circles with black edge color mark the mean. An independent 2-sample t-test with Bonferroni correction was used for statistical analysis.

The $\sqrt{\overline{BIAS^2}}$ showed a significant increase with stimulus size across tested stimulus distributions A, B and C (1.642 $\pm$ 0.690 vs. 2.214 $\pm$ 0.954 vs 3.059 $\pm$ 1.202, H = 53.373, p = 2.572 $\times 10^{-12}$; independent 2-sample t-test, A vs. B: T = -3.122, p $\leqslant$ 0.01, B vs. C: T = -3.533, p $\leqslant$ 0.01, A vs. C: T = -6.885, p $\leqslant$ 0.001), suggesting a stronger regression effect for the long stimulus ranges (Figure 3.3a). Similarly, and following scalar variability, the standard deviation was larger for the longer ranges than the shorter ranges (1.362 $\pm$ 0.401 vs. 1.792 $\pm$ 0.455 vs. 2.321 $\pm$

0.400, H = 65.352, p = 6.443 $\times 10^{-15}$; independent 2-sample t-test, A vs. B: T = -4.502, p $\leqslant$ 0.001, B vs. C: T = -5.762, p $\leqslant$ 0.001, A vs. C: T = -11.581, p $\leqslant$ 0.001) (Figure 3.3b), and so was the RMSE for the tested stimulus distributions A, B and C (1.831 $\pm$ 0.854 vs. 2.526 $\pm$ 1.143 vs 3.391 $\pm$ 1.228, H = 52.398, p = 4.187 $\times 10^{-12}$; independent 2-sample t-test, A vs. B: T = -3.124, p $\leqslant$ 0.01, B vs. C: T = -3.348, p $\leqslant$ 0.01, A vs. C: T = -7.06, p $\leqslant$ 0.001) (Figure 3.3c). Calculating the (signed) bias revealed a general underestimation for all ranges. This effect massively increased with stimulus magnitude A, B, and C (-0.278 $\pm$ 0.465 vs. -0.809 $\pm$ 0.541 vs. -1.447 $\pm$ 0.916, $F_{2,131}$ = 33.837, p = 1.423 $\times 10^{-12}$; independent 2-sample t-test, A vs. B: T = 4.756, p $\leqslant$ 0.001, B vs. C: T = 3.778, p $\leqslant$ 0.001, A vs. C: T = 7.645, p $\leqslant$ 0.001) (Figure 3.3d). This linear increase in (signed) bias helped to explain the increase in $\sqrt{\overline{\text{BIAS}^2}}$ across stimulus distributions.

3.1.2 *Time estimation in humans.*

The same task structure was applied for experiments with six young adults aged between 21 and 32 years. Instead of reproducing the time estimate via a self-motion response, participants controlled their virtual movement through the virtual maze via a joystick. Figure 3.1b shows the reproduction times depending on the stimulus times tested for each stimulus range of one representative participant. Data of all human individuals are shown in Figure 6.2. As with the gerbils, the standard deviation increased with increasing stimulus size (Figure 3.2b). Regression effects were visible and increased with the magnitude of the stimulus distribution. Within the human-subject group, effects of regression were more diverse than compared to gerbils (Figure 3.4c; example subject marked with an asterisk).

Similarly to gerbils, time reproduction correlated with stimulus range and showed an increased $\sqrt{\overline{\text{BIAS}^2}}$ (1.276 $\pm$ 0.592 vs. 1.551 $\pm$ 0.643 vs 2.227 $\pm$ 0.922, $F_{2,33}$ = 4.894, p = 0.014; independent

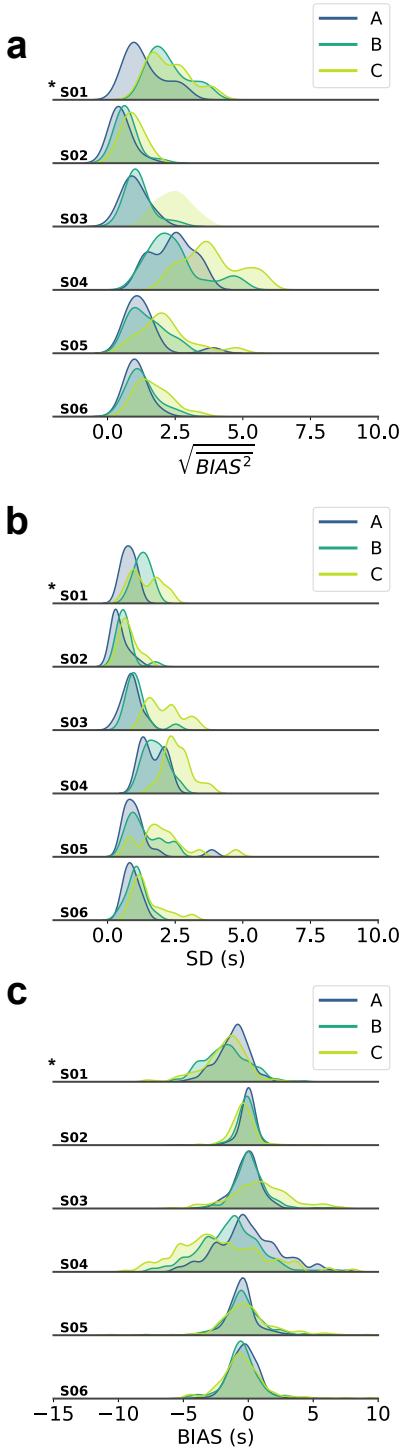

Figure 3.4: Comparison parameters $\sqrt{\overline{BIAS^2}}$, SD, and BIAS of time reproductions of humans. Selected parameters are shown for each subject individually as density estimates for $\sqrt{\overline{BIAS^2}}$ (a), standard deviation (b) and BIAS (c). $\sqrt{\overline{BIAS^2}}$ and standard deviation increased with stimulus size (scalar variability). The signed bias decreased with increasing stimulus size. $\sqrt{\overline{BIAS^2}}$ density was calculated as the square root of the mean squared BIAS for response values per stimulus, presented in each session within each stimulus distribution. The density of the signed bias was calculated as the averaged bias per response of all sessions. Standard deviation density was calculated as the standard deviation of all responses per stimulus, in each stimulus range. The representative participant indicated in Figure 3.1 is marked with an asterisk. Colors identify stimulus distributions (cf. Figure 2.2c).

2-sample t-test, A vs. B: T = -1.044, p = 0.922 failed to reach significance, B vs. C: T = -1.993, p = 0.176 failed to reach significance, A vs. C: T = -2.877, $p \leqslant 0.05$) (Figure 3.5a), an increased SD (0.938 $\pm$ 0.335 vs. 1.185 $\pm$ 0.311 vs 1.694 $\pm$ 0.633,

$F_{2,33}$ = 8.039, $p \leqslant 0.01$; independent 2-sample t-test, A vs. B: T = -1.786, p = 0.263 failed to reach significance, B vs. C: T = -2.395, p = 0.077 failed to reach significance, A vs. C: T = -3.5, $p \leqslant 0.01$) (Figure 3.5b), an increased RMSE (1.386 $\pm$ 0.608 vs. 1.660 $\pm$ 0.680 vs 2.329 $\pm$ 0.949, $F_{2,33}$ = 4.481, $p \leqslant 0.05$; independent 2-sample t-test, A vs. B: T = -0.997, p = 0.988 failed to reach significance, B vs. C: T = -1.9, p = 0.212 failed to reach significance, A vs. C: T = -2.774, $p \leqslant 0.050$) (Figure 3.5c), and overall negative bias for all tested stimulus ranges. The (signed) bias did not decrease as strongly as for gerbils, which was expected due to obtained values of $\sqrt{\overline{\text{BIAS}^2}}$ (-0.378 $\pm$ 0.402 vs. -0.650 $\pm$ 0.635 vs -0.649 $\pm$ 1.086, $F_{2,33}$ = 0.465, p = 0.632 failed to reach significance; independent 2-sample t-test, A vs. B: T = 1.199, p = 0.73 failed to reach significance, B vs. C: T = -0.002, p = 1.0 failed to reach significance, A vs. C: T = 0.777, p = 1.0 failed to reach significance) (see Figure 3.5d).

3.1.3 *Comparison of gerbils and humans*

To compare the performance of humans versus animals and species-specific performance across tested stimulus distributions, I calculated dimensionless analysis parameters, i.e., coefficient of variation (CV) and slope (Figure 3.6 and Figure 3.7). The differences within species were evaluated across stimulus distributions with one-way repeated measures ANOVA. The differences between species were calculated using a two-way repeated-measures ANOVA.

Coefficient of variation. The CV was calculated comparably to the selected parameters in subsection 3.1.1 and subsection 3.1.2: Data were tested for normality, and depending on the outcome further analyzed with one-way ANOVA or Kruskal-Wallis test respectively. Differences in stimulus range pairs were evaluated with an independent 2-sample t-test with Bonferroni-corrected p-value. The CV showed no significant

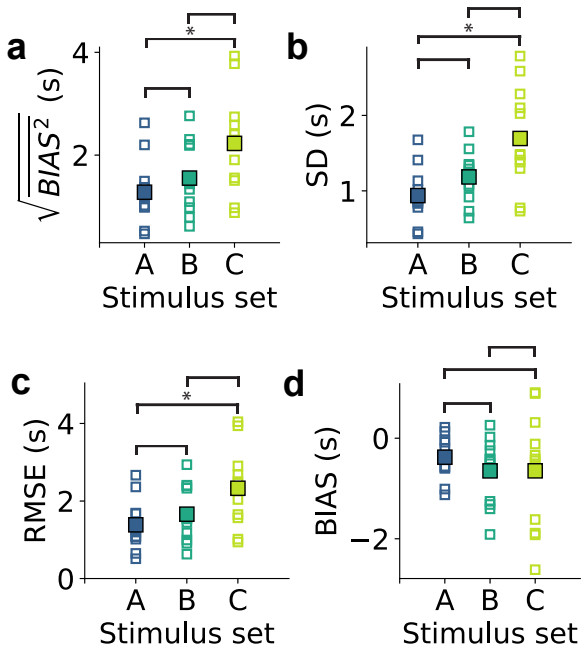

Figure 3.5: Comparison parameters $\sqrt{\overline{BIAS^2}}$, SD, RMSE, and BIAS of time reproductions of humans pooled across all participants. Selected parameters include values from each experimental session and are pooled across all participants. $\sqrt{\overline{BIAS^2}}$ (a) as well as standard deviation (b) differed significantly only between tested stimulus distributions A and C. Both parameters increased across the magnitude of the tested stimulus ranges but could not yield significance due to high variability between subjects. Analogously, the RMSE (c) showed significant differences only for stimulus set A compared to C. The signed bias (d) showed no significant differences. Colors identify stimulus distributions (cf. Figure 2.2c). Filled squares with black edgecolor mark the mean. An independent 2-sample t-test with Bonferroni correction was used for statistical analysis.

differences for the human test group across the tested stimulus sets (A vs. B vs. C: 0.176 ± 0.081, 95% CI [0.155, 0.198] vs. 0.149 ± 0.063, 95% CI [0.132, 0.167] vs. 0.160 ± 0.073, 95% CI [0.145, 0.175]; η^2 = 0.168, H = 2.098, p = 0.35; Figure 3.7a). Analysis with independent 2-sample t-test of stimulus range pairs further confirmed that all set pairs did have a very similar mean and showed strongly overlapping distributions (Figure 3.7a). Thus,

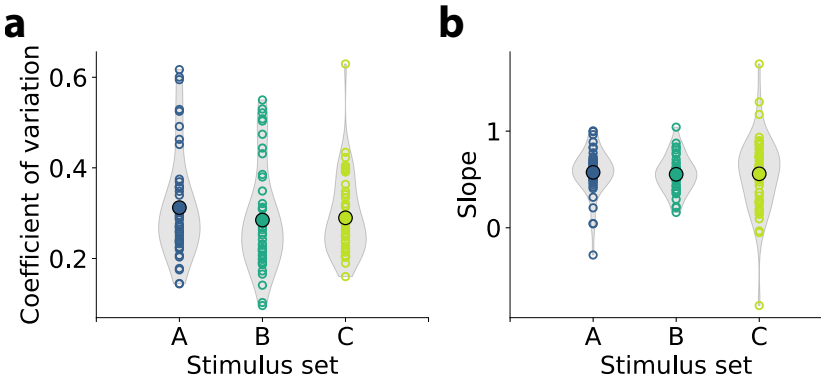

Figure 3.6: Time estimation performance in gerbils. Coefficient of variation (a) and slope (b). Violin plots illustrate the distribution of the population. Marker colors identify the stimulus range. Filled circles mark the distribution mean. Open circles depict the average CV per subject for each stimulus interval included in the tested range (a). The slope was calculated using a linear regression algorithm fitted to the means of the responses, obtained for each stimulus within the tested stimulus distribution (b).

none of the set pairs differed significantly from each other (AB: T = 1.795, p = 0.228, BC: T = -0.745, p = 1.0, AC: T = 1.035, p = 0.91). The same observation was made in the data of the gerbil population. The CV showed no significant differences across the tested stimulus sets (A vs. B vs. C: 0.312 $\pm$ 0.114, 95% CI [0.293, 0.331] vs. 0.285 $\pm$ 0.111, 95% CI [0.271, 0.298] vs. 0.290 $\pm$ 0.086, 95% CI [0.272, 0.308]; η^2 = 0.242, H = 2.258, p = 0.323; Figure 3.6a), which was further confirmed by an independent 2-sample t-test (AB: T = 1.195, p = 0.705, BC: T = -0.239, p = 1.0, AC: T = 1.098, p = 0.825) The variability of the responses was not affected by the stimulus range, since the average CV was at about 0.3 for all ranges and animals. The analysis revealed a significant difference between species ($F_{1,43}$ = 136.276, p = 7.649×10^{-6}, η^2 = 4.943) which was confirmed with an independent 2-sample t-test ($A_{gerbils}$ vs. A_{humans}: t = 9.224, p = 4.635×10^{-7}; $B_{gerbils}$ vs. B_{humans}: t = 12.055, p = 2.831×10^{-8}; $C_{gerbils}$ vs. C_{humans}: t = 10.857, p = 1.156×10^{-7}). The interaction of species and stimulus set was not significant.

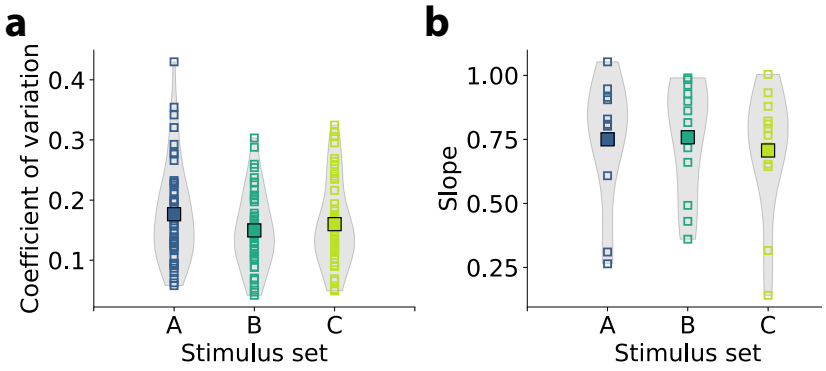

Figure 3.7: Time estimation performance in humans. Coefficient of variation (a) and slope (b). Violin plots illustrate the distribution of the population. Marker colors identify stimulus range. Filled squares mark the distribution mean. Open squares depict the average CV per participant for each stimulus interval included in the tested range (a). The slope was calculated using a linear regression algorithm fitted to the means of the responses, obtained for each stimulus within the tested stimulus distribution (b).

Slope. To extract the slopes, data of individual subjects were pooled across experimental sessions. The slope was then calculated by using a least-squares linear regression algorithm, fitted to the means of the responses obtained for each stimulus within the stimulus distribution. Within animals, slopes showed a slight decrease only. No significant differences were detected across stimulus distributions (A vs. B vs. C: 0.573 ± 0.238, 95% CI [0.522, 0.689] vs. 0.553 ± 0.191, 95% CI [0.522, 0.607] vs. 0.558 ± 0.379, 95% CI [0.462, 0.658]; η^2 = 0.043, H = 0.727, p = 0.695; Figure 3.6b). Considering significance between pairs of tested stimulus sets further confirmed the obtained results (A vs. B: T = 0.414, p = 1.0; B vs. C: T = -0.739, p = 1.0; A vs. C: T = 0.227, p = 1.0). For humans, the decrease in slopes with increasing stimulus range was more pronounced compared to gerbils, but yet did not yield significance either (A vs. B vs. C: 0.750 ± 0.232, 95% CI [0.545, 0.953] vs. 0.758 ± 0.215, 95% CI [0.585, 0.936] vs. 0.706 ± 0.239, 95% CI [0.520, 0.897]; η^2 = 0.01, H = 0.619, p = 0.734; Figure 3.7b). Further evaluation with an independent 2-sample t-test confirmed that there was no significance between pairs of tested stimulus sets (A vs. B : T = -0.086, p = 1.0; B vs. C: T = 0.533, p = 1.0; A vs. C: T =

0.434, p = 1.0). The difference between species failed to reach significance ($F_{1,37}$ = 0.216, p = 0.809, η^2 = 0.005). The interaction of species and stimulus range was not significant.

3.1.4 *Influence of movement parameters on reproduction performance*

Movement parameters were analyzed to check whether animals used specific running strategies to solve the task. Therefore, correlations and interactions of the presented stimulus interval, the reproduced time, and the distance traveled during the reproduction phase were evaluated. Further, I investigated whether animals could and did take advantage of the applied gains by adjusting their running speeds and thereby infer information about the time passed. Additionally, running trajectories were analyzed to exclude the possibility that animals used characteristic running patterns to precisely estimate, and reproduce time.

Time stimuli tested in each stimulus range were evenly distributed and equally frequent. The stimulus size strongly correlated with the distance traveled (path length) (r = 0.49, p $<$ 0.01) (Figure 3.8a) - which was expected by the nature of the task - and so did the reproduced intervals (r = 0.58, p $<$ 0.01) (Figure 3.8b). In both cases, the provided kernel density estimates (KDEs) on the marginal y-axis showed an upward shift for the larger stimulus distributions and peaked from approximately 1 meter to 3 meters. The virtual running speed, which is the real running speed multiplied with the applied gain, peaked around 0.25 m/s for all tested stimulus distributions and did not show a significant correlation with presented stimuli (r = 0.02, p = 0.2) (Figure 3.8c). However, Pearson's correlation coefficient did reveal a significant positive correlation of the reproduced intervals with the virtual running speed (r = 0.04, p $<$ 0.01; Figure 3.8d). Also, the path length correlated positively with the virtual running speed (r = 0.78, p $<$ 0.01; Figure 3.8e). The magnitude of the tested stimulus distribution did not affect

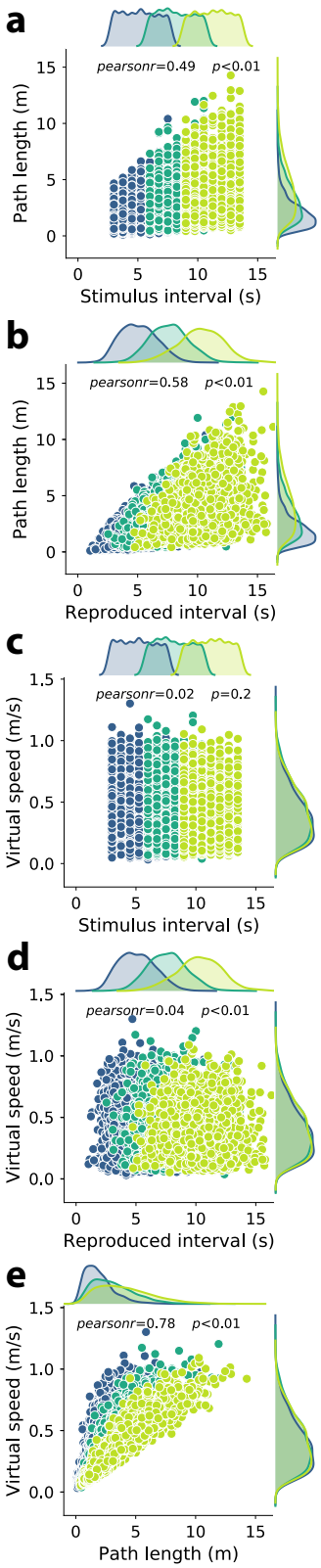

Figure 3.8: Trajectory parameters of temporal reproduction for gerbils – part I. Correlation of stimulus intervals with path length and reproduced intervals with path length (a and b) as well as correlation of virtual movement speed with stimulus intervals and virtual movement speed with reproduced intervals (c and d). (e) Correlation of path length with virtual speed. Kernel density estimates on the marginal plots show the data distributions on the respective axis. Pearson's correlation coefficients r and corresponding p-values are provided. Data were pooled within the animal's test group. Same color conventions as in Figure 3.1.

the interactions of the virtual running speed with the tested stimulus intervals or reproduced intervals, as depicted by the strongly overlapping corresponding kernel density estimates for the tested stimulus distributions. The described correlations could be detected for almost all animals individually. The individual subjects only showed minor deviations from the overall impression and found correlations depicted in Figure 3.8. Interactions of reproduction performance of each individual are shown in Figure 6.4.

The applied gain factors, ranging from 0.25 to 2.25 were evenly applied to all stimulus ranges and were not correlated with stimulus intervals ($r = 0.0$, $p = 0.94$). Although the KDEs were fairly similar for the interaction of reproduced intervals and gain, Pearson correlation assigned significance to this interaction ($r = 0.04$, $p < 0.01$) (see Figure 3.9a and Figure 3.9b). Analysis of the physical running speed revealed, that animals ran with an average speed of 3 m/s and did not adjust running speed for presented stimuli ($r = 0.03$, $p = 0.01$) nor for time reproduction ($r = -0.01$, $p = 0.42$) (see Figures 3.9c and 3.9d). The applied gain factors showed a significant negative correlation with the physical running speed, but kernel density estimates showed substantial overlap for the tested stimulus ranges, indicating that there were no significant differences across stimulus distributions ($r = -0.02$, $p < 0.01$; Figure 3.9e). The movement parameter running speed appeared to be much more diverse when considered for each animal individually (Figure 6.5). When considered separately, all animals showed a significant relationship of running speed with presented stimulus interval, of running speed with reproduced intervals and running speed with applied gain. Only with minor exceptions, a shifted KDE distribution for increasing stimulus ranges was apparent.

The relationship of stimulus intervals with starting latency as well as the relationship of reproduced intervals with starting latency was evaluated to exclude possibly applied strategies facilitating time estimation. The starting latency incorporates the time from trial onset to the start of the running response. The starting latency peaked at approximately 7.5 s, 11 s and 14 s for the stimulus ranges A, B, and C. It was strongly correlated with the stimulus interval and the reproduced interval (Figure

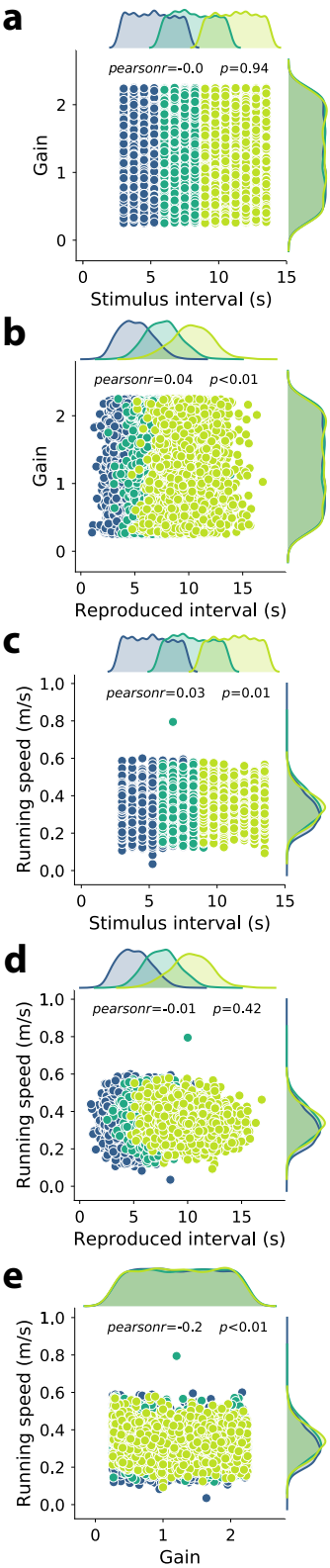

Figure 3.9: Trajectory parameters of temporal reproduction for gerbils – part II. Correlation of stimulus intervals with gain and reproduced intervals with gain (a and b) as well as the correlation of stimulus intervals with animals' running speed and reproduced intervals with animals' running speed (c and d). (e) Correlation of gain with the animals' running speed. Kernel density estimates on the marginal plots show the data distributions on the respective axis. Pearson's correlation coefficients r and corresponding p-values are provided. Data were pooled within the animal's test group. Same color conventions as in Figure 3.1.

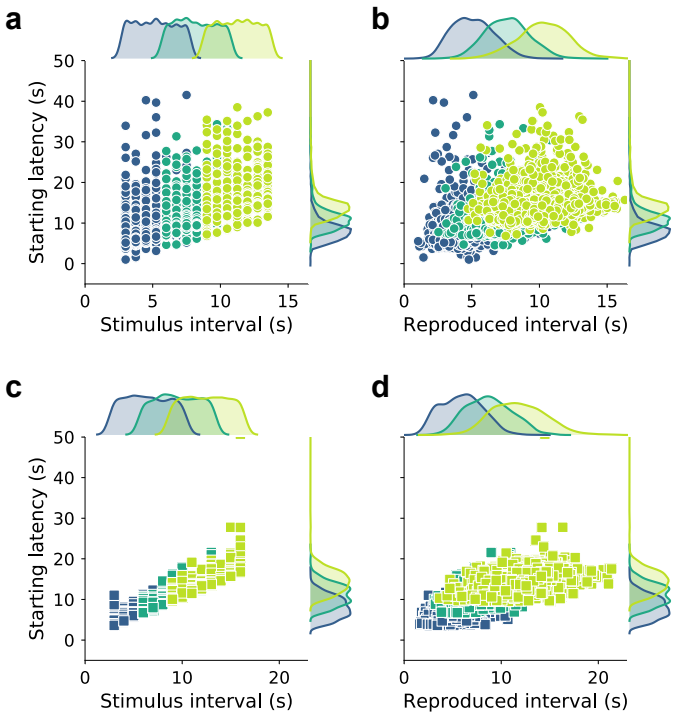

Figure 3.10: Starting latency correlates with time stimuli and reproduction. Correlation of stimulus interval with the animals' starting latency and reproduced interval with the animal's starting latency (a and b). Increasing starting latencies observed for humans (c and d). Kernel density estimates on the marginal plots show distributions on the respective axis. Data were pooled across all subjects within each group of the tested species. Same color conventions as in Figure 3.1.

3.10a and Figure 3.10b). As the stimulus's presentation time increased with stimulus size, the correlation is strongly positive by nature. Also, the correlation between starting latency and reproduced intervals is naturally affected by stimulus size, but it might also be affected by other factors. The KDEs reinforce the impression of the increase in starting latency across tested stimulus magnitude with an upward shift towards larger magnitudes. The found interactions are also visible when evaluated for animal subjects individually (see Figure 6.6). In order to get a better comparison for the evaluation of the starting latencies of the animals, I also looked at the starting latencies of the human test group. Starting latencies scaled with the size of

the stimulus distribution and the duration of the reproduced interval. The mean starting latencies for all participants reached a comparable maximum to the values described for gerbils. The variability of starting latency, however, was significantly different in gerbils and humans. Gerbil data appeared to be much more variable than human data and spread across longer starting latencies. Nevertheless, the main mass of data points, representing the starting latencies, was equal or showed minor differences as depicted by comparable density functions.

The evaluation of running trajectories showed directed running paths with constant speeds throughout the whole path (see Figure 6.7) for all animals. Also, here some variability was visible across subjects. Some animals did not use the dimension of the virtual corridor's width, and others irregularly traversed the corridor. Several animals did favor one side of the corridor, as indicated by the right-side or left-side accumulated running paths.

3.1.5 *Context dependence*

Context dependence was analyzed with a subset of stimuli in the overlapping stimulus ranges. Therefore, stimulus pairs of overlapping stimulus sizes each were compared. A stimulus pair included reproduced values of a tested time stimulus that was one time embedded at the upper bound of the smaller stimulus distribution and the other time embedded at the lower bound of the larger stimulus distribution. This grouping of stimuli yielded two pairs (AB, BC) for the overlapping stimulus intervals with durations of 6.0 s, 6.75 s, and 7.5 s (AB) and 9.0 s, 9.75 s, and 10.5 s (BC) for gerbils and 6.0 s, 7.0 s, 8.0 s, 9.0 s and 10.0 s (AB) and 9.0 s, 10.0 s, 11.0 s, 12.0 s, 13.0 s (BC) for humans.

Within this subset of tested stimulus values, the mean responses increased with the size of the stimulus (Table 3.1 and Table 3.2). This effect was stronger for humans compared to gerbils (see Figure 3.11 and Figure 3.12).

Stimulus interval [s] \ Pair	AB	
6.0	5.36 ± 0.9	6.15 ± 0.98
6.75	5.78 ± 1.27	6.64 ± 0.8
7.5	6.33 ± 0.98	7.01 ± 1.06

Stimulus interval [s] \ Pair	BC	
9.0	7.69 ± 1.31	8.61 ± 1.7
9.75	7.94 ± 0.94	8.87 ± 1.46
10.5	9.07 ± 1.25	9.4 ± 1.8

Table 3.1: Summary of results for pair-wise comparison of mean response values for overlapping stimuli in gerbils. Mean values ± standard deviation are given for the subset of overlapping stimuli in range pairs AB and BC.

Stimulus interval [s] \ Pair	AB	
6.0	5.87 ± 0.59	6.05 ± 0.52
7.0	6.68 ± 0.37	6.79 ± 0.68
8.0	7.18 ± 0.69	7.7 ± 0.45
9.0	8.03 ± 0.76	8.71 ± 0.37
10.0	8.61 ± 1.07	9.23 ± 0.76

Stimulus interval [s] \ Pair	BC	
9.0	8.71 ± 0.37	9.33 ± 0.89
10.0	9.23 ± 0.76	10.1 ± 1.09
11.0	10.27 ± 0.74	10.9 ± 0.94
12.0	10.89 ± 1.12	11.47 ± 1.2
13.0	11.17 ± 1.57	12.02 ± 1.34

Table 3.2: Summary of results for pair-wise comparison of mean response values for overlapping stimuli in humans. Mean values ± standard deviation are given for the subset of overlapping stimuli in range pairs AB and BC.

However, for both species, the mean of responses for each stimulus was larger when embedded in the larger stimulus range than when embedded in the smaller stimulus range ($AB_{gerbils}$ [6.0 s]: t = -3.78, $p < 0.001$; [6.75 s]: t = -3.54, $p < 0.001$; [7.5 s]: t = -3.01, $p < 0.01$, $BC_{gerbils}$ [9.0 s]: t = -2.76, $p < 0.01$; [9.75 s]: t = -3.4, $p < 0.01$; [10.5 s]: t = -0.95, p = 0.34 (see Figure 3.11); AB_{humans} [6.0 s]: t = -0.73, p = 0.47; [7.0 s]: t = -0.49, p = 0.63; [8.0 s]: t = -2.09, $p < 0.05$; [9.0 s]: t = -2.67, $p < 0.05$; [10.0 s]: t = -1.56, p = 0.13; BC_{humans}[9.0 s]: t = -2.14, $p < 0.05$; [10.0 s]: t = -2.19, $p < 0.05$; [11.0 s]: t = -1.76, p = 0.09; [12.0 s]: t = -1.18, p = 0.25; [13.0 s]: t = -1.36, p = 0.19 (see Figure 3.12)).

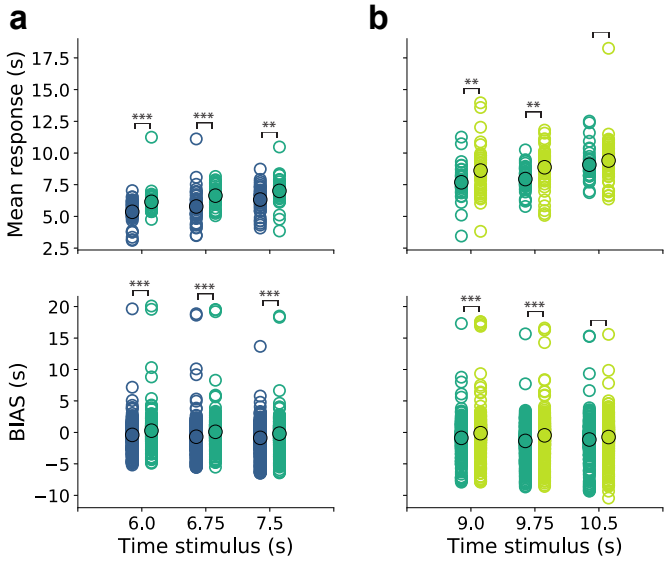

Figure 3.11: Context dependence in gerbils. The overlapping stimuli of stimulus pair AB (blue (A) and green (B)) (a) and BC (green (B) and yellow (C)) (b) for all animals pooled across sessions. Mean response values (filled circles) increased with stimulus size. The BIAS decreased with stimulus size and was larger for the stimuli embedded in the longer stimulus range. Same color conventions as in Figure 3.1.

The BIAS was stable or showed a limited, yet significant decrease across stimulus size, stronger for gerbils than for humans ($AB_{gerbils}$ [6.0 s]: t = -4.31, p = 1.86×10^{-5}; [6.75 s]: t = -4.46, p = 9.22×10^{-6}; [7.5 s]: t = -4.32, p = 1.73×10^{-5}, $BC_{gerbils}$ [9.0 s]: t = -3.34, p = 0.87×10^{-2}; [9.75 s]: t = -4.23, p = 2.58×10^{-5}; [10.5 s]: t = -1.85, p = 0.06; AB_{humans} [6.0 s]: t = -0.42, p = 0.67; [7.0 s]: t = -1.74, p = 0.08; [8.0 s]: t = -3.82, p = 0.16×10^{-3}; [9.0 s]: t = -3.51, p = 0.51×10^{-3}; [10.0 s]: t = -2.51, p = 0.01; BC_{humans} [9.0 s]: t = -3.48, p = 0.56×10^{-3}; [10.0 s]: t = -4.65, p = 4.93×10^{-6}; [11.0 s]: t = -2.08, p = 0.04; [12.0 s]: t = -2.22, p = 0.03; [13.0 s]: t = -4.75, p = 3.04×10^{-6} (Table 3.3 and Table 3.4; see Figure 3.11 and Figure 3.12).

To assess the regression and get a better understanding of the BIAS and the slope, I analyzed the transition point when overestimation turned to underestimation. I investigated whether this transition point corresponded to the mean of the stimulus distribution as predicted by Bayes (see subsection

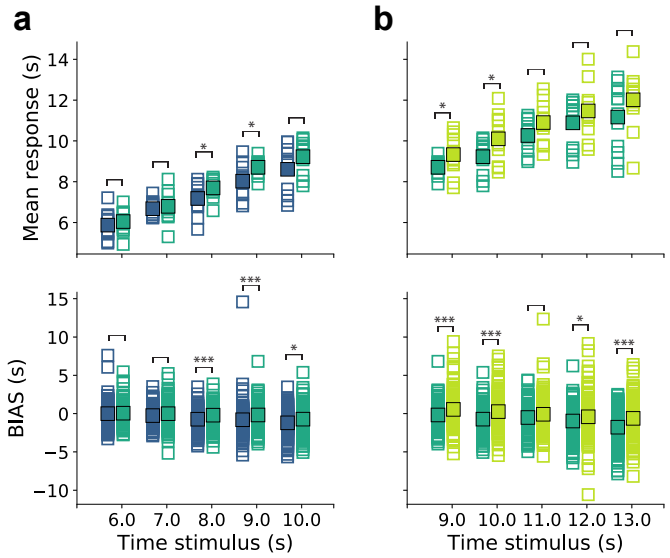

Figure 3.12: Context dependence in humans. The overlapping stimuli of stimulus pair AB (blue (A) and green (B)) (a) and BC (green (B) and yellow (C)) (b) for all humans pooled across sessions. Mean response values (filled circles) increased with stimulus size. The BIAS decreased with stimulus size and was larger for the stimuli embedded in the longer stimulus range. Same color conventions as in Figure 3.1.

Stimulus interval [s] \ Pair	AB	
6.0	-0.39 ± 1.96	0.28 ± 2.28
6.75	-0.69 ± 2.41	0.1 ± 2.43
7.5	-0.87 ± 2.16	-0.2 ± 2.3

Stimulus interval [s] \ Pair	BC	
9.0	-0.88 ± 2.58	-0.12 ± 3.18
9.75	-1.37 ± 2.64	-0.47 ± 2.01
10.5	-1.13 ± 2.86	-0.74 ± 2.73

Table 3.3: Summary of results for pair-wise comparison of the BIAS for overlapping stimuli in animals. Mean values ± standard deviation are given for the subset of overlapping stimuli in range pairs AB and BC.

1.4.4) according to the central tendency effect, or if deviations occurred. To test this, I fitted a least-squares linear regression to the average responses of each stimulus per session. From this fit, the BIAS was calculated and used to determine the

Stimulus interval [s] \ Pair	AB	
6.0	-0.005 ± 1.31	0.05 ± 1.18
7.0	-0.26 ± 1.05	-0.009 ± 1.45
8.0	-0.73 ± 1.29	-0.2 ± 1.18
9.0	-0.8 ± 1.81	-0.18 ± 1.44
10.0	-1.2 ± 1.71	-0.72 ± 1.6

Stimulus interval [s] \ Pair	BC	
9.0	-0.18 ± 1.45	0.55 ± 2.25
10.0	-0.72 ± 1.6	0.26 ± 2.14
11.0	-0.51 ± 1.6	-0.09 ± 2.03
12.0	-0.97 ± 1.92	-0.41 ± 2.5
13.0	-1.77 ± 2.2	-0.62 ± 2.16

Table 3.4: Summary of results for pair-wise comparison of the BIAS for overlapping stimuli in humans. Mean values ± standard deviation are given for the subset of overlapping stimuli in range pairs AB and BC.

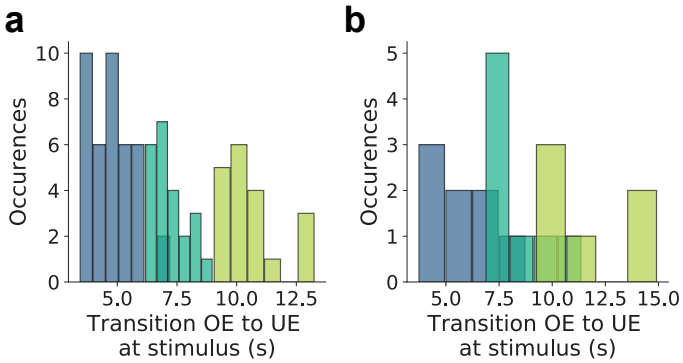

Figure 3.13: Transition from overestimation to underestimation. Occurrences of transition points from overestimation (OE) to underestimation (UE) in gerbils (a) and humans (b). Time values derived from a least-squares linear regression fitted to the average response per stimulus size were counted in single sessions of the tested ranges and accumulated. Data were pooled within subject groups. Same color conventions as in Figure 3.1.

exact stimulus value (transition point) when a change in sign occurred.

The analysis of transition point for the animal test group revealed that time values of 5.0 seconds to 6.0 seconds and 4.0 seconds to 4.5 seconds were encountered as transition point 6 times, each within this given range from all animals in stimulus

range A. Each possible time point within the limited range of 0.5 seconds to 1.0 seconds and 4.5 seconds to 5.0 seconds was counted ten times as transition point within stimulus range A, each. The main mass of occurrences was encountered for time values around 5.0 seconds, which is only 95% of the actual distribution mean at 5.25 seconds (Figure 3.13a). For stimulus distribution B, the occurrences peaked at 7.0 seconds, at only 85% of the actual mean of 8.25 seconds. 89% of the actual mean of 11.25 seconds of stimulus distribution C served as transition point, which had its most occurrences as 10.0 seconds (Figure 3.13a).

In humans, the transition point was at only 70% of the actual mean of 6.5 seconds, with the most occurrences at 4.5 seconds for stimulus range A (Figure 3.13b). With approximately 80% of the actual mean in stimulus distribution B, the most occurrences for transition from over- to underestimation were encountered at the time value of 7.5 seconds. In stimulus range C, the transition point was detected at a value of 10.0 seconds, which is 80% of the actual mean at 12.5 seconds (Figure 3.13b).

3.2 SINGLE NEURON DYNAMICS DURING TEMPORAL PROCESSING OF RETROSPECTIVE AND PROSPECTIVE INTERVAL DURATION ESTIMATES

The animals participating in electrophysiology experiments were trained for 6-8 weeks on two well distinguishable stimuli and afterward on a continuous stimulus distribution. Daily, the performance was evaluated using the RMSE as well as the presence of a positive linear correlation of stimulus time and reproduction time. When the daily check of behavioral data let assume that animals had understood the task structure, the microdrive was implanted. After recovery, animals were tested on stimulus distributions A and stimulus distribution B, with simultaneous recording of the underlying neuronal activity. The data obtained during electrophysiological experiments can be split up in 3 categories: (i) Behavior only (see subsection 3.2.1), (ii) electrophysiology only (see subsection 3.2.3) and (iii) behavior combined with electrophysiology (see subsection 3.2.4), in order to detect sources of behavior encoded by neuronal firing.

3.2.1 *Behavioral output of underlying neuronal activity*

First, the pure behavior of the three animals' subset was analyzed to ensure that animals did estimate and reproduce the presented time interval. Further, it was investigated whether the neuronal substrates recorded during task execution showed correlations.

All animals managed to learn the timing task without using specific running patterns (example sessions shown in Figure 3.14f and Figure 3.14i). Animals showed a positive correlation of tested stimuli with reproduced values, and behavioral data indicated Bayesian effects like regression effect and scalar variability, for both tested stimulus distributions A and B (example animal shown in Figure 3.14a and Figure 3.14b).

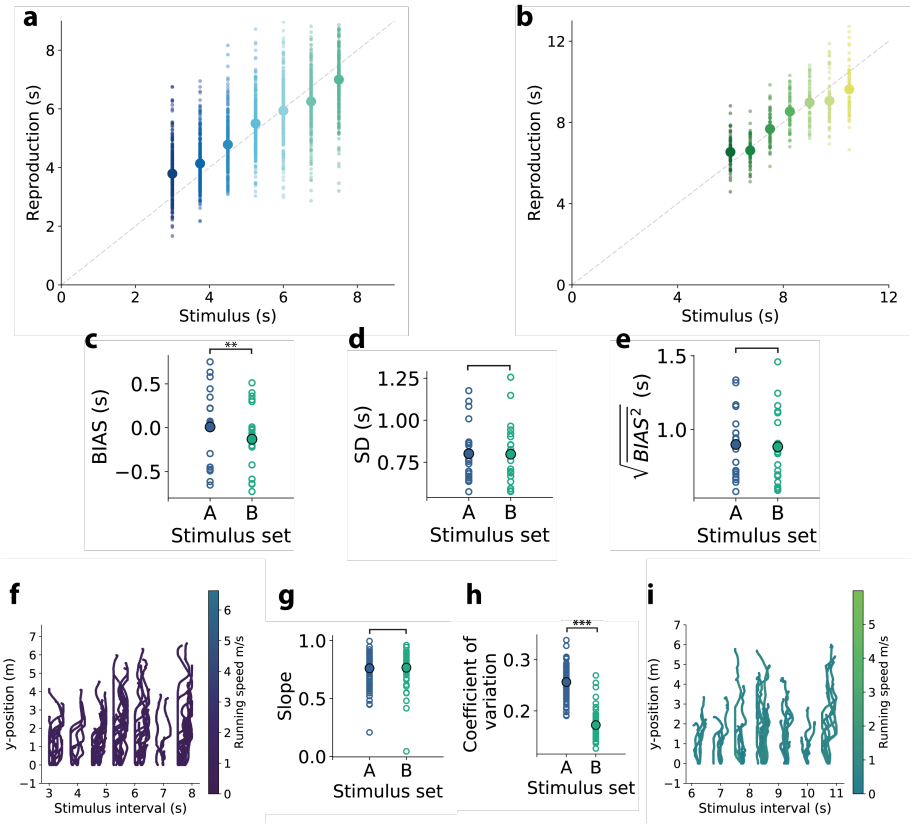

Figure 3.14: Behavioral output during electrophysiology experiments. Time reproductions of all sessions tested on stimulus range A (a) and B (b) of one representative subject. Individual reproduced values for stimulus intervals are given as small dots, and averages for each stimulus are depicted as filled circles. Colors identify stimulus size within stimulus distribution and are adapted to colors used for stimulus distributions of Figure 3.1. Parameters like BIAS (c), SD (d), $\sqrt{\overline{\text{BIAS}^2}}$ (e), slope (g), and CV (h) were extracted from behavioral data, analogously to section 3.1, and compared for the two tested stimulus distributions. Except for the CV, none of the analyzed parameters showed significant differences between the tested stimulus ranges. Running trajectories split by stimulus size of one session tested in range A (f) and another one tested in B (i) did not show characteristic running patterns.

Behavioral parameters of SD, BIAS, $\sqrt{\overline{\text{BIAS}^2}}$, coefficient of variation, and slope were assessed and tested for normality with

Shapiro-Wilk test. Differences in SD, BIAS, and $\sqrt{\overline{BIAS^2}}$ for the tested stimulus distributions were calculated by using a paired t-test or Mann-Whitney-U test, respectively. Differences of CV and slope for the tested stimulus distributions were determined using an independent 2-sample t-test or Mann-Whitney-U test.

Standard deviation. Responses of each animal were grouped by stimulus size, and SD calculated separately for each of the tested stimulus distributions (n = 21). Stimulus set A and B did not show significant differences in standard deviation (A vs. B: 0.801 $\pm$ 0.165 vs. 0.798 $\pm$ 0.179, U = 220.0, p = 0.5; Figure 3.14d)

BIAS and $\sqrt{\overline{BIAS^2}}$. BIAS was calculated as the average of biases for all responses, grouped by stimulus size for each animal individually, and accordingly assigned to stimulus distribution (n=21). Similarly, the $\sqrt{\overline{BIAS^2}}$ was calculated for each stimulus size and animal and assigned according to the stimulus distributions tested (n = 21). Significant differences were only observed for BIAS (A vs. B: 0.008 $\pm$ 0.409 vs. -0.131 $\pm$ 0.366, t = 3.438, p < 0.01; Figure 3.14c), but not for $\sqrt{\overline{BIAS^2}}$ (A vs. B: 0.899 $\pm$ 0.211 vs. 0.8841 $\pm$ 0.229, t = 0.407, p = 0.688; Figure 3.14e).

CV. The coefficient of variation was calculated session-wise. Data was tested on normality, and depending on the outcome, further analyzed with Mann-Whitney-U test or independent 2-sample t-test. The CV showed significant differences across the tested stimulus sets (A vs. B: 0.256 $\pm$ 0.027 vs. 0.172 $\pm$ 0.025, U = 191.0, p $<$ 0.001; Figure 3.14h).

Slope. The slope was calculated analogously to CV, but in contrast did not show significant differences between stimulus sets A and B (A vs. B: 0.761 $\pm$ 0.125 vs. 0.766 $\pm$ 0.03, U = 3867.0, p = 0.5; Figure 3.14g).

3.2.2 *Unit classification*

A total of 4109 well-isolated single units were extracellularly recorded from three animals, in 50-65 sessions for each animal, along the dorsoventral axis of the mPFC. Unit signals were isolated by manual cluster cutting, as described in subsection 2.6.3. Recorded unit signals were classified into putative pyramidal cells and putative interneurons based on mean discharge rate and spike width (see Figure 3.15a). Both types of neurons were included in the analyses. Those neurons with a mean firing rate $<$ 6.44 Hz and a spike width $>$ 0.4 ms were classified as putative pyramidal cells (PC; n = 728, 17.7%), and the remaining cells were classified as putative interneurons (IntN; n = 3381, 82.3%). However, as this result appeared unrepresentative compared to literature, I tried an approximation of cell classification by using a firing rate limit of 8.8 Hz and a width limit of 0.28 ms, as reported by Kim et al. (2013). With this approximation, the obtained classification yielded a populational majority of PC (n = 2975, 72.4%) in comparison to IntN (n = 1134, 27.6%).

3.2.3 *Activity profiles of individual neurons*

I successfully targeted all subregions of the mPFC and recorded a portion of 0.4% (n = 16) from subarea M2, 34.1% (n = 1401) from subarea Cg1, 23.1% (n = 949) from Cg2, 41.6% (n = 1710) from PrL, and 0.8% (n = 33) from IL (Figure 3.15b). Only cells with a total number of spikes $\geqslant$ 100 were included. Only those units with a mean firing rate of 0.3 Hz were subject to further analysis. Therefore, the obtained cell population included all types of putative cells, homogeneously collected from all subareas of mPFC, but was not divided by either category for successive analysis. Diverse types of neuronal activity profiles were observed for retrospective and prospective interval duration estimates (Fig. 3.16 - Fig. 3.18). Of these, the most abundant type was a monotonically changing

activity profile ("ramping activity") (Fuster, 1991; Durstewitz and Seamans, 2006), represented by many neurons which gradually increased or decreased their activity over time.

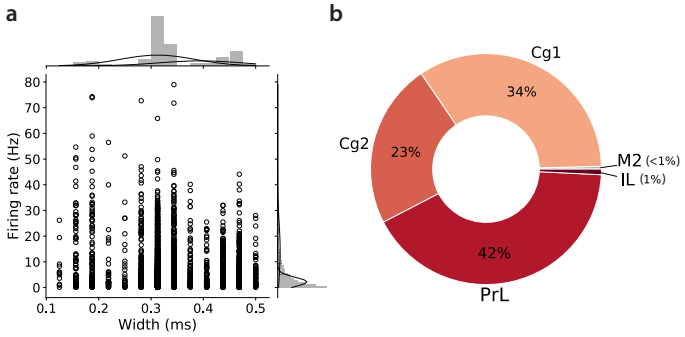

Figure 3.15: Cells recorded from subregions of the mPFC. (a) Unit classification. Recorded units (n = 4109) were classified into two groups based on the mean discharge rate and spike width. Those neurons with a mean firing rate < 6.44 Hz and spike width > 0.4 ms were classified as putative pyramidal cells (PC; n = 728, 17.7%), and the remaining cells were classified as putative interneurons (IntN; n = 3381, 82.3%). An approximation with specified values of 8.8 Hz and 0.276 ms, as reported by Kim et al. (2013), classified 2975 cells (72.4%) as PC and 1134 cells (27.6%) as IntN (adapted classification not shown). A Gaussian mixture model was used for cell classification, which identified two populational clusters. (b) Overview of cell portions recorded from targeted subareas of the mPFC.

For each neuron, the whole spike train of a recording session was time-sliced into the individual trials and sorted according to each presented interval duration (n = 7). Each resulting spike raster was aligned to session events of measurement onset, measurement offset, reproduction onset, and reproduction offset to evaluate the resulting peri-stimulus time histograms (see subsection 2.6.5). Thereby, activity profiles, present at the beginning and the end of the two task phases, could be evaluated to investigate the neural code underlying time estimation.

Among the recorded cells, I could identify subgroups of neurons with differentiated firing for the individual phases of the timing task: measurement, reproduction, and evaluation

phase, introduced as ITI in subsection 2.3.2. The present activity profiles of each subgroup will be introduced in the following. However, besides the modulated activity profiles, cells also showed sustained firing across task phases, which indicated no involvement of these cells in the process of time encoding during retrospective and prospective duration estimation (see Figure 6.8 in Appendix).

3.2.3-I. Neurons show modulated activity in measurement phase

The first presented group of neurons showed modulated activity during the measurement phase. This activity profile class can be subdivided into cells that differed in their average firing activity during measurement from reproduction, and cells, which additionally showed integration of the presented stimulus size during measurement.

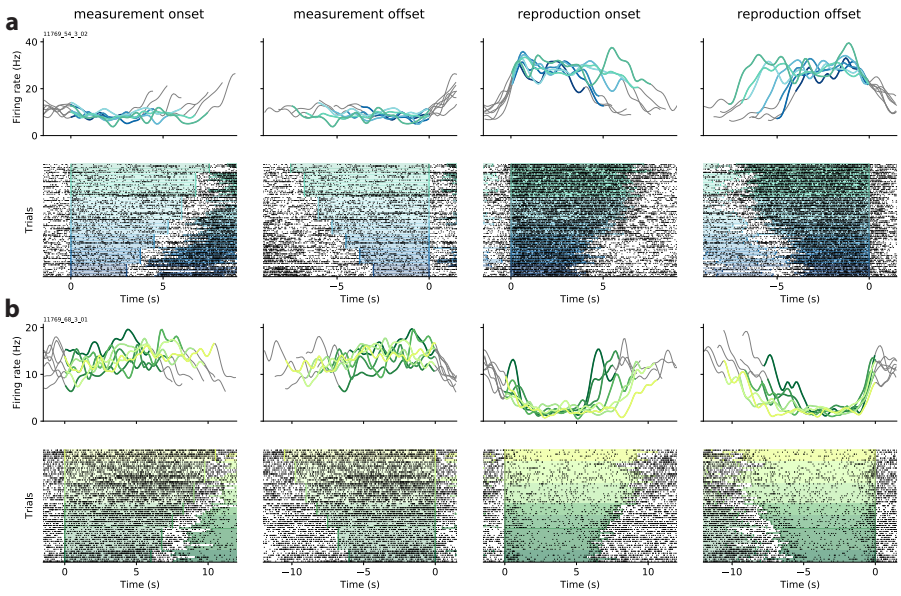

Figure 3.16: Different mean firing rate during measurement and reproduction. Spike raster plots and PSTHs (σ = 100 ms) are shown for mPFC example neurons, recorded during interval timing in stimulus distribution A (a) and stimulus distribution B (b). A subset of cells showed a higher mean discharge rate in measurement vs. reproduction (b), or a lower mean discharge rate in measurement phase than in reproduction phase (a). Colors identify stimulus size within the distribution (cf. Figure 3.14a and Figure 3.14b). Each row represents one trial. Trials were sorted according to the length of the sampled interval and aligned to measurement onset, measurement offset, reproduction onset, and reproduction offset. Color shaded areas in raster plots mark the respective phase in each trial.

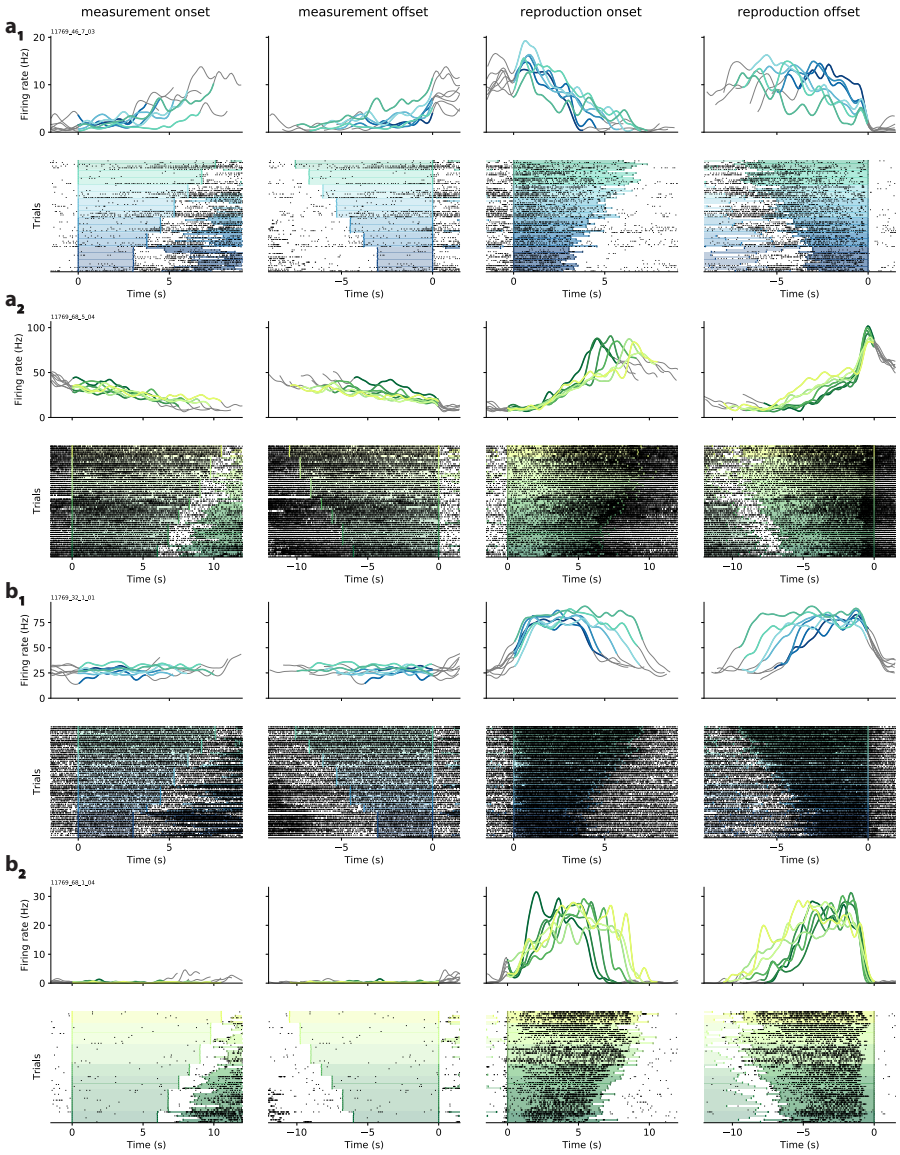

Figure 3.17: Tonic activity modulation during measurement and reproduction phase. Spike raster plots and PSTHs (σ = 100 ms) are shown for mPFC example neurons, recorded in stimulus distribution A (a_1 and b_1) and B (a_2 and b_2). Diverse combinations of non-monotonic with monotonic activity during measurement and reproduction could be observed e.g., a monotonic activity increase in MP with monotonic activity decrease in RP (a_1), a monotonic decreasing activity in MP with monotonic increasing firing in RP (a_2), or non-monotonic activity in MP and RP at different average discharge rates (b_1), or even no activity in MP with non-monotonic firing in RP (b_2). Colors identify stimulus size within the distribution as shown in Figure 3.16.

Average firing rate differs in measurement and reproduction. The majority of cells showed a mean firing at different rates during measurement and reproduction. A higher mean discharge rate in measurement vs. reproduction was present as well as a lower mean discharge rate in measurement than in reproduction phase. Various types of activity combinations in measurement and reproduction were observed within this cell type due to high diversity: cells with non-monotonic activity in measurement and a modulated activity profile during reproduction and vice versa (Figure 3.16) Also, non-monotonic, or monotonic activity to different extents in both, measurement and reproduction were present (Figure 3.17). Within this population, a subset of neurons showed differentiated activity by the size of the presented stimulus.

Stimulus encoding during measurement phase. Although a vast number of observed activity patterns during measurement phase did reflect a uniform activity profile for the tested stimulus intervals, a subpopulation of cells, which adapted their firing according to the size of the presented stimulus, was identified. Here, two types of activity adaptations were observed: 1) The firing rate adapted to stimulus size over the entire measurement phase (Figure 3.18a and Figure 3.18b), and activity terminated at equal discharge rate levels for all stimuli. 2) The overall activity pattern was congruent for the individual stimulus sizes, but terminated at different levels of discharge rate towards the end of the measurement phase, and thereby represented stimulus size (Figure 3.18c and Figure 3.18d).

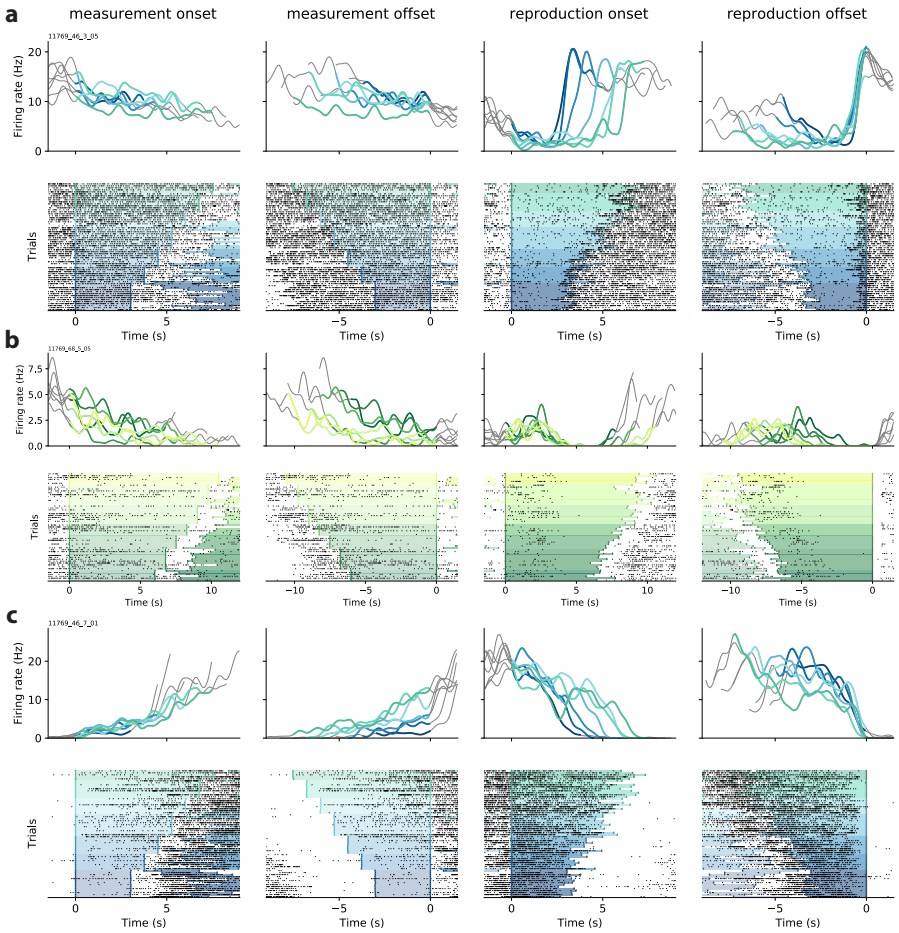

Figure 3.18: Stimulus integration during measurement phase. Spike raster plots and PSTHs (σ = 100 ms) are shown for mPFC example neurons, recorded for stimulus distribution A (a and c) and B (b). Cells integrated the length of the presented stimulus by adapting the intensity of their firing to the presented stimulus size. The activity was adapted over the entire measurement phase and terminated with converging activity profiles towards the end of the measurement phase (a and b). Stimulus size was represented by an overall congruent activity for the individual stimuli, but the discharge rate adapted to the stimulus size towards the end of the measurement phase (c). Figure conventions are as depicted in Figure 3.16.

3.2.3-II. Modulated activity in reproduction phase

Temporally fixed activity in reproduction. A particular subset of cells exhibited firing at a fixed time point throughout the reproduction phase. This activity pattern was reflected by either one single peak right at the beginning of reproduction, or represented by a single peak right at the beginning of reproduction, followed by a second smaller peak a few seconds after (Figure 3.19). The width and height, as well as the center of the second peak, varied in the found examples. The activity profile did not show any adaptations to stimulus size, e.g., no adaptation of the mean firing rate to stimulus size, nor was the time course of the activity pattern compressed or stretched. This activity pattern was observed in both tested stimulus ranges A and B. However, this activity profile was only present in reproduction but not in measurement.

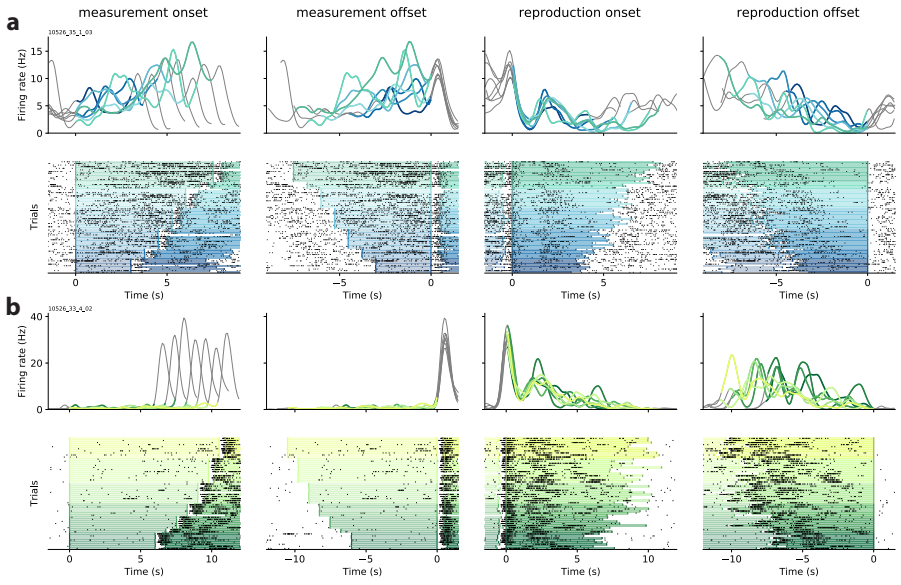

Figure 3.19: Examples of individual neurons exhibiting a temporally fixed activity. Spike raster plots and PSTHs (σ = 100 ms) are shown for mPFC example neurons, recorded during interval timing in stimulus distribution A (a) and B (b). Colors identify stimulus size within the distribution (cf. Figure 3.14a and Figure 3.14b). Figure conventions are as depicted in Figure 3.16.

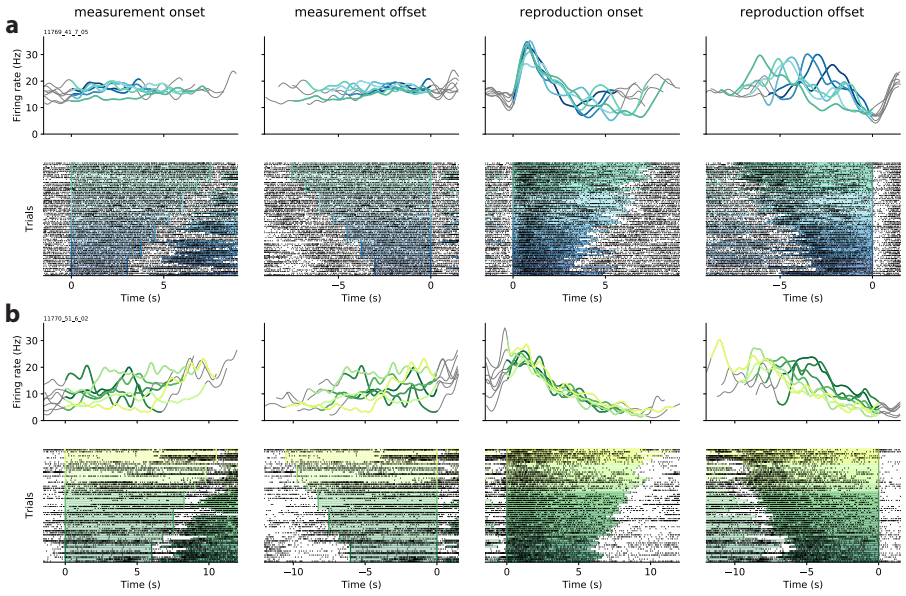

Figure 3.20: Examples of individual neurons responding with monotonic decreasing activity during reproduction. Spike raster plots and PSTHs (σ = 100 ms) are shown for mPFC example neurons, recorded during interval timing, tested in stimulus distribution A (a) and B (b). Gradually decreased activity profile resulted in a ramp-like PSTH, which span the entire reproduction phase (b) or only fractions of it (a). Colors identify stimulus size within the tested distribution (cf. Figure 3.14a and Figure 3.14b). Figure conventions are as depicted in Figure 3.16.

Ramping activity. The most frequently observed activity profile during reproduction was a monotonic response pattern, in which activity gradually increased or decreased over time. These ramps occurred in a multi-faceted fashion, e.g., appeared at the beginning, or the end of reproduction, and also could span the entire reproduction phase (Figure 3.20b), or only fractions of it (Figure 3.20a). Although this type of activity pattern was most abundant in reproduction phase, it was also observed in measurement phase (Figure 3.18d). Here, the ramping effect was rarely as strong as in reproduction and was hence described as monotonic activity in contrast. Other cells exhibited ramp-like activity and responded with an extraordinary feature. They adapted the time course of their response profile to the length of the stimulus or, as seen during

measurement phase, modulated their firing activity according to stimulus size.

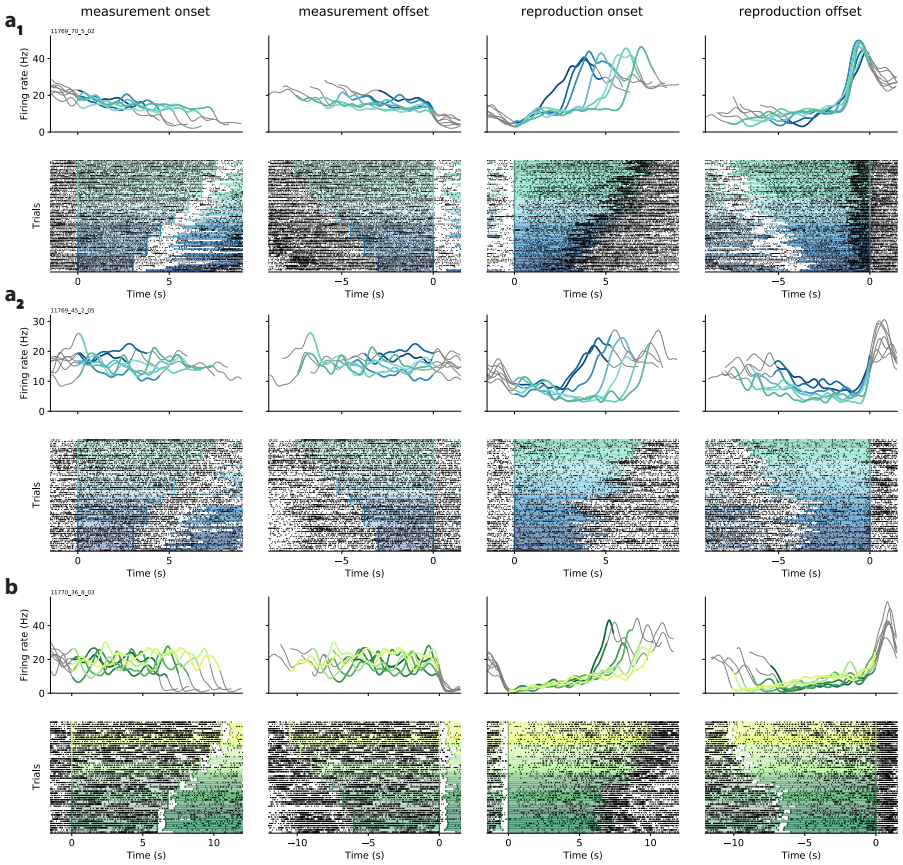

Figure 3.21: Representative neurons exhibiting scaled activity profiles dependent on stimulus size. Spike raster plots and PSTHs (σ = 100 ms) are shown for mPFC example neurons, recorded during interval timing, tested in stimulus distribution A (a_1 and a_2) and B (b). Cells changed the time course of their firing pattern, which affects the speed of the up-ramping activity towards the end of the reproduction phase. The build-up rate correlated with stimulus size. Colors identify stimulus size within the tested distribution (cf. Figure 3.14a and Figure 3.14b). Figure conventions are as shown in Figure 3.16.

Stimulus-dependent integration in reproduction. A selected response type found in the ramping profiles adapted the time course of their activity pattern to the stimulus's length, i.e., by scaling their response. This feature was represented by the activity profile being stretched or compressed for the individual tested stimulus intervals. At the end of the reproduction phase, activity strength was comparably high for all tested stimulus intervals tested in the stimulus distribution. This temporal scaling resulted in a change of time to establish the ramp and thereby an adapted steepness (slope) of the ramp (Figure 3.21). Follow-up analysis should show whether the build-up of the ramp correlated with stimulus size. As a second extraordinary response type during reproduction, cells continuously represented stimulus size with a graded magnitude of neural activity, reflected by the average firing rate being correlated with stimulus size. Positively correlated relationships were found (Figure 3.22), as well as firing rates negatively correlated with stimulus size.

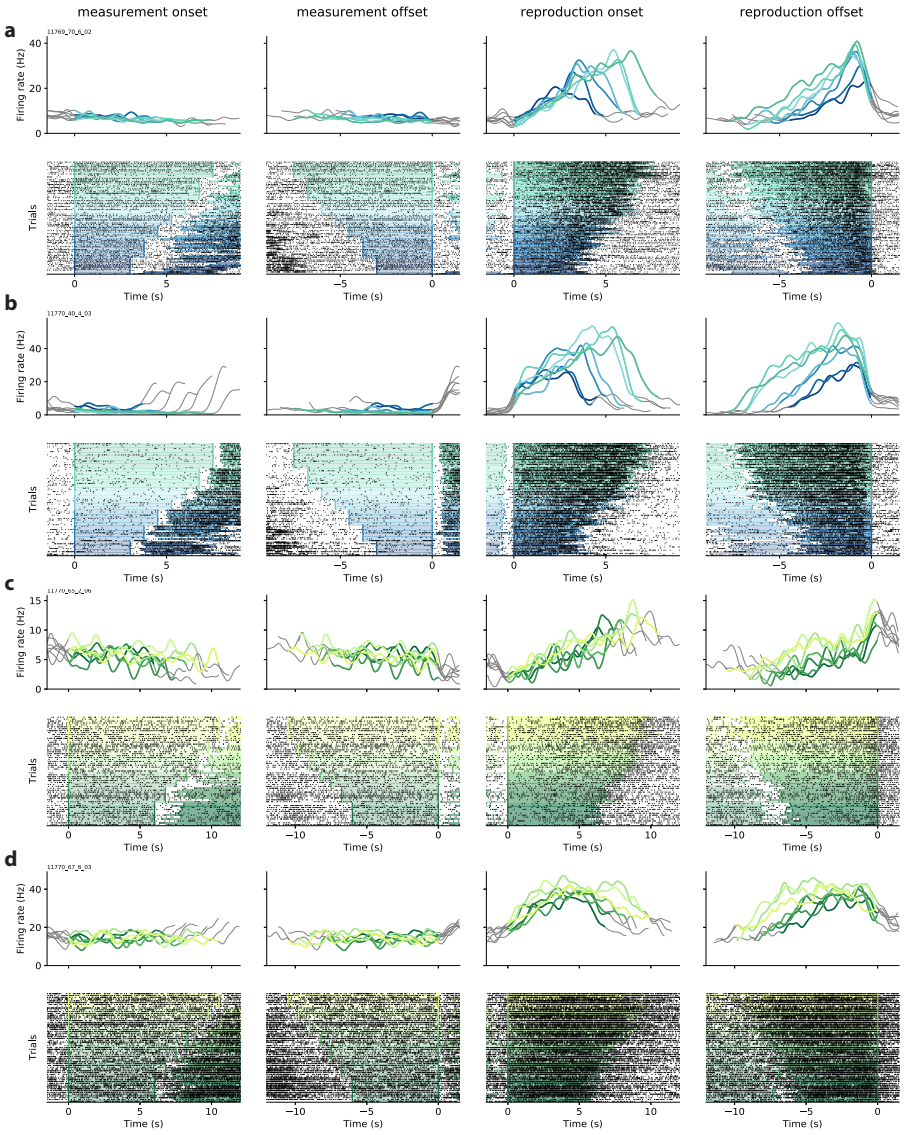

Figure 3.22: Integration of stimulus size during reproduction phase. Spike raster plots and PSTHs (σ = 100 ms) are shown for mPFC example neurons, recorded during interval timing, tested in stimulus distribution A (a and b) and B (c and d). Cells integrated the length of the presented stimuli by changing the magnitude of firing relative to stimulus size over the entire reproduction phase, which resulted in different magnitudes of firing at the end of the response. Small time stimuli were encoded by lower firing rates, in contrast to large stimuli, represented with high firing rates, and likewise vice versa. Figure conventions are as shown in Figure 3.16.

3.2.3-III. Reward encoding during ITI

Although previously described activity profiles might be the source which lead to success or not by reflecting the underlying process of timing, neural information conveyed during ITI might give rise to the intrinsic evaluation of performance and how reward is encoded.

mPFC neurons modulate activity during ITI. A subset of cells presented firing rate modulations and adaptations of activity patterns, possibly reflecting the reward's meaning. Some cells did show no activity at all. Thus, they did not contribute to the encoding of reward. Other cells, in contrast, did modulate their activity towards the evaluation phase, e.g., drastically increased their firing at the transition of the reproduction phase to ITI (Figure 3.23a and Figure 3.23c, or increased their firing during the evaluation phase (Figure 3.23b). Nevertheless, a steady activity profile for all tested stimuli and a relative to stimulus duration gradually adapted activity profile was observed.

3.2.4 *Neural correlates of behavior*

Multiple firing rate combinations during measurement phase and reproduction phase were present in the recorded cell population. Nevertheless, the combinations *per se* did not give information about if, and to which extent, the activity might be correlated with timing processes or correlates with behavioral parameters. In order to investigate this issue, activity profiles of the subpopulations were assessed. To evaluate the activity differences, a modulation index (MI) was calculated (see section 2.6.6). The modulation index identified the cell populations, responding with pronounced activity in either measurement or reproduction. Additionally, with the help of the modulation index, modulated activity in each of the phases was detected.

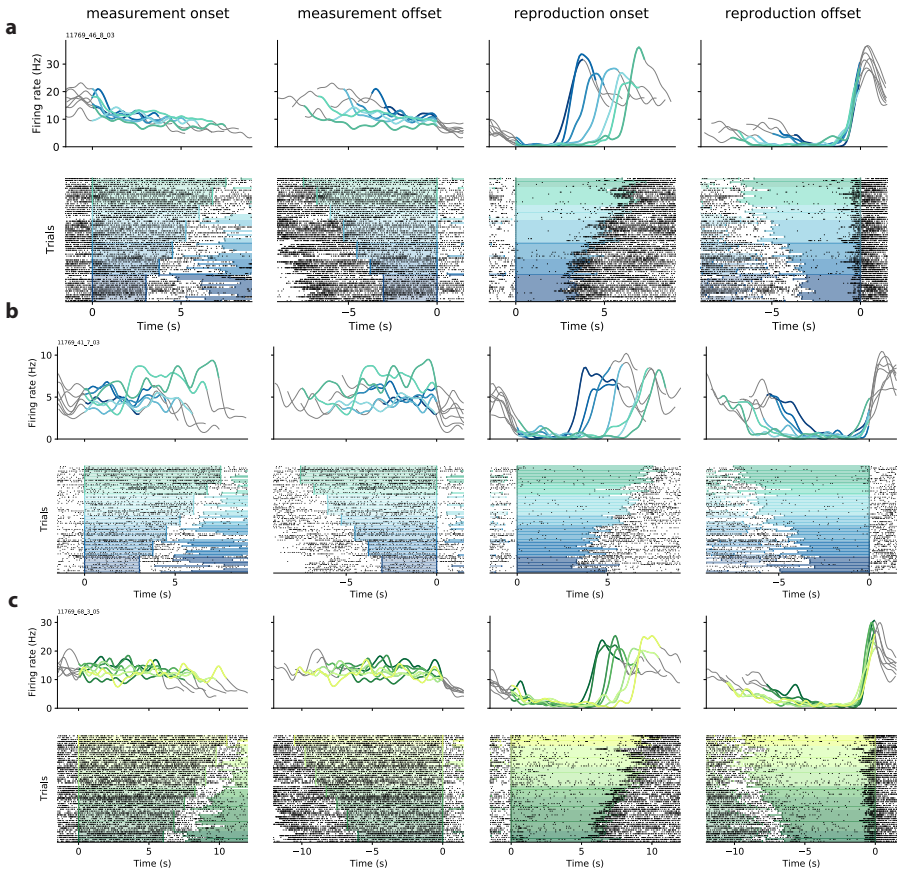

Figure 3.23: Encoding of reward phase. Spike raster plots and PSTHs (σ = 100 ms) are shown for mPFC example neurons, recorded in test sessions of stimulus distribution A (a and b) and B (c). Cells increased activity towards the onset of ITI (depicted right-side to reproduction offset), whereas activity during reproduction was clearly reduced. Change in activity appeared towards reproduction offset and excludes activity solely based on noise from eating. Figure conventions are as shown in Figure 3.16.

Therefore, the two non-overlapping periods encompassing the first third and the last third of the stimulus-wise PSTH were compared. The firing rate difference was tested using a paired t-test or Wilcoxon-test. Cells, yielding test statistics of $p < 0.05$, were considered to be significantly modulated during the time estimation period. The resulting MI was used to classify the modulation profile (monotonic increase (+1), monotonic decrease (-1), or nonmonotonic changes (0)) during the time-estimation periods.

Significantly different firing in measurement phase compared to reproduction phase was found in almost two-thirds of the cells (n=2342, 57%) (Figure 3.24, row c). Approximately the same portion of cells showed higher average firing in measurement phase than in reproduction phase and vice versa (Figure 3.24c_2). 25% of this cell population exhibited monotonic activity in reproduction, and 19% modulated their activity monotonically during measurement (Figure 3.24b_3). Fewer cells, i.e., only 22% (n = 904) showed significant differences in activity when the last and the first third of measurement phase were compared (Figure 3.24, row b). The histogram of the modulation indices indicates, that higher activity was preferably observed towards the end of the measurement phase (Figure 3.24b_2). 16% and 17% of the measurement-active subpopulation responded with monotonic activity (Figure 3.24b_3). The majority of the recorded cells (70%, n = 2876) showed modulated activity during reproduction (Figure 3.24, row a). Of these, increased activity was observed towards the end of the reproduction phase compared to reproduction onset (Figure 3.24a_2). Comparably, only a small fraction of 18% and 25% responded with monotonic activity during the reproduction, either at the start or the end of the phase (Figure 3.24a_3).

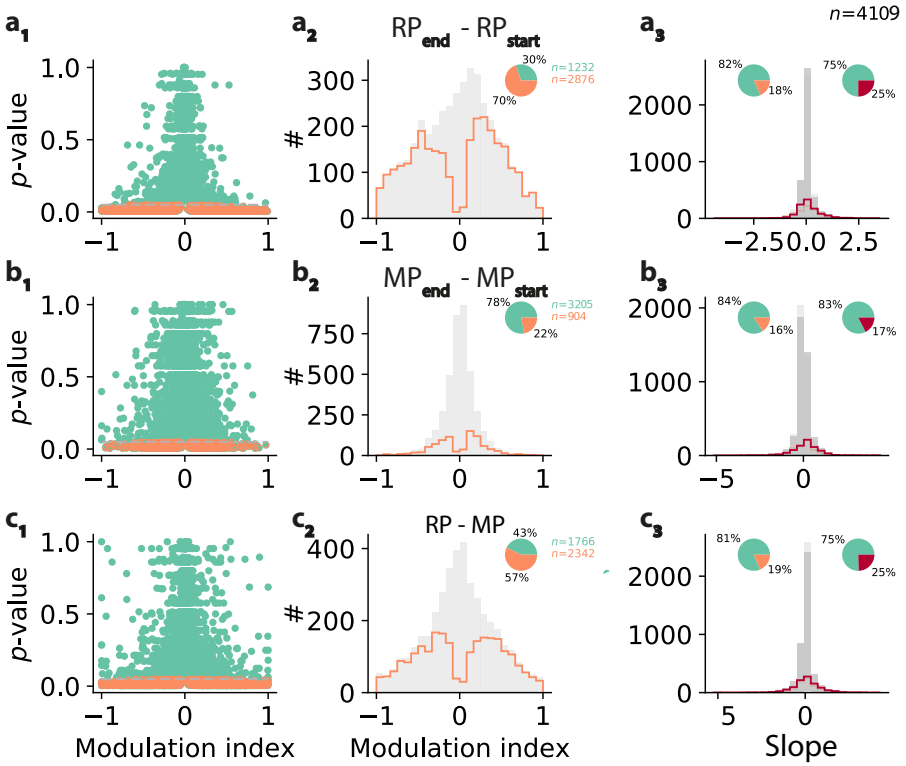

Figure 3.24: Neuronal activity during measurement phase and reproduction phase. The majority of cells showed modulated activity in reproduction phase (RP) (a_1). Here 70% (n = 2876) of all recorded cells significantly modulated their activity during reproduction (a_2). However, only a small fraction of 18% and 25% exhibited monotonic activity at the beginning and the end of reproduction phase (a_3). Only 22% (n = 904) showed significant differences (b_1 and b_2) in activity when the last and first third of measurement phase (MP) were compared. Monotonic activity was visible in 16% and 17% of the subpopulation modulating activity in measurement phase (b_3). More than half of the cells (n=2342, 57%) exhibited significantly different firing in measurement phase compared to reproduction phase (c_1 and c_2). The portion of cells exhibiting higher firing rates in reproduction (MI: 0 to 1) phase was comparably similar to those cells which responded with enhanced activity in measurement phase (MI: -1 to 0). 25% of this cell population exhibited monotonic activity in reproduction phase, and 19% modulated their activity monotonically during measurement phase (c_3).

Integration of stimulus size. In the recorded population, some cells adapted their activity during the time estimation period and thereby integrated the stimulus size in two different manners: a) Single cells integrated the size of the presented stimulus by adapting the overall magnitude of firing during the reproduction phase. b) Others adapted the time course of their activity profile during reproduction to the size of the presented stimulus. These two different kinds of stimulus size integration during reproduction were further analyzed in the upcoming subsection. A detailed analysis should verify the hypothesis that cells encode stimulus time by their firing magnitude. Therefore, cells responding with ramping activity during reproduction phase were sorted, and the obtained subpopulation split into up-ramping cells and down-ramping cells.

I found that 1456 (35.42%) neurons of the recorded population exhibited higher average firing rates for small stimulus intervals in comparison to large stimuli, which were represented with a low mean discharge rate (Pearson's r = -0.103, p = 0.002; Figure 3.25a). Another subset of 1692 cells (41.17%), responding in a positively correlated manner for stimulus size and average firing rate, was identified. Here, the average discharge rate scaled positively with the represented time interval (Pearson's r = 0.098, p = 0.002, Figure 3.25c). However, significance was not detected for cells tested in stimulus distribution B, although they encoded the stimulus size in the same fashion (decreased: Pearson's r = -0.067, p = 0.127; Figure 3.25b and increased: Pearson's r = 0.065, p = 0.103, failed to reach significance; Figure 3.25d). In contrast, during measurement, this stimulus-related activity was less observed. Here only 749 (18.22%) responded with decreased firing to increasing stimulus size, and only 805 cells (19.53%) increased their firing with increasing stimulus size, accordingly.

Further, only up-ramping cells with modulated "build-up rate" property, i.e., adapted speed of the up-ramping activity to stimulus size, were analyzed. The build-up rate was calculated as the stimulus-wise PSTH signal divided by the corresponding PSTH time, thereby giving information about the increase's slope. The slope was calculated by fitting a linear least-squares regression to the PSTHs of each stimulus size and their

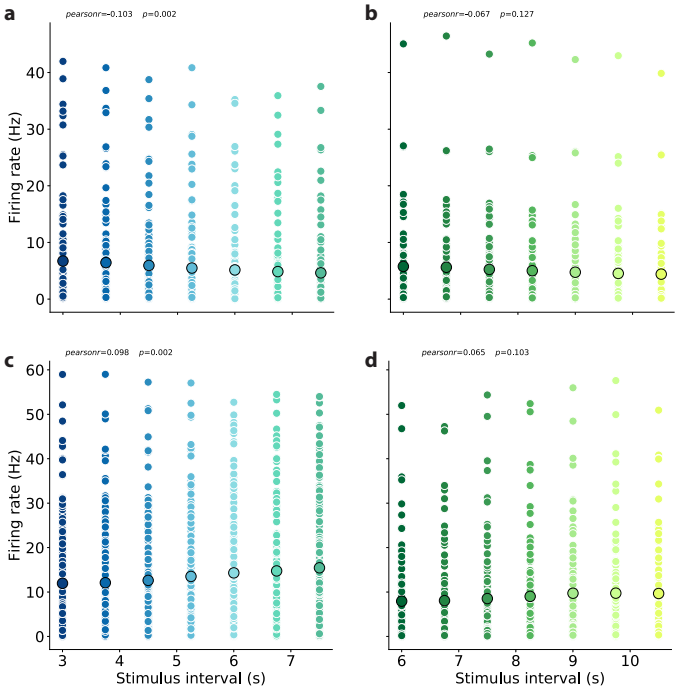

Figure 3.25: Stimulus size is encoded in average firing rate. Cells showed significant differences in firing rate for the tested stimulus intervals. A negative (a and b) as well as a positive (c and d) relationship of average firing rate with stimulus size was observed. The magnitude of the average firing rate scaled with presented stimulus size: small stimuli were encoded with low average firing compared to large stimulus intervals, especially for the tested stimuli presented in distribution A (Pearson's r = 0.098, p = 0.002). The positive correlation for tested values with the firing rate in stimulus distribution B did not reach significance (Pearson's r = 0.065, p = 0.103). Equivalently, the negative correlation of average firing rate with stimulus intervals, tested in the distributions A and B, was similarly strong pronounced (A: Pearson's r = -0.103, p = 0.002; B: Pearson's r = 0.067, p = 0.127, failed to reach significance.

corresponding average firing rates. Cells were assigned to have the build-up rate property if the Spearman's coefficient was significant for the correlation of stimulus size and its average firing rate.

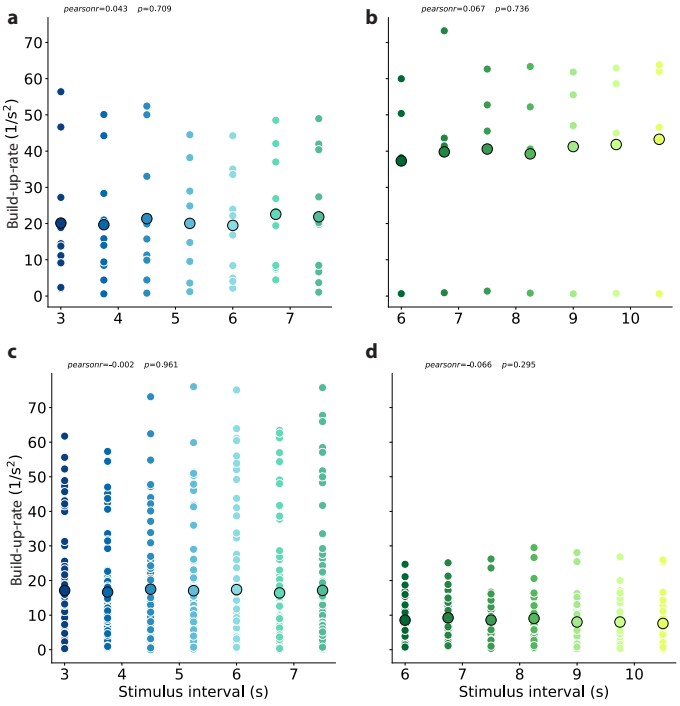

Figure 3.26: Correlation of firing rate with ramping speed. The speed of ramping activity strongly encoded the size of the tested stimulus intervals for single cells (data not shown). This effect reduced when observed on a populational level. Two types of ramping speed adaptation of were found in the population. Stimulus size was either represented with increased ramping speed for long intervals (a and b) (A: Pearson's r = 0.043, p = 0.709; B: Pearson's r = 0.067, p = 0.736) or encoded by reduced ramping speed for long stimulus intervals (c and d) (A: Pearson's r = -0.002, p = 0.961; B: Pearson's r = -0.066, p = 0.295).

Analogously to the adaptation of firing rate to stimulus size, two different response patterns regarding the speed of the up-ramping activity for increasing stimulus size, were found. A minority of 105 cells (2,55%) did increase the speed of the ramp with increasing stimulus size. This observation was not significant in none of the two tested stimulus distributions (A: Pearson's r = 0.043, p = 0.709; B: Pearson's r = 0.067, p = 0.736; Figure 3.26a and Figure 3.26b). A small portion of 791 cells (n = 19,24%) decreasing the speed of their ramp up activity with increasing stimulus size was detected. However, effects were rather small (A: Pearson's r = -0.002, p = 0.961; B: Pearson's r

= -0.066, p = 0.295, Figure 3.26c and Figure 3.26d) when the total number of build-up-modulated cells was tested. Single-cell examples did impressively represented this adaptation to the speed of the ramp (see Figure 3.21).

Cells with the build-up property, exhibited a uniform activity pattern, for the different tested time stimuli. The activity profiles only differed by the signal traces being stretched or compressed on the time axis. Further analysis quantified the temporal scaling property by the best temporal scaling factor. The best scaling factor was calculated as the scaling factor, given the minimum difference after scaling between the smallest presented stimulus interval and the consecutive stimuli. Therefore, the average PSTH of each consecutive stimulus size using scaling factors from 0.2 to 1.25, with boundaries defined by sample length, was linearly compressed (Figure 3.27a and Figure 3.27b). The MSE of each stimulus-wise PSTH to the PSTH of the smallest presented stimulus was assessed using the following equation:

$$\mathrm{MSE}(f) = \frac{1}{n}\sum_{n}^{i=1}[\mathrm{PSTH}_{\mathrm{minStim}}(t_i) - \mathrm{PSTH}_{\mathrm{Stim}}(f * t_i)]^2 \qquad (3.1)$$

The scaling factor f, which resulted in the minimum MSE, was taken as the best scaling factor (Figure 3.27a and Figure 3.27b). Cells with a significant correlation of scaling with stimulus size were included in analysis.

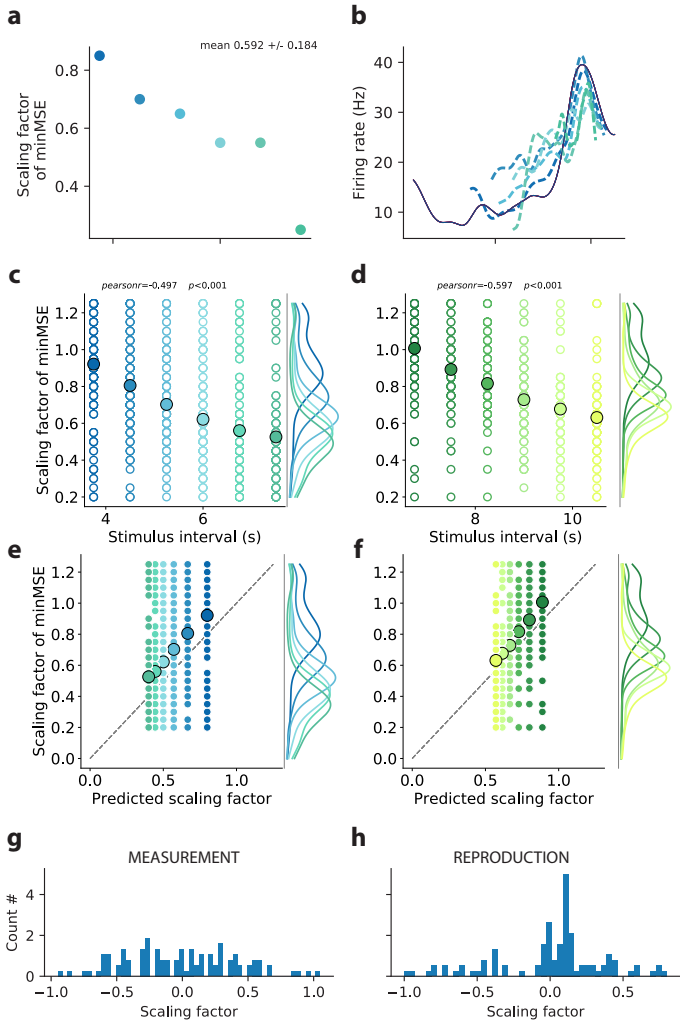

Figure 3.27: Temporal scaling represents stimulus size. The best scaling factor for each presented stimulus size (a) was determined by calculating the minimum MSE for temporally scaled PSTH signals (b), with factors of 0.2 - 1.25. The best scaling factors decreased with stimulus size (c and d) and complied with predicted scaling factors obtained from the calculated ratios of minimum and tested stimulus intervals (e and f). Scaling preferably occurred towards the end of the reproduction phase (h), but not in measurement phase (h). Color conventions are as shown in Figure 3.14a and Figure 3.14b.

A total of 2340 cells (56.9%) showed significant temporal scaling of their activity profile during the timing task. The scaling factors significantly decreased for large stimulus intervals in

both tested stimulus distributions (stimulus range A: Pearson's r = -0.497, $p < 0.001$; stimulus range B: Pearson's r: -0.597, $p < 0.001$; Figure 3.27c and Figure 3.27d). However, the averaged best scaling factors for each time stimulus in distribution A and B did not differ significantly ($t = -1.21$, $p = 0.25$). Actual scaling factors were correlated with the predicted scaling factors, calculated from the ratio of the smallest stimulus size and the consecutive large stimuli, each, to test if scaling factors follow prediction. The data did not show a perfectly veridical match. Instead, actual scaling factors were larger than prediction. Deviation from predicted values was small, and the distribution of scaling factors peaked between 0.4 and 0.8 for stimulus distribution A and peaked between 0.6 to 0.9 for stimulus distribution B. Despite the deviation, the results obtained corresponded to the prediction in either stimulus distribution (Figure 3.27e and Figure 3.27f). Deviation from prediction was comparably smaller for stimulus distribution B than for stimulus distribution A. To compare scaling in measurement phase and reproduction phase, I looked at the scaling factors in both time-related phases, with alignments on phase onset and phase offset. Scaling was preferably found in reproduction phase (Figure 3.27g), than in measurement phase (Figure 3.27h). Additionally, the scaling appeared more pronounced towards the end, in both phases (Figure 3.27h).

Neural correlates of reward. To gain insight into how the cells' population activity reflected and represented the outcome of the animal's decisions, i.e., the interaction with the environment, I focused on the time after the reproduction. I investigated if the quality of the response, i.e., being rewarded or not, considering tested stimulus size, was correlated with the neural activity. To investigate this issue, I focused on cells that showed activity during ITI compared to reproduction phase. The following analyses were hence performed on the 3.5 seconds time period from the end of the reproduction phase till right before the start of the next trial. Only cells with an overall firing rate > 0.3 Hz were included in analysis. As a second refinement, only cells with a mean firing rate > 0.3 Hz, specifically during ITI (n = 3610; 87.67%), were subject to analysis. I examined, whether precision and accuracy of response were encoded

during ITI or reproduction. Therefore, the correlation of firing rate and behavioral outputs of time estimation of individual trials was assessed in quantitative analysis. For each animal, the session-wise correlation of firing rate with the behavioral response-time parameter BIAS was evaluated. The average firing rate of each trial during ITI was extracted and related to the behavioral parameter's deviation value from the mean value per tested stimulus size. Thereby, the obtained results were evaluated considering the "internal settings" of the animal during this session, i.e., the attentional state, motivation, or prior knowledge of the tested stimulus distribution. However, a negative or positive bias, and also the strength of it, does not give information about the time reproduction's success. The success of performance, i.e., the encoding of time reproduction success, was evaluated by assessing the neural activity during ITI, further subdivided by rewarded ("hits") and non-rewarded ("non-hits") trials.

The results show that a wide range of firing magnitudes applied for small biases, whereas the variety of activity magnitudes decreased with the increasing values of absolute bias. This observation was captured by the triangular distribution of the data shown in Figure 3.28. The data showed a slight right-sided inclined asymmetry, indicating that overestimation, resulting in a negative value for the mean bias of stimulus s minus the actual bias of the trial, is represented with lower firing, in contrast to underestimation (Figure 3.28a and Figure 3.28c). The subdivided BIAS, sorted by "hits" and "nonhits" revealed, that regardless of over- or underestimation, the reward modality was encoded and processed with a higher firing rate for "hits", in contrast to "nonhits" (Figure 3.28b and Figure 3.28d). However, activity during ITI was not significantly correlated with stimulus size, neither for "hits", nor for "nonhits" ($hits_A$: Spearman's ρ = 0.29, p = 0.53; $hits_B$: Spearman's ρ = -0.68, p = 0.09; $nonhits_A$: Spearman's ρ = -0.28, p = 0.53; $nonhits_B$: Spearman's ρ = -0.14, p = 0.76).

The session-wise standard deviation for each presented stimulus interval was correlated with the cells' average firing to check if the scalar property of timing was represented in the neuronal activity. Additionally, I investigated if neuronal firing reflected

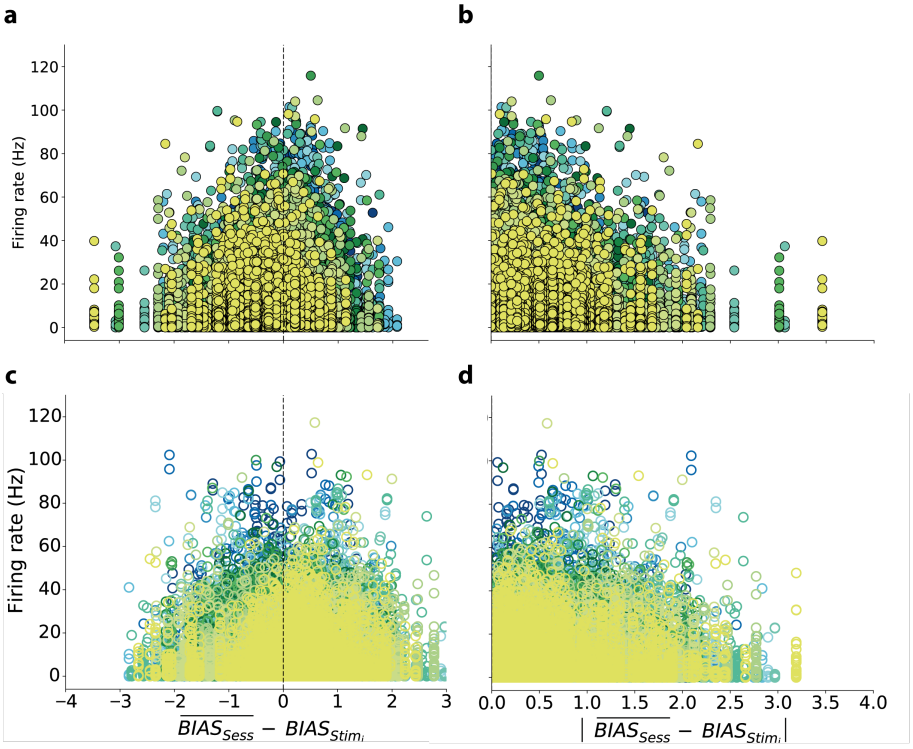

Figure 3.28: Encoding of performance during ITI. Small biases were encoded with a wide range of activity magnitudes, whereas the variety was reduced for large biases. Higher activity was preferably exhibited for small biases (a and c). High overall activity was observed for "hits" (a and b) compared to "nonhits"(c and d). Overestimation, in contrast to underestimation, was represented with low firing rates, as depicted by the right-side inclined asymmetry of the data for "hits" and "nonhits".

regression effects. Therefore, the $\sqrt{\overline{BIAS^2}}$ for each presented stimulus was calculated and the resulting data analyzed for correlation with the average firing rate. The parameters SD and $\sqrt{\overline{BIAS^2}}$ were calculated in relation to the sessions' mean of the respective parameter for each animal and session.

The assessed parameter of $\sqrt{\overline{BIAS^2}}$ drew a similar picture as the assessment of the BIAS for all stimuli . A huge variety of firing magnitude was observed for small values of $\sqrt{\overline{BIAS^2}}$ in comparison to large ones (Figure 3.29a and Figure 3.29b). The variety of firing magnitudes decreased with

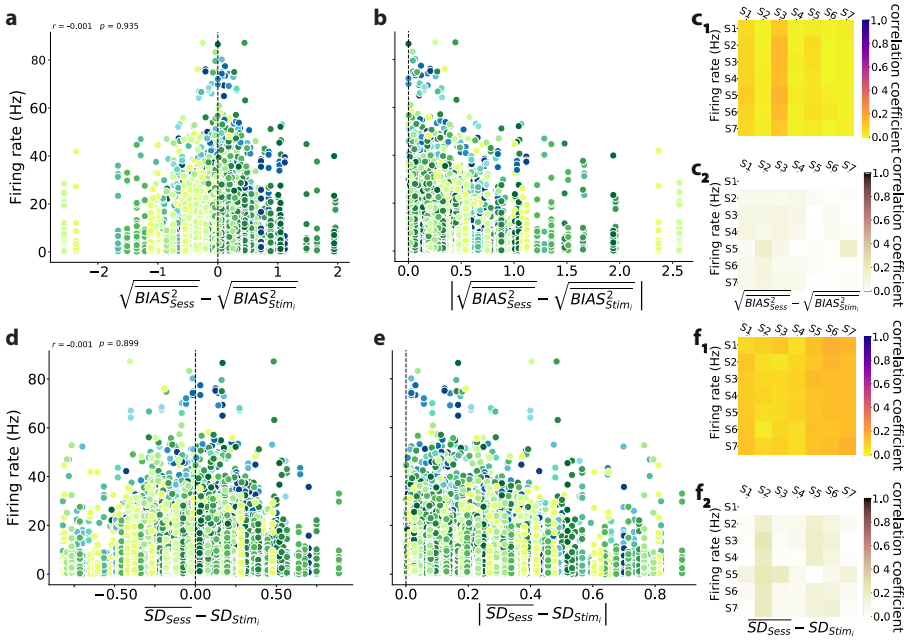

Figure 3.29: Regression strength but not SD is encoded during ITI. Small activity magnitudes potentially represented strong regression compared to weak regression, which in contrast, was encoded with a wide range of activity magnitudes (a and b). Stimulus-wise firing rate was correlated with the stimulus-wise absolute behavioral parameter $\sqrt{\overline{\text{BIAS}^2}}$ in stimulus distribution A (c_1) and B (c_2), but had no significant effect. The behavioral parameter SD was analyzed analogously, and likewise did not correlate with activity strength nor correlated with tested stimulus size in stimulus distribution A (f_1) or B (f_2). Instead, preferably higher activity was observed for values matching the referenced session mean (d and e).

increasing $\sqrt{\overline{\text{BIAS}^2}}$. Data evaluation of the parameter $\sqrt{\overline{\text{BIAS}^2}}$, reflected that strong regression was preferably encoded with low activity, whereas weak regression was represented with a vast number of activity magnitudes (Figure 3.29a and Figure 3.29b). The stimulus-wise correlation of activity with $\sqrt{\overline{\text{BIAS}^2}}$ in the tested stimulus distributions did not reveal a significant difference in firing magnitude (Figure 3.29c_1 and Figure 3.29c_2). However, it supports the impression of increased activity for small values of $\sqrt{\overline{\text{BIAS}^2}}$. Quantitative analysis of SD also reflected a triangular distribution of the data (Figure 3.29d). Generally, a small SD, referenced to the session's mean, and

thereby resulting in positive values, as well as a large SD, resulting in negative values, were not specifically encoded by the magnitude of activity (Figure 3.29d). Instead, deviation from the session-wise reference, potentially shaped by internal parameters, was encoded in the magnitude of activity, which was reflected by the accumulation of large activity magnitudes up to 80 Hz (Figure 3.29e.) The correlation of activity magnitude with the strength of SD did not reveal a significant effect for stimulus sizes in stimulus range A and B (Figure 3.29f_1 and Figure 3.29f_2).

4

DISCUSSION

The first goal of this thesis was to establish a time estimation task for physiological recordings in gerbils, which can be used to investigate on the behavioral effects of interval timing. To this end, I developed a production-reproduction procedure (a modified "ready-set-go" timing task) that required retrospective and prospective time estimation. This paradigm could be used in a virtual environment for humans and rodents alike. As a second objective, activity profiles occurring were evaluated and it was analyzed whether estimation performance during the timing task was represented by the neuronal response.

4.1 THE BEHAVIOR OF INTERVAL TIMING

With the present study, I aimed to investigate the characteristic biases namely, regression effect and range effects, in the estimation of the magnitude of temporal stimuli. I used a retrospective-prospective combining behavioral paradigm, in which subjects, first estimated and then reproduced the elapsed time, while moving in a virtual environment. Experiments were performed with six human adults and seven rodents. As a central finding, regression effects were found for gerbils and humans. Both groups showed stronger regression effects for large stimulus ranges compared to small stimulus ranges. However, the overall differences were rather small. The gerbil's reproduced intervals showed greater variability than humans, and therefore the increased regression effect appeared to be more pronounced with larger stimulus sizes in

humans compared to gerbils. The animals showed increased heterogeneity in reproductive performance, so the effect of regression on the mean was not as pronounced. Nevertheless, the average performance of the animals was quite high overall. The weak regression effect in large magnitudes might have appeared as a phenomenon, resulting from "over-training". Ellard et al. (1984) and also Legg and Lambert (1990) reported the absence of regression to the mean when animals were trained over a long period of time with a large number of training sessions. Whereas the behavior of the rats showed regression to the mean at the beginning of the training for a gap jump task with different gap sizes. The weak regression effect in the human data possibly resulted from pooling the populational data and thereby canceled out individual differences between the tested distributions. Because half of the people performed almost perfectly with appropriate time estimation and showed an exact time estimate. Whereas in contrast, the performance of the participants included in the other half was rather weak. Modality effects and individual differences are well known in literature of interval timing (Shi et al., 2013). Cicchini et al. (2012) showed that percussionists precisely reproduce temporal intervals and display feeble regression effects in contrast to normal subjects. Indeed, one of the human participants also played a musical instrument and responded with veridical time estimation. Internal and external factors influence the ability to discriminate physical stimuli. An internal factor is quantified by the so-called signal-to-noise ratio (SNR), which inversely corresponds to the Weber fraction. It was shown that Weber fractions depend on the stimulus modality and are subject-specific (Kautzky and Thurley, 2016).

4.1.1 *Advantage of using virtual reality*

Since the first reports of successful application of VR for rodents (Hoelscher et al., 2005; Dombeck et al., 2007), VR setups became very popular. This popularity is primarily due to the fact that VR setups enable the use of advanced recording techniques in

behaving animals, such as intracellular recordings (Harvey et al., 2009; Domnisoru et al., 2013; Haas et al., 2019), or optical imaging of neuronal populations (Harvey et al., 2012; Keller et al., 2012). The behavioral paradigms in use, however, are usually very limited. Time estimation and time perception are generally investigated by using peak-procedures, forced choice tasks, or symbolic matching-to-sample tasks (Jazayeri and Shadlen, 2015). Nevertheless, some studies already used paradigms implemented in VR, e.g. two-alternative-forced choice tasks in rodents (Harvey et al., 2012; Thurley et al., 2014; Kautzky and Thurley, 2016). These implemented paradigms have been used to measure psychometric functions of time and other stimulus sizes. So far, time estimates in the supra-second time range of rodents have only been reported bases of ordinal judgments, but not on continuous scales (Cordes and Meck, 2014). My study was particularly characterized by the fact that it successfully implemented a time estimation task on a continuous scale, in which rodents learned rule-based responding, and applied the learned on a broad range of temporal durations in VR.

4.1.2 *Context and range effect*

The results of the conducted experiments with humans and animals showed that the same stimuli tested led, on average, to different responses when embedded in different, but overlapping stimulus distributions. Estimates of stimuli thus depend on the stimulus context, or the environment's statistics (Jazayeri and Shadlen, 2010). The occurrence of context-dependency has been shown in experiments probing interval timing in the sub-second range (Jazayeri and Shadlen, 2010) and experiments testing for distance estimation (Petzschner and Glasauer, 2011; Petzschner et al., 2012) in humans. Jazayeri and Shadlen (2015) showed that regression effects exist in animals, but not that the central tendency toward the mean increases with stimulus magnitude. Especially overlapping stimulus ranges, the phenomenon of increasing regression quantifies the range effect. In my study, I could

show that the range effect is present in time estimation of gerbils and humans. The mean response values for the tested stimuli were always larger when presented in the large stimulus distribution compared to being presented in the short one. The stimulus' pair-wise comparison of the signed bias in the tested stimulus distributions revealed an increased absolute bias for the stimuli embedded in the large than in the small stimulus distribution. This finding indicates that the same durations were preferably underestimated if they represented the comparatively large stimuli within the distribution. Whereas they were overestimated if they were considered small stimuli within the range tested. This finding emphasizes that magnitude estimates are not solely influenced by internal factors. These results demonstrate how stimulus statistics influence magnitude judgments, and hence how subjects adapt to the environment. In section 1.5, I raised the question, how the boundary for perceptual categories in time estimation might be classified. The results of the analysis on context-dependency suggest that there is an adaptive instead of a fixed boundary. On the one hand, the same stimuli were underestimated when embedded in a small stimulus range, but on the other hand, were overestimated when presented in a large stimulus range. This finding indicates that the perceptual categories applied for time estimation follow the Bayesian framework. However, the further analysis did reveal that in most cases, it was not the mean of the tested stimulus distribution, which turned out to be the transition point from over- to underestimation. In some animals, there was no transition at all. However, some gerbil subjects underestimated all stimuli, especially in the largest stimulus range C. Again, also here the Bayesian framework comes into play: One hypothesis could be, that the animal's prior was set such, that all stimuli presented in the largest stimulus range were underestimated because the "mean in mind" was smaller as the true mean for the tested stimulus range. In this case, the consecutive trials within the single sessions or even across all sessions for this test distribution were not sufficient to update the prior ('mean in mind') to the current stimulus range. Another hypothesis could be that the animal had an entirely updated prior but operated on a minimum-cost - maximum profit strategy: "How much can I risk but still save energy, to get maximum reward under known

constraints"? The overall underestimation could also be partly driven by error minimization due to uncertainty and partly by a minimum-cost vs. maximum-profit strategy. Nevertheless, the mathematical mean of the tested stimulus range could not be identified as crux of the matter. The transition point from overestimation to underestimation was different not only across the individual subjects of one species but also across the several sessions within one tested stimulus range for each subject.

4.1.3 *Bayesian integration of temporal judgments*

Statisticians have known for centuries that Bayesian integration is the optimal strategy for handling uncertain information. When we are uncertain about something, we automatically rely on our prior experiences to optimize behavior (Jazayeri and Shadlen, 2010; Petzschner and Glasauer, 2011; Cicchini et al., 2012; Petzschner et al., 2015). Even subjects that can reliably perform at magnitude estimation show remaining errors. These are due to uncertainties from the stimulus statistics that can not be controlled by the subject. However, these statistics define the lower limit of error, represented in the subject's responses. The stimulus statistics can be quantified by the ratio between the mean and the variance of the stimulus distribution and can be classified as external uncertainty e.g., stimulus context. The regression effect counteracts this uncertainty by treating different stimuli similar to the mean of the tested stimulus distribution. According to Weber-Fechner law, the decreased discriminability for more difficult magnitude estimation tasks will lead to stronger regression effects (Teghtsoonian and Teghtsoonian, 1978; Petzschner et al., 2015). Therefore, systematic over- and underestimation are strategic tools to minimize reproduction errors and, hence, optimize judgments. Recent studies on time estimation and distance estimation reported that humans have knowledge of this uncertainty inherent in their measurements, and use mechanisms to reduce the average error (Jazayeri and Shadlen, 2010; Petzschner and Glasauer, 2011; Cicchini et al., 2012). With this study, I

provide evidence that this problem is not exclusively present in human or primate species but also rodent species. The relation between the present work and the Bayesian approaches is not investigated in detail. Nevertheless, it follows the architecture of the Bayesian framework, and also, the results are in line with Bayesian assumptions. The measurement phase results in an internal estimate of a stimulus drawn from a likelihood distribution. The reproduction process gives a posterior estimate, the reproduced stimulus, drawn from the distribution. The obtained results are in line with the Bayesian findings: (i) Scalar variability implies decreased reliability and increased uncertainty of measurements of relatively longer temporal intervals. Scalar variability was visible for both rodents and humans. (ii) Estimates tend towards the mean (regression effect). (iii) This effect scales with stimulus size and also is dependent on the stimulus context (range effect).

4.1.4 *Influence of movement parameters*

Analyzing the influence of movement parameters on reproduction performance revealed that animals did not use any modulation of physical running speed, the starting latency, or a directional running pattern to solve the task and precisely estimate time intervals. A positive correlation of stimulus interval with path length and a positive correlation of reproduced interval with path length is in nature of the task design. The resulting KDEs, representing the distribution of traveled path length, gave sufficient reason to believe that animals indeed performed time estimation and not distance estimation. This finding was represented by an increased shift of density estimates for reproduced intervals across the tested stimulus distributions, in contrast to the strongly overlapping KDEs, representing the path length traveled. As mentioned above, traveled distance correlated naturally with the size of the tested stimulus, as well as with the magnitude of the tested stimulus distribution. However, by applying virtual gain factors, this correlation was effectively reduced. Additionally, the applied gains hindered distance estimation as the animals

could not infer traveled distance from steps taken. Also, the starting latencies naturally increased with the stimulus size and distribution's magnitude. Both species produced comparable data distributions, which oppose the theory that either group used a specific strategy e.g., adapting the running response related to the starting latency, to solve the task other than time estimation or to improve estimation performance. Thus, both tested groups served as a control group for the respective other because results are strikingly congruent. The possibility that both species yielded strongly similar results as they used the same strategy is eliminated by the different cognitive abilities of the two species. The virtual speed showed a homogeneous distribution across all stimulus ranges, and also for reproduced intervals across all stimulus ranges. This observation indicates, that animals randomly varied their running speed for the applied gain factors as well as for the stimulus presented. All animals used different running speed adaptations: One example animal, ran with a constant running speed for increasing stimulus magnitudes. Others reduced their running speeds for larger magnitudes. As the running response implies physical exhaustion, it is understandable that animals used constant running speeds for all magnitudes or even decreased it for larger ones. So why then increase it for larger magnitudes? From an energy-effort point of view, it seems rather disadvantageous. However, reward expectations might be higher the more time passes, and therefore animals are "enthusiastic" to finish the trial. The behavioral data revealed a negative correlation of gain factors with running speeds, indicating that animals reduced their running speeds. This seems reasonable as the visual impression changed dramatically with the applied gain. The results suggest that animals preferred a constant visual flow, which explains the equally distributed virtual speeds. The running trajectories showed no specific running pattern, like Zick-zack or other geometric patterns, which would help to solve the task. Also, running speeds for distinct sections of the running path within one trial did not reveal significant modulations. Summarizing, animals did not use movement parameter interactions to improve their estimation performance on time intervals nor developed idiosyncratic and stereotypic behavioral strategies unlike it has been reported by Gouvêa et al. (2014).

4.1.5 *The cognitive effort of time perception*

Prospective time estimation is implicit in nature because, for most tasks, the timing aspect is secondary to the real task being performed. Therefore, many studies have used a prospective paradigm, but relatively few have used a retrospective paradigm. The main reason for this imbalance is that, after a participant is asked to provide a retrospective judgment, the participant is then aware that he or she may be asked to judge a subsequent duration, which commonly reflects the defined characteristic of prospective time judgment. The experimental design used in my study lacks the possibility to track the active information processing of time during the measurement phase. During this phase, the time period in passing is passively being perceived by the subject or participant; to the contrary in the reproduction phase the subject's or participant's experience of time passing was reflected by the proactive movement response. Prospective duration timing depends on attention-demanding processes that occur concurrently with the processing of nontemporal information (Pouthas and Perbal, 2004). In my study, the reproduction phase, encompassing the executive function of movement response and attending to time reflects a dual-task condition and can therefore be characterized as prospective paradigm (Pouthas and Perbal, 2004). During measurement phase, uncertainty remains on whether the subject's attention is purely directed to the dimension of time or on the time point, when the dimension of time is in focus of attention. Nevertheless, the presented results indicate that temporal information must be assessed in any way, which can not be clearly identified with the current behavioral paradigm. Therefore, the terms "retrospective" and "prospective" could rather be understood in a non-classical sense, namely as a cognitive load affecting factor as proposed by Brown (1985) and Zakay and Block (2004), in contrast to a past or future-directed estimation of duration. Hence, different cognitive processes may underlie prospective and retrospective timing. This interpretation follows attentional models (Thomas and Weaver, 1975; Zakay and Block, 1996), which suggest divided attentional resources between nontemporal and temporal information Because retrospective and prospective duration judgements show clear differences in

the information processing involved, they historically have been studied as separate phenomena. Yet, they also share unifying aspects, such as disruption from the demands of untimed tasks, experience an increase from a rise in physical duration; the order in which the stimulus duration occurs, and certain involved factors affecting stimulus context (Brown and Stubbs, 1992) All these aspects are believed to be intimately related. Consequently they should not be considered as distinct phenomena (French et al., 2014).

I successfully could reproduce the results of Jazayeri and Shadlen (2010), and additionally could implement the behavioral task with rodents using a VR. I obtained comparable results for humans and gerbils, although the two tested species groups were very limited in size. Due to the limited sample size regarding the number of subjects and participants itself, the current study should be seen as a "slim-line" version of a pilot study probing the possibility of testing an equivalent timing task in humans and rodents. The obtained results can, therefore, be understood as an indication, rather than a state-of-the-art for similarities in rodent and human species. Under the scope of the present study, I did find generic principles that apply to the behavior of temporal judgments in human and non-primate species. This success offered the possibility to investigate the underlying neuronal mechanisms of prospective and retrospective time estimation in rodents. Therefore, in the second part of the thesis, the experimental design was extended to electrophysiological recordings in rodents.

4.2 NEURONAL DYNAMICS OF DURATION ESTIMATES

In the second part of this thesis, I examined whether and how neuronal activity in the medial prefrontal cortex represents interval timing for a retrospective-prospective time-estimation task. The majority of cells exhibited ramping activity, which was previously assigned to play a crucial role in timing. The observed ramping activity specifically occurred in two different kinds: Stimulus duration could be encoded in ramping magnitude, or be encoded by the slope of the up-ramping activity. I found that 57% of the recorded neurons exhibited temporal scaling during prospective time estimation in their firing activity, adapted to stimulus size presented. In contrast, a comparable scaling property during retrospective time estimation was not observed. Further, I found diverse activity patterns that provide a basis for the understanding of time encoding in the brain. In detail, I found that neurons encoded stimulus size by adapting their activity related to the estimated time. These observations were not exclusively present in prospective timing. However, activity adaptations to the interval to be estimated was less notable in retrospective time estimation. Also, I provide evidence that the accuracy and precision of the duration estimation behavior, related to the environmental demands, are encoded by PCF neurons. These findings indicate that the PFC can not solely be attributed to have an inherent clock function but might play a crucial role at the memory stage by evaluating new to existing knowledge and updating memory. These results provide a basis for further studies for the investigation of the neuronal mechanisms underlying interval timing.

4.2.1 *Activity patterns in mPFC*

The highly diverse firing patterns during time estimation, observed in PFC neurons, are consistent with findings in monkeys (Freedman et al., 2001; Wallis et al., 2001; Nieder et

al., 2002) and other rodent species (Baeg et al., 2003; Narayanan and Laubach, 2006; Mainen and Kepecs, 2009; Kim et al., 2009, 2013; Xu et al., 2014). Because the mentioned studies employed various timing paradigms, this finding presents the heterogeneity of PFC neurons involved in regulating diverse aspects of timing behavior. Among the variety of neural responses, I identified cells responding with persistent firing in measurement phase or reproduction phase, or in both phases, as well as temporally fixed activity. Activity patterns that were well correlated with different phases of the task, including measurement offset, the onset and offset of reproduction, and reward onset, represented the involvement of regulatory actions of mPFC neurons in sensory and motor systems. Likewise, other research groups successfully recorded cells with various temporal profiles, including phasic, tonic, and ramping activities during cue and delay periods, whilst monkeys performed an interval timing task. Their studies proposed neurons in PFC that may play a variety of roles in temporal processing, including the monitoring of cue duration and memory encoding (Sakurai et al., 2004; Genovesio et al., 2009; Matell et al., 2011). I successfully recorded cells from all subregions of the prefrontal cortex, which homogeneously presented the mentioned activity profiles over all subareas of the PFC. However, the experimental design cannot delineate if particular response patterns are exclusively present in devoted subregions of the PFC, as the tetrode position during experiments was approximated but could only be verified post mortem. Nevertheless, the majority of cells recorded from all subregions of the mPFC exhibited firing with a monotonic increase or decrease in activity over time, commonly referred to as "ramping" (Narayanan and Laubach, 2009; Kim et al., 2013; Bekolay et al., 2014; Parker et al., 2014).

Ramps - ramps everywhere. Neurons in the medial frontal cortex robustly ramp (Niki and Watanabe, 1976, 1979) - Ramping activity is one type of neuronal activity patterns in the cortex, which is thought to robustly encode temporal information. With its consistent changes, typically starting at the beginning of the to-be-timed interval until the end, ramping activity could encode evidence accumulation of temporal information, which is, that temporal expectation correlates with time passing

and thereby leads to increased or decreased activity. Thus, ramping activity can be understood as temporal integration of information, which was already well captured by drift-diffusion processes and integrative models (Durstewitz, 2003; Simen et al., 2011; Thurley, 2016). One might argue that activity observed especially during reproduction is conflicted with motor response or motor planning. With the data provided, I can not fully disentangle the contributions of PFC neurons to motor activity and their contribution to timing activity. However, ramping activity predicts actions, often beginning several seconds before animals initiate their response (Kim et al., 2013; Parker et al., 2014; Xu et al., 2014). This makes the signal unlikely to be explicitly movement-related. Ramping activity readily scales over a variety of intervals (Kim et al., 2013; Xu et al., 2014). In premotor areas, movements are typically initiated when activity reaches a threshold (Hanes and Schall, 1996; Balcı and Simen, 2016), although it is unclear how this threshold is determined. Controversially, I found cells, which ramped to a specific threshold toward the termination of the movement. The pattern of ramping activity is not only limited to appear in a linear fashion and can in contrast, be represented with exponential features when needed, e.g. to encode hazard functions (Simen et al., 2011; Kim et al., 2013). The precision of the temporal estimate can therefore be encoded in the magnitude of activity or the slope of the ramp (Reutimann et al., 2004). Ramping was not exclusively observed for single cells but might also occur across a population of neurons via recurrent network interactions (Wong and Wang, 2006). This network activity could explain ramping activity profiles of cells, which did not span the entire phase or showed temporally fixed responses. In this respect, cells coordinately responded as a network to represent the timed interval. Such a neural network that spans the entire duration of an interval by coordinated ensemble activity has already been described in striatum (Gouvêa et al., 2015), hippocampus (Macdonald et al., 2011), or parietal areas (Jazayeri and Shadlen, 2015). Alternatively, ramping features can be represented in persistent activity and encode mnemonic information (Funahashi et al., 1989). Consequently, ramping understood as the integral or cumulative cum of persistent activity, might encode other cognitive variables than timing,

which imply decision-making or working memory (Bekolay et al., 2014).

Telling time by scalable firing. Despite the observed diversity of firing patterns of mPFC neurons, a substantial portion (57%) of the overall population exhibited temporal scaling of their firing patterns while performing the prospective timing task. The observed scaling property correlated with the timed interval's size and thereby matched the applied magnitude system. The results of properly scaled activity, to match the activity of the smallest presented stimulus in either of the tested stimulus distributions, demonstrated that the brain uses generalized patterns modified and adapted on a when-needed basis. Although scaling appeared to be highly adaptive, it was arranged, as expected by the math of the stimulus ratio. This could be interpreted that timing is represented in a distinct manner of numerosity, which was previously shown by Xu et al. (2014). In a time discrimination task, neurons in the lateral intraparietal area showed ramping activity at slow and fast speeds, correspondingly for long or short intervals (Leon and Shadlen, 2003), representing the feature of temporal scaling. Similar temporal scaling of PFC neural activity has been reported during the delay period for the working memory task in monkeys (Brody et al., 2003). My results correspond to the reported findings of the studies mentioned above and indicate that temporally scalable firing-rate modulation may serve as a mechanism for mPFC neurons to represent the timed of different magnitudes. Also, this finding is consistent with the model that timing information is inherent in the neural network dynamics (Brody et al., 2003; Ivry and Schlerf, 2008; Reutimann et al., 2004).

The math of time representation. The interaction of numerosity and time in prefrontal cortex has already been addressed by the neuroscience community. It was suggested that a two-stage model represents numerosity–time interactions whereby the interaction at the perceptual level occurs within the parietal region and the interaction at categorical decisions takes place in the prefrontal cortex (Hayashi et al., 2013). With

my study, I provided evidence that stimulus-correlated activity related to timing is in line with the proposed numerosity-time interactions. However, it needs to be discussed how the two different representations of stimulus size by firing magnitude, observed during my experiments, can be explained. I found positive as well as negative correlations of neural firing with stimulus size. Some cells encoded small stimuli with low firing rates, compared to large intervals being represented with high firing rates. A substantial portion of cells responded with reversed firing rates, which is, that small intervals were encoded with high firing rates, whereas low firing rates represented long durations. The applied order of magnitudes was therefore bound to stimulus features, which suggests that the prefrontal cortex contributes to temporal perception (Genovesio et al., 2009). Following the argumentation of order-based activity or representation bound to stimulus magnitude, I expect that firing increases with stimulus size. However, this representation was only visible in a subset of the magnitude-adapting population, which showed correlated firing with stimulus size. Still, a significant portion of cells, in which stimulus-size-dependent correlation has been detected, represented the size of the tested stimulus in a reciprocal order. From a physiological point of view, extensive firing is energy-consuming and should be kept to a minimum. Nevertheless, how to keep the necessary information under constraints of energy savings? One possibility is to convey the most energy-consuming information in the shortest possible time interval, and degrade it when adapted to large stimulus sizes. This encoding would advantage in preserving the transmission of information at a moderate energy-consuming level even for long intervals, but sacrifices the precision of the conveyed content. As an alternative hypothesis, cells, exhibiting a specific response type on a continuous scale, are tuned to the time stimuli involved and only afford a limited number of spikes. Temporally compressing the spikes represents short intervals and thereby results in a high discharge rate. Stretching the time period for long intervals with a consistent number of spikes, reduces the spike density, leading to a low discharge rate. This hypothesis for time encoding by neural firing would be supported by the Bayesian framework, which implies that retrieved information depends on the incorporate mean of a stimulus distribution

and causes errors when deviating from it. To which extent, and if at all, both hypotheses raised apply can not be clarified within this thesis. However, what unifies both theories, is that they would, in either case, lead to reduced spike density given a long stimulus interval. This reduction in spike density then, leads to increased variance, thereby reflecting increased uncertainty, which in turn represents the scalar property of timing (Gibbon et al., 1984; Leon and Shadlen, 2003). The two types of discharge rate adaptation demonstrate that separating subpopulations, considering the stimulus size's correlation, is essential. Analysis of a mixed population lead to blurred effects and hide essential information needed to clarify the role of discharge rate adaptations.

Time in context. However, all of the described activity modulations share the common fact that PFC neurons process time in a highly context-dependent fashion. The influence of external parameters, such as the magnitude of time stimuli, or the sequence of presented stimulus intervals define the temporal context. Genovesio et al. (2016) provided evidence that temporal processing in the PFC is linked to specific past events, and they showed that PFC activity in primates is profoundly affected in a context-dependent way. Thus, adaptive coding (Everling et al., 2002; Duncan, 2010) involves recruiting cells in highly demanding conditions and changes the degree of neuronal specialization. The PFC was consequently assigned not to signal durations abstractedly, as expected of a general temporal encoder, but instead does so in a highly context-dependent manner. For example, Genovesio et al. (2016) showed, that different durations were distinguished as short or long, but only in one out of two tasks or intervals. Thereby, neurons signaled information about duration in an uncorrelated or just weakly correlated manner and responded in dependence of context. To investigate context-dependence with the timing paradigm I used, it would be mandatory to compare the activity of tracked neurons when presented with two overlapping stimulus distributions. An experimental approach using high resolution techniques, like silicon probes, might be helpful to get multi-unit recordings without reduced data size.

4.2.2 *The prefrontal cortex and interval timing*

Timing-related neuronal activity has been observed in a variety of brain regions, including PFC (Duncan, 2001; Rao et al., 2001; Genovesio et al., 2006; Oshio et al., 2006), pre-supplementary and supplementary motor areas (Mita et al., 2009), basal ganglia (Rao et al., 2001; Matell et al., 2003; Meck et al., 2008), cerebellum (Ivry and Spencer, 2004) or lateral intraparietal area (Leon and Shadlen, 2003; Janssen and Shadlen, 2005). Recent studies already provided converging evidence of the involvement of the mPFC in timing. Temporary inactivation of mPFC neurons in rats was shown to result in impaired neural processes that are related to time interval discrimination (Dietrich and Allen, 1998), especially in the range of a few seconds (Kim et al., 2009). So by now, there exists profound evidence that the PFC is crucially involved in discriminating and estimating time intervals in humans (Mangels et al., 1998; Koch et al., 2003; Jones et al., 2004) and animals (Glickstein et al., 1964; Rosenkilde and Divac, 1976; Dietrich et al., 1997; Dietrich and Allen, 1998; Onoe et al., 2001; Kim et al., 2009, 2013; Xu et al., 2014). However, the exact role of the PFC in interval timing behavior has not been clear.

With this thesis, I tried to shed light on how the prefrontal cortex encodes time. I could show that neurons in the prefrontal cortex exhibit a variety of response patterns while performing a time estimation task. Here, I presented neurons that showed more complex timing activity, extending the monotonic ramping activities. Example neurons exhibited a generic activity profile for all tested stimulus durations, but adapted the activity profile towards the end of the reproduction phase until reaching a threshold. This adaptation was reflected by ramping activity, which scaled with the size of the stimulus. Generally, small stimuli were represented with temporally compressed signals, which resulted in a fast up-ramping activity, whereas large stimuli were temporally stretched respectively, and represented in a slow ramp to a threshold. Thereby, cells modulated the speed of their ramp-like activity to a certain threshold in relation to stimulus size. Interestingly, this speed-correlated modulation, with respect to stimulus size, was not observed when analyzing this feature across the subpopulation of ramping speed-adapting

cells. This was caused by the fact that data containing mixed variants of ramping activity obscure correlation effects. In particular, single-cell examples were shown to undoubtedly represented adaptation of ramping speed.

Clock or memory function? Data from the present study can be used to differentiate various hypotheses on time representations in PFC. One such hypothesis is that timing relies critically on ramping neuronal activity in PFC. Indeed, changes in mPFC neurons' firing patterns have been identified during the performance of timed behavior (Niki and Watanabe, 1979; Xu et al., 2014). However, the procedures used in these studies are relatively different from the timing task I used. Moreover, ramping neuronal activity in the mPFC has also been reported in simple reaction time tasks (Narayanan and Laubach, 2009), or during the delay in delayed-response tasks in primates (Quintana et al., 1988; Tsujimoto et al., 2004). Here it was interpreted to presumably represent mnemonic processing of stimulus attributes rather than timing on a clock stage. Therefore, it is unlikely that ramping neuronal activity in the mPFC solely codes for time. Hence, other putative time coding mechanisms are worth considering. The final question remains whether PFC activity is specific to timing, or another, more general process, like attention, working memory, or response selection. It has been suggested that estimation of a time interval, its storage and retrieval, and comparison with a newly estimated time interval, are the three basic processes for all internal time operations (Wearden, 1999). The PFC might be in charge of one or more of these steps. An alternative hypothesis would be that contribution of the PFC to interval timing behavior is of general executive functional reasons (Mangels et al., 1998; Tregellas et al., 2006; Livesey et al., 2007) such as attentional control. Biochemical manipulation experiments support the idea that the mPFC may be involved in either attention or working memory processes, rather than timing *per se* (Matthews et al., 2012). Animal and human studies alike have implicated the mPFC in a wide variety of cognitive processes. Indeed, contributions to structural functions of attention (Arnsten, 2009; Paneri and Gregoriou, 2017), working memory (Funahashi, 2017; Spaak et al., 2017), planning and decision making (Padoa-Schioppa and

Conen, 2017), and action selection (Ridderinkhof et al., 2004) have been demonstrated.

Sequential effects have been shown to occur during estimation tasks (Thurley and Schild, 2018). The sequential order of events during the presented timing task required retrieving information, based on previous experience from reference memory, and simultaneously monitor the experienced duration. This supports the idea that both working and reference memory, would have been required for the prospective phase of the time estimation task, which required associating a given duration with a representation of intervals or knowledge of conventional time units. The representation of conventional time units is stored in the reference memory (Perbal-Hatif, 2012). According to Perbal-Hatif (2012), reference memory is assimilated with semantic memory, which stores general knowledge of the world, including time representation. Thus, accurate time estimation, as measured by the task of the present work, required both working and reference memory, supporting the idea of the prefrontal cortex in the memory stage of the SET. A further indication for PFC neurons involved in the memory or comparison/decision stage rather than the clock stage would be if activity increases after the offset of the estimated time intervals but not during their presentation. This would suggest that information concerning comparison and or updating of internally stored knowledge is conveyed. Previous physiological studies have found neuronal activity possibly related to the storage and comparison processes in the PFC. Some neurons in the rat's ACC showed different activity between two different interval durations (Matell et al., 2003). Also, when monkeys were required to discriminate durations of two successfully presented stimuli, some PFC neurons showed duration-dependent activity during the time period between the two stimuli (Sakurai et al., 2004; Oshio et al., 2006; Genovesio et al., 2009), suggesting the involvement of the PFC in holding the information on the first time interval as working memory, which might be a step toward long-term storage of temporal information (Wearden, 1999). After the presentation of the second stimulus, some PFC neurons signaled relative durations of the two stimuli (Genovesio et al., 2009), suggesting the involvement of the PFC in the comparison process as well. They also found that some neurons in the rat's

mPFC modulated their activity according to sample interval duration after sample interval offset. These results suggest the involvement of the mPFC in maintaining temporal information as working memory, and possibly in comparing this information with a reference time interval stored in long-term memory. Collectively, the present and previous physiological studies in rats and monkeys suggest the involvement of the PFC in multiple processes of time-interval discrimination, raising the possibility that the PFC might be part of a central neural system controlling interval timing behavior. Usually, physiological studies employing a fixed interval or peak interval procedure suffer from confounding of timing with motor activity, because animals emit motor responses that vary with the elapse of time. The current study also involved a time estimation period that might easily be confounded with motor activity. Thus, it is difficult to isolate clock function-related neural activity from motor response-related neural activity. For this reason, the current study presented in the thesis focused on those neurons that showed differential activity between the tested interval durations as it was previously reported by Matell et al. (2003). Kim et al. (2018) compared timing activity in striatal and prefrontal neurons and found that both brain areas contributed significantly to temporal processing. However, striatal neurons rarely showed a full-interval spanning ramping activity, which was, in contrast, frequently observed in mPFC. Striatal neurons preferably fired briefly during sample intervals. Their study provides evidence that brain areas dedicated to timing convey temporal information via distinct neural processes or even adapt to the demanded task. Bakhurin et al. (2017) share the idea, that temporal information is encoded in a widely distributed manner throughout multiple brain areas, but state that the striatum may have a privileged role in timing because it has a more accurate "clock" as it integrates information across multiple cortical areas. In contrast to PFC, the striatum has been shown to be a more reliable timing system, as the precision of neural time decoding became progressively worse with increasing time duration in the mPFC, but not in the striatum (Kim et al., 2018). Therefore, the exact role of PFC in interval timing behavior to date could not be clarified.

The body of literature provides evidence that timing is an emergent property of brain-wide interactions of the brain areas where timing signals have been identified on a population level. These brain areas include the hippocampus (Pastalkova et al., 2008; Macdonald et al., 2011), medial prefrontal cortex (Kim et al., 2013; Xu et al., 2014), parietal cortex (Leon and Shadlen, 2003; Janssen and Shadlen, 2005), motor areas (Lebedev et al., 2008), and the cerebellum (Mauk and Buonomano, 2004) . Contrasting brain-wide interactions, it was proposed that the brain has several distributed timing stages which are activated on specific timing needs. Simultaneous recordings in multiple brain areas during time estimation tasks could enlighten the knowledge of the numerous time-related functions we and other organisms rely on for survival.

4.2.3 *Reward encoding*

Reward signals in the brain. Rewards are defined by their action on behavior and are crucial for the survival of the organism. They are vital in the control of homeostasis, sustain learning of new behaviors, the induction of approach behavior, and serve as goals for voluntary, intentional behavior. Reward related activity has been found in various brain regions, i.e., the hippocampus (Gauthier and Tank, 2018), striatum (Samejima et al., 2005) and also prefrontal areas like the anterior cingulate cortex (Amiez et al., 2006). For example, in the hippocampus and subiculum, reward-associated cells were shown to exhibit activity fields that strongly correlated with reward location, and these cells entirely accounted for the excess density of fields near reward (Gauthier and Tank, 2018). In contrast, in the prefrontal cortex, reward-related units were not limited to specific subregions. Instead, they were found anywhere in the prefrontal cortex. Association with reward is common with widely scattered neuronal groups all over the prefrontal surface. In the monkey as in the rat, however, most promising regions in this regard appeared to be orbital and medial prefrontal areas (Amiez et al., 2006; Kobayashi et al., 2010; Chiang and Wallis,

2018; Setogawa et al., 2019). However, it has been suggested that the orbitofrontal cortex (OFC) and the medial frontal cortex (MFC) do not encode reward associations completely autonomously, instead, amygdala, a structure essential for the evaluation of motivational significance was assigned to play a crucial role in shaping the encoding in OFC and MFC (Rudebeck et al., 2017).

Reward encoding for survival. In natural environments, the distance and terrain that one might encounter to obtain food (or traveling to new habitats) produce energetic costs, which is a critical component in optimal choice (Stevens et al., 2005; Rangel and Hare, 2010; Walton et al., 2006). Guidance of responding to maximize benefits vs. costs was suggested to be a major role of the PFC in optimizing behavior (Moorman and Aston-Jones, 2015). The execution of behavior requires that animals interact with and respond to changes in their environment. This implies that the nervous system must represent both the internal state and the external world in the form of neuronal activity. Therefore, the spatial and temporal precision of these representations fosters many behaviors crucial to survival. Growing evidence suggests that the ACC may have a specialized role in influencing effort-based decision making. ACC disruptions bias animals toward actions that are associated with less effort even when a more rewarding option is available (Walton et al., 2002; Schweimer and Hauber, 2005; Floresco and Ghods-Sharifi, 2007). To improve efficacy and increase chances of survival, the representations of the to be timed interval has to be updated when environmental reward contingencies are modified. Researchers have proposed that a circular process modifies the estimated value depending on the outcome because updating of the estimated values by integrating outcomes is fundamental to rapid adaptations of behavior. Consecutively, outcomes have to be evaluated in relation to existing stored values constructed through successive trials (Amiez et al., 2006). Consequently, the relative encoding of outcomes is essential for appropriate reactions to particular contexts and expectancies. Nevertheless, it has to be taken into consideration that reward-related activity can only be distinguished with difficulty from its possible relationship to any of the various

sensory stimuli that accompany its delivery. Nonetheless, by use of appropriate controls, it has been determined that the activity of some of those units is indeed related to the ingestion of the appetitive reinforcement, whereas that of others is related to its absence if a reward is expected (Fuster, 2008).

Reward-related activity represents precision and accuracy. In the last part of my experimental work, I tried to find the neural correlates of reward. Therefore, a time period of 3.5 seconds from reproduction offset to the start of the next consecutive trial was evaluated. I found that the accuracy and precision, represented by the behavioral parameters of BIAS, SD, and $\sqrt{BIAS^2}$ were encoded by neural activity. Surprisingly, a majority of PFC neurons (88%) showed activity during ITI, although no active timing process had to be performed at this stage. This finding affirmed the hypothesis that PFC neurons provided clock functions by representing actual timing in neural activity and are responsible for evaluating and updating memory values. Furthermore, the quantitative analysis revealed that low behavioral bias occurring in time estimation was encoded with a large variety of magnitudes of discharge rates, whereas large biases were represented only on a limited range of discharge magnitudes. The same observations were made for the $\sqrt{BIAS^2}$. These results indicate that the strength of regression is encoded by neural activity. What is the advantage of spending energy in encoding a past event? Integration of experiences and thereby updating the current knowledge to improve performance and efficacy for future events represents the most likely rational. Thereby, I suggest that evaluating performance-indicating parameters during ITI update the internal prior, thereby leading to adaptation of behavior and neural representation. With this property, the mPFC encodes the accuracy of duration estimation following Bayesian inference. In this context,the SD was not significantly correlated with neural activity but demonstrated that precision was one of the encoded features of PFC during ITI. Therefore, I propose that all persistent neuronal activity during ITI of the timing task is an expression of the involvement of cells that exhibit activity contributing to working memory – that is, of their participation in a network that has been activated

temporarily for the withholding of information toward the attainment of the reward.

Hence, as a key discovery, I found that irrespective of the neurons' activity pattern, the adaptation of discharge rate depended on the time interval required. On a populational level, I could show that firing rate adaptations, representing performance accuracy, reflected regression effects, resulting from strategies to cope with uncertainty about sensory information. The precision of duration estimates was captured by the neural activity as well, although for an internal reference instead of an external value determined by the statistics of the stimulus distribution. Using higher firing rates to provide higher information content, causing less regression, and low variance corroborates the fact that the objective of timed behavior is maximal accuracy and minimal variance.

4.2.4 *Neurophysiological predictions in humans*

Magnetoencephalography (MEG) and electroencephalography (EEG) are completely noninvasive tools that reflect the human brain's real-time operations in experimental conditions. Due to inter-species differences, rodent data can not always be directly translated to the human situation. Therefore, these methods could be used to reproduce the neurophysiology experiments and generate a data set of neuronal activity during the duration estimation task comparable to the animal study presented in this thesis. These neuroimaging techniques could help gain insights into the sensory and cognitively controlled neuronal responses during the duration estimation task. MEG specifically, enables to separately measure a single brain process rather than an amalgamate of multiple temporally overlapping processes, which cannot be unequivocally disentangled based on location or orientation. By using this technique, process-specific information can be used to disambiguate event-related potential data (ERP) recorded from the same experimental situation. Experiments probing the estimation of the dimension of time

while recording the underlying neural activity, have mainly been performed using a time to contact (TTC) paradigm e.g., when a participant has to estimate the time when an object reaches a target (Chang and Jazayeri, 2018; Daneshi et al., 2020). However, using EEG or MEG does not allow for assessing single-neuron activity in humans as comparably done in this study. Without the possibility of sorting specific response patterns of cells, the overall detected activity while performing the time estimation task might give no meaningful results. Separate populations of cells with heterogeneous activity profiles analogous to these found in the neurophysiological experiments performed with rodents in this study, i.e., up-ramping vs. down-ramping activity profiles, cancel out prominent activity patterns when represented by separate subpopulations of cells simultaneously. Nevertheless, data obtained from humans with neuroimaging techniques, such as MEG or EEG, could be used to compare the neuronal activity of a population as an entity and thereby enable assessment inter-species differences or similarities of neuronal activity while performing the duration estimation task and draw conclusions between animals and humans. Additionally, EEG or MEG could be used as noninvasive tools to examine the structural activation of the prefrontal cortex or other brain areas involved as well as the structural activation of related subareas during the different phases of the duration estimation task and identify their cognitive load.

Adding to the existing body of evidence, my results show that the mPFC provides timing-related neural signals for prospective time estimation in the supra-second range in gerbils, and that the PFC plays an essential role in interval timing in animal species. Although the presented complex patterns of activity correlated strongly with stimulus size, it can not be disentangled, that this activity was not associated with movement-related signals or that the the signals originated because the PFC rules as the central area where interval timing takes place. On a basis, I agree that the distinction between sensory and motor timing is essential, but is was shown, that these two timing systems can also overlap. Many models of motor timing can account for simple sensory timing tasks like interval and duration discrimination (Paton and Buonomano, 2018) of time.

My results, therefore, demonstrate that the medial prefrontal cortex of rodents profoundly provides timer functions at an internal clock stage. However, the prefrontal cortex does not exclusively code for time but also fulfills mnemonic functions by integrating the outcome and interaction of the decision with the environment. This integration might serve to compare the present outcome with previously stored values in memory. Activity during the delay phase supports the idea that the prefrontal cortex concurrently acts as a memory stage, integrating prior knowledge and updating posterior knowledge about the stimulus duration following Bayesian inference.

Strikingly similar neural correlates of timing have been observed in rodents and humans, i.e., ramping activity and delta/theta rhythms that synchronize single neurons (Narayanan et al., 2013). Humans with Parkinson's Disease and rodents with medial frontal dopamine depletion showed attenuated spectral delta/theta power (Parker et al., 2015), which is coupled with cortical ramping activity in rodents (Parker et al., 2014, 2015). Using model organisms like rodents might help establish how the prefrontal cortex encodes and instantiates the temporal control of actions, thereby paving the way to identifying diseases that degrade cortical function and potentially cause disorders due to disrupted timing. As we continue to understand more about time in the brain, I hope that the research community will discover other contact points with clinical neuroscience.

5

REFERENCES

Acerbi L, Wolpert DM, Vijayakumar S (2012) Internal representations of temporal statistics and feedback calibrate motor-sensory interval timing. *PLoS computational biology* 8:e1002771.

Adesnik H, Scanziani M (2010) Lateral competition for cortical space by layer-specific horizontal circuits. *Nature* 464:1155–1160.

Adler A, Katabi S, Finkes I, Israel Z, Prut Y, Bergman H (2012) Temporal convergence of dynamic cell assemblies in the striato-pallidal network. *Journal of Neuroscience* 32:2473–2484.

Ahrens MB, Sahani M (2011) Observers exploit stochastic models of sensory change to help judge the passage of time. *Current Biology* 21:200–206.

Alexander GE, DeLong MR, Strick PL (1986) Parallel organization of functionally segregated circuits linking basal ganglia and cortex. *Annual review of neuroscience* 9:357–381.

Alvarez JA, Emory E (2006) Executive function and the frontal lobes: a meta-analytic review. *Neuropsychology review* 16:17–42.

Amiez C, Joseph JP, Procyk E (2006) Reward encoding in the monkey anterior cingulate cortex. *Cerebral Cortex* 16:1040–1055.

Applebury ML, Antoch MP, Baxter LC, Chun LL, Falk JD, Farhangfar F, Kage K, Krzystolik MG, Lyass LA, Robbins JT (2000) The murine cone photoreceptor: a single cone type expresses both S and M opsins with retinal spatial patterning. *Neuron* 27:513–523.

Arnsten AFT (2009) Toward a new understanding of attention-deficit hyperactivity disorder pathophysiology: an important role for prefrontal cortex dysfunction. *CNS drugs* 23 Suppl 1:33–41.

Aton SJ, Herzog ED (2005) Come together, right...now: synchronization of rhythms in a mammalian circadian clock. *Neuron* 48:531–534.

Avni-Babad D, Ritov I (2003) Routine and the perception of time. *Journal of Experimental Psychology: General* 132:543–550.

Baeg EH, Kim YB, Huh K, Mook-Jung I, Kim HT, Jung MW (2003) Dynamics of population code for working memory in the prefrontal cortex. *Neuron* 40:177–188.

Bailey N, Areni CS (2006) Background music as a quasi clock in retrospective duration judgments. *Perceptual and motor skills* 102:435–444.

Bakhurin KI, Goudar V, Shobe JL, Claar LD, Buonomano DV, Masmanidis SC (2017) Differential Encoding of Time by Prefrontal and Striatal Network Dynamics. *Journal of Neuroscience* 37:854–870.

Balcı F, Simen P (2016) A decision model of timing. *Current Opinion in Behavioral Sciences* 8:94 – 101 Time in perception and action.

Baylor DA (1987) Photoreceptor signals and vision. Proctor lecture. *Investigative ophthalmology & visual science* 28:34–49.

Bechara A, Tranel D, Damasio H, Damasio AR (1996) Failure to respond autonomically to anticipated future outcomes following damage to prefrontal cortex. *Cerebral Cortex* 6:215–225.

Bekolay T, Laubach M, Eliasmith C (2014) A spiking neural integrator model of the adaptive control of action by the medial prefrontal cortex. *Journal of Neuroscience* 34:1892–1902.

Block RA, Zakay D (1997) Prospective and retrospective duration judgments: A meta-analytic review. *Psychonomic bulletin & review* 4:184–197.

Brody CD, Hernández A, Zainos A, Romo R (2003) Timing and Neural Encoding of Somatosensory Parametric Working Memory in Macaque Prefrontal Cortex. *Cerebral Cortex* 13:1196–1207.

Brown GD, Preece T, Hulme C (2000) Oscillator-based memory for serial order. *Psychological Review* 107:127–181.

Brown SW, Stubbs DA (1992) Attention and interference in prospective and retrospective timing. *Perception* 21:545–557.

Brown SW (1985) Time perception and attention: The effects of prospective versus retrospective paradigms and task demands on perceived duration. *Perception & Psychophysics* 38:115–124.

Brunia C, de Jong B, van den Berg-Lenssen M, Paans A (2000) Visual feedback about time estimation is related to a right hemisphere activation measured by pet. *Experimental Brain Research* 130:328–337.

Buhusi CV, Meck WH (2005) What makes us tick? Functional and neural mechanisms of interval timing. *Nature Reviews Neuroscience* 6:755–765.

Buonomano DV, Bramen J, Khodadadifar M (2009) Influence of the interstimulus interval on temporal processing and learning: testing the state-dependent network model. *Philosophical Transactions of the Royal Society B: Biological Sciences* 364:1865–1873.

Buonomano DV, Maass W (2009) State-dependent computations: spatiotemporal processing in cortical networks. *Nature Reviews Neuroscience* 10:113.

Burgess PW, Fellows LK (2013) *Decision makingExecutive Functions Meet Motivation* Oxford, UK.

Buzsáki G (2004) Large-scale recording of neuronal ensembles. *Nature Neuroscience* 7:446–451.

Cantlon JF, Cordes S, Libertus ME, Brannon EM (2009) Comment on "log or linear? distinct intuitions of the number scale in western and amazonian indigene cultures". *Science* 323:38–38.

Caras ML, Sanes DH (2019) Neural variability limits adolescent skill learning. *Journal of Neuroscience* pp. 2878–18.

Caselli L, Iaboli L, Nichelli P (2009) Time estimation in mild Alzheimer's disease patients. *Behavioral and brain functions : BBF* 5:32.

Catani M, de Schotten MT (2012) *Atlas of Human Brain Connections* Oxford, UK.

Catania A (1970) Reinforcement schedules and psychophysical judgments: A study of some temporal properties of behavior, the theory of reinforcement schedule. *Meredith, New York* .

Cavada C, Goldman-Rakic PS (1989) Posterior parietal cortex in rhesus monkey: II. Evidence for segregated corticocortical networks linking sensory and limbic areas with the frontal lobe. *The Journal of comparative neurology* 287:422–445.

Cenquizca LA, Swanson LW (2007) Spatial organization of direct hippocampal field CA1 axonal projections to the rest of the cerebral cortex. *Brain research reviews* 56:1–26.

Chahl JS, Srinivasan MV (1997) Reflective surfaces for panoramic imaging. *Appl Opt* 36:8275–8285.

Chang CJ, Jazayeri M (2018) Integration of speed and time for estimating time to contact. *Proc Natl Acad Sci U S A* 115:E2879–E2887.

Chao LL, Knight RT (1998) Contribution of human prefrontal cortex to delay performance. *Journal of cognitive neuroscience* 10:167–177.

Chazotte B (2011) Labeling Lysosomes in Live Cells with Neutral Red. *Cold Spring Harbor Protocols* 2011:pdb.prot5570–pdb.prot5570.

Cheal ML (1986) The gerbil: a unique model for research on aging. *Experimental aging research* 12:3–21.

Chen BH, Park JH, Ahn JH, Cho JH, Kim IH, Lee JC, Won MH, Lee CH, Hwang IK, Kim JD, Kang IJ, Cho JH, Shin BN, Kim YH, Lee YL, Park SM (2017) Pretreated quercetin protects gerbil hippocampal CA1 pyramidal neurons from transient

cerebral ischemic injury by increasing the expression of antioxidant enzymes. *Neural regeneration research* 12:220–227.

Chiang FK, Wallis JD (2018) Neuronal encoding in prefrontal cortex during hierarchical reinforcement learning. *Journal of Cognitive Neuroscience* 30:1197–1208 PMID: 29694261.

Church RM (1984) Properties of the internal clock. *Annals of the New York Academy of Sciences* 423:566–582.

Church RM, Broadbent HA (1990) Alternative representations of time, number, and rate. *Cognition* 37:55–81.

Church RM, Gibbon J (1982) Temporal generalization. *Journal of Experimental Psychology: Animal Behavior Processes* 8:165–186.

Cicchini GM, Arrighi R, Cecchetti L, Giusti M, Burr DC (2012) Optimal encoding of interval timing in expert percussionists. *J Neurosci* 32:1056–1060.

Close B, Banister K, Baumans V, Bernoth EM, Bromage N, Bunyan J, Erhardt W, Flecknell P, Gregory N, Hackbarth H, Morton D, Warwick C (1996) Recommendations for euthanasia of experimental animals: Part 1. DGXI of the European Commission. *Lab Anim* 30:293–316.

Close B, Banister K, Baumans V, Bernoth EM, Bromage N, Bunyan J, Erhardt W, Flecknell P, Gregory N, Hackbarth H, Morton D, Warwick C (1997) Recommendations for euthanasia of experimental animals: Part 2. DGXT of the European Commission. *Lab Anim* 31:1–32.

Cole MW, Reynolds JR, Power JD, Repovs G, Anticevic A, Braver TS (2013) Multi-task connectivity reveals flexible hubs for adaptive task control. *Nature neuroscience* 16:1348–1355.

Conchedda M, Gabriele F, Bortoletti G (2006) Development and sexual maturation of Echinococcus granulosus adult worms in the alternative definitive host, Mongolian gerbil (Meriones unguiculatus). *Acta tropica* 97:119–125.

Cordes S, Meck WH (2014) Ordinal judgments in the rat: An understanding of longer and shorter for suprasecond, but not subsecond, durations. *J Exp Psychol Gen* 143:710–720.

Coull JT, Vidal F, Nazarian B, Macar F (2004) Functional anatomy of the attentional modulation of time estimation. *Science* 303:1506–1508.

Coull JT, Cheng RK, Meck WH (2011) Neuroanatomical and neurochemical substrates of timing. *Neuropsychopharmacology* 36:3.

Coutlee CG, Huettel SA (2012) The functional neuroanatomy of decision making: prefrontal control of thought and action. *Brain Res* 1428:3–12.

Cummings JL (1993) Frontal-subcortical circuits and human behavior. *Archives of neurology* 50:873–880.

Daneshi A, Azarnoush H, Towhidkhah F, Bernardin D, Faubert J (2020) Brain activity during time to contact estimation: an EEG study. *Cognitive neurodynamics* 14:155–168.

Darlington TK, Wager-Smith K, Ceriani MF, Staknis D, Gekakis N, Steeves TD, Weitz CJ, Takahashi JS, Kay SA (1998) Closing the circadian loop: CLOCK-induced transcription of its own inhibitors per and tim. *Science (New York, N.Y.)* 280:1599–1603.

Dehaene S (2003) The neural basis of the Weber-Fechner law: a logarithmic mental number line. *Trends in cognitive sciences* 7:145–147.

Dehghani N, Peyrache A, Telenczuk B, Le Van Quyen M, Halgren E, Cash SS, Hatsopoulos NG, Destexhe A (2016) Dynamic Balance of Excitation and Inhibition in Human and Monkey Neocortex. *Scientific Reports* 6:23176–12.

Demers G (2006) ANIMAL RESEARCH: Enhanced: Harmonization of Animal Care and Use Guidance. *Science* 312:700–701.

Deng K, Liu W, Wang D (2017) Inter-group associations in Mongolian gerbils: Quantitative evidence from social network analysis. *Integrative zoology* 12:446–456.

Dietrich A, Allen JD (1998) Functional dissociation of the prefrontal cortex and the hippocampus in timing behavior. *Behavioral neuroscience* 112:1043.

Dietrich A, Allen J, Bunnell BN (1997) Is the hippocampus involved in temporal discrimination and the memory of short intervals? *International journal of neuroscience* 90:255–269.

Ding BY, Chi QS, Liu W, Shi YL, Wang DH (2018) Thermal biology of two sympatric gerbil species: The physiological basis of temporal partitioning. *Journal of thermal biology* 74:241–248.

Dombeck DA, Khabbaz AN, Collman F, Adelman TL, Tank DW (2007) Imaging large-scale neural activity with cellular resolution in awake, mobile mice. *Neuron* 56:43–57.

Domnisoru C, Kinkhabwala AA, Tank DW (2013) Membrane potential dynamics of grid cells. *Nature* 495:199–204.

Drewe EA (1974) The effect of type and area of brain lesion on Wisconsin card sorting test performance. *Cortex; a journal devoted to the study of the nervous system and behavior* 10:159–170.

Duncan J (2001) An adaptive coding model of neural function in prefrontal cortex. *Nature reviews. Neuroscience* 2:820–829.

Duncan J (2010) The multiple-demand (MD) system of the primate brain: mental programs for intelligent behaviour. *Trends in cognitive sciences* 14:172–179.

Durstewitz D, Seamans J (2006) Beyond bistability: Biophysics and temporal dynamics of working memory. *Neuroscience* 139:119 – 133.

Durstewitz D (2003) Self-organizing neural integrator predicts interval times through climbing activity. *J Neurosci* 23:5342–5353.

Effron DA, Niedenthal PM, Gil S, Droit-Volet S (2006) Embodied temporal perception of emotion. *Emotion (Washington, D.C.)* 6:1–9.

Ehrat H, Isenbügel E, Wissdorf H (1973) Postnatale entwicklung und verhalten von meriones unguiculatus (milne edwards, 1867) vom zeitpunkt der geburt bis zum absetzen der jungtiere im alter von 30 tagen. *Zeitschrift für Säugetierkunde : im Auftrage der Deutschen Gesellschaft für Säugetierkunde e.V.* 39:41–50.

Ekman G, Hosman B, Lindman R, Ljungberg L, Akesson CA (1968) Interindividual differences in scaling performance. *Perceptual and motor skills* 26:815–823.

Ellard CG, Goodale MA, Timney B (1984) Distance estimation in the Mongolian gerbil: the role of dynamic depth cues. *Behavioural brain research* 14:29–39.

Erhardt W, Henke J, Haberstroh J, Baumgartner C, Tacke S, Kölle P, Korbel R, Kroker R, Lendl C, Lierz M (2011) *Anästhesie und Analgesie beim Klein- und Heimtier mit Exoten, Labortieren, Vögeln, Reptilien, Amphibien un Fischen* Schattauer GmbH, Stuttgart, 2nd edition.

Etienne AS, Jeffery KJ (2004) Path integration in mammals. *Hippocampus* 14:180–192.

Everling S, Tinsley CJ, Gaffan D, Duncan J (2002) Filtering of neural signals by focused attention in the monkey prefrontal cortex. *Nat Neurosci* 5:671–676.

Fechner G (1860) *Elemente der Psychophysik* Number Bd. 1 in Elemente der Psychophysik. Breitkopf und Härtel.

Ferrandez AM, Hugueville L, Lehéricy S, Poline JB, Marsault C, Pouthas V (2003) Basal ganglia and supplementary motor area subtend duration perception: an fMRI study. *Neuroimage* 19:1532–1544.

Fiala JC, Grossberg S, Bullock D (1996) Metabotropic glutamate receptor activation in cerebellar purkinje cells as substrate for adaptive timing of the classically conditioned eye-blink response. *Journal of Neuroscience* 16:3760–3774.

Flaherty MG, Freidin B, Sautu R (2005) Variation in the perceived passage of time: a cross-national study. *Social Psychology Quarterly* 68:400–410.

Fletcher PC, Shallice T, Dolan RJ (1998a) The functional roles of prefrontal cortex in episodic memory. I. Encoding. *Brain* 121 (Pt 7):1239–1248.

Fletcher PC, Shallice T, Frith CD, Frackowiak RS, Dolan RJ (1998b) The functional roles of prefrontal cortex in episodic memory. II. Retrieval. *Brain* 121 (Pt 7):1249–1256.

Floresco SB, Ghods-Sharifi S (2007) Amygdala-prefrontal cortical circuitry regulates effort-based decision making. *Cerebral Cortex* 17:251–260.

Fortin C, Breton R (1995) Temporal interval production and processing in working memory. *Perception & psychophysics* 57:203–215.

Freedman DJ, Riesenhuber M, Poggio T, Miller EK (2001) Categorical representation of visual stimuli in the primate prefrontal cortex. *Science* 291:312–316.

French RM, Addyman C, Mareschal D, Thomas E (2014) GAMIT – A Fading-Gaussian Activation Model of Interval-Timing: Unifying Prospective and Retrospective Time Estimation. *Timing & Time Perception Reviews* 1:1–17.

Frenz H, Lappe M (2005) Absolute travel distance from optic flow. *Vision research* 45:1679–1692.

Fujisawa N, Maeda Y, Yamamoto Y, Sato NL, Niimura S (2003) Newly established low seizure susceptible and seizure-prone inbred strains of Mongolian gerbil. *Experimental animals* 52:169–172.

Funahashi S (2017) Working Memory in the Prefrontal Cortex. *Brain sciences* 7.

Funahashi S, Bruce CJ, Goldman-Rakic PS (1989) Mnemonic coding of visual space in the monkey's dorsolateral prefrontal cortex. *Journal of neurophysiology* 61:331–349.

Fuster JM (2001) The prefrontal cortex–an update: time is of the essence. *Neuron* 30:319–333.

Fuster JM, Bodner M, Kroger JK (2000) Cross-modal and cross-temporal association in neurons of frontal cortex. *Nature* 405:347–351.

Fuster J (2011) *The Prefrontal Cortex* Amazon Digital Services.

Fuster JM (1991) [book review] the prefrontal cortex, anatomy, physiology, and neuropsychology of the frontal lobe. *American Journal of Psychiatry* 148:130–130.

Fuster JM (2002) Frontal lobe and cognitive development. *Journal of Neurocytology* 31:373–385.

Fuster JM (2008) Chapter 2 - anatomy of the prefrontal cortex In Fuster JM, editor, *The Prefrontal Cortex (Fourth Edition)*, pp. 7 – 58. Academic Press, San Diego, fourth edition edition.

Gallistel CR (1990) Representations in animal cognition: an introduction. *Cognition* 37:1–22.

Gallistel CR, Gibbon J (2000) Time, rate, and conditioning. *Psychol Rev* 107:289–344.

Garbers C, Henke J, Leibold C, Wachtler T, Thurley K (2015) Contextual processing of brightness and color in Mongolian gerbils. *J Vis* 15:15.1.13–13.

Gauthier JL, Tank DW (2018) A dedicated population for reward coding in the hippocampus. *Neuron* 99:179 – 193.e7.

Genovesio A, Seitz LK, Tsujimoto S, Wise SP (2016) Context-Dependent Duration Signals in the Primate Prefrontal Cortex. *Cerebral Cortex* 26:3345–3356.

Genovesio A, Tsujimoto S, Wise SP (2006) Neuronal activity related to elapsed time in prefrontal cortex. *J Neurophysiol* 95:3281–3285.

Genovesio A, Tsujimoto S, Wise SP (2009) Feature- and order-based timing representations in the frontal cortex. *Neuron* 63:254–266.

Gibbon J, Church RM, Meck WH (1984) Scalar timing in memory. *Ann N Y Acad Sci* 423:52–77.

Gibbon J, Malapani C, Dale CL, Gallistel C (1997) Toward a neurobiology of temporal cognition: advances and challenges. *Curr Opin Neurobiol* 7:170–184.

Gibbon J (1977) Scalar expectancy theory and weber's law in animal timing. *Psychological Review* 84:279–325.

Glickstein M, Quigley WA, Stebbins WC (1964) Effect of frontal and parietal lesions on timing behavior in monkeys. *Psychonomic Science* 1:265–266.

Goldman-Rakic PS (2011) *Circuitry of Primate Prefrontal Cortex and Regulation of Behavior by Representational Memory*, pp. 373–417 American Cancer Society.

Gouvêa TS, Monteiro T, Soares S, Atallah BV, Paton JJ (2014) Ongoing behavior predicts perceptual report of interval duration. *Frontiers in neurorobotics* 8:10.

Gouvêa TS, Monteiro T, Motiwala A, Soares S, Machens C, Paton JJ (2015) Striatal dynamics explain duration judgments. *Elife* 4.

Griffiths TL, Tenenbaum JB (2011) Predicting the future as Bayesian inference: people combine prior knowledge with observations when estimating duration and extent. *J Exp Psychol Gen* 140:725–743.

Grondin S (2010) Timing and time perception: a review of recent behavioral and neuroscience findings and theoretical directions. *Attention, perception & psychophysics* 72:561–582.

Grothe B, Pecka M (2014) The natural history of sound localization in mammals–a story of neuronal inhibition. *Frontiers in neural circuits* 8:116.

Grzimek BH (1960) Systematische Übersicht. *Grzimeks Tierleben, Enzyklopädie des Tierreichs. Verlag Kindler, Zürich* Band 11:517–519.

Haas OV, Henke J, Leibold C, Thurley K (2019) Modality-specific Subpopulations of Place Fields Coexist in the Hippocampus. *Cerebral Cortex* 29:1109–1120.

Hanes DP, Schall JD (1996) Neural control of voluntary movement initiation. *Science* 274:427–430.

Harvey CD, Coen P, Tank DW (2012) Choice-specific sequences in parietal cortex during a virtual-navigation decision task. *Nature* 484:62–68.

Harvey CD, Collman F, Dombeck DA, Tank DW (2009) Intracellular dynamics of hippocampal place cells during virtual navigation. *Nature* 461:941–946.

Hayashi MJ, Kanai R, Tanabe HC, Yoshida Y, Carlson S, Walsh V, Sadato N (2013) Interaction of numerosity and time in prefrontal and parietal cortex. *J Neurosci* 33:883–893.

Heidbreder C, Groenewegen H (2003) The medial prefrontal cortex in the rat: evidence for a dorso-ventral distinction based upon functional and anatomical characteristics. *Neurosci Biobehav Rev* 27:555–579.

Henke J, Erhardt W (2001) *Schmerzmanagement bei Klein- und Heimtieren* Enke, 1st edition.

Hoelscher C, Schnee A, Dahmen H, Setia L, Mallot HA (2005) Rats are able to navigate in virtual environments. *J Exp Biol* 208:561–569.

Hollingworth HL (1910) The central tendency of judgment. *The Journal of Philosophy, Psychology and Scientific Methods* pp. 461–469.

Hoover WB, Vertes RP (2007) Anatomical analysis of afferent projections to the medial prefrontal cortex in the rat. *Brain structure & function* 212:149–179.

Howard MW, Eichenbaum H (2015) Time and space in the hippocampus. *Brain Res* 1621:345–354.

Hudspeth AJ (1997) How hearing happens. *Neuron* 19:947–950.

Ingle DJ (1981) New methods for analysis of vision in the gerbil. *Behav Brain Res* 3:151–173.

Isaacson JS, Scanziani M (2011) How inhibition shapes cortical activity. *Neuron* 72:231–243.

Itskov V, Curto C, Pastalkova E, Buzsáki G (2011) Cell assembly sequences arising from spike threshold adaptation keep track of time in the hippocampus. *J Neurosci* 31:2828–2834.

Ivry RB (1996) The representation of temporal information in perception and motor control. *Current Opinion Neurobiology* 6:851–857.

Ivry RB, Keele SW, Diener HC (1988) Dissociation of the lateral and medial cerebellum in movement timing and movement execution. *Exp Brain Res* 73:167–180.

Ivry RB, Richardson TC (2002) Temporal control and coordination: the multiple timer model. *Brain and cognition* 48:117–132.

Ivry RB, Schlerf JE (2008) Dedicated and intrinsic models of time perception. *Trends in Cognitive Sciences* 12:273–280.

Ivry RB, Spencer RMC (2004) The neural representation of time. *Curr Opin Neurobiol* 14:225–232.

Jacobs GH, Deegan JF (1994) Sensitivity to ultraviolet light in the gerbil (Meriones unguiculatus): characteristics and mechanisms. *Vision research* 34:1433–1441.

Jacobs GH, Neitz J (1989) Cone monochromacy and a reversed Purkinje shift in the gerbil. *Experientia* 45:317–319.

James W, Burkhardt F, Bowers F, Skrupskelis IK (1890) *The principles of psychology*, Vol. 1 Macmillan London.

Janssen P, Shadlen MN (2005) A representation of the hazard rate of elapsed time in macaque area LIP. *Nature Neuroscience* 8:234–241.

Jarvers C, Brosch T, Brechmann A, Woldeit ML, Schulz AL, Ohl FW, Lommerzheim M, Neumann H (2016) Reversal Learning in Humans and Gerbils: Dynamic Control Network Facilitates Learning. *Frontiers in neuroscience* 10:535.

Jay TM, Witter MP (1991) Distribution of hippocampal CA1 and subicular efferents in the prefrontal cortex of the rat studied by means of anterograde transport of Phaseolus vulgaris-leucoagglutinin. *The Journal of comparative neurology* 313:574–586.

Jazayeri M, Shadlen MN (2010) Temporal context calibrates interval timing. *Nat Neurosci* 13:1020–1026.

Jazayeri M, Shadlen MN (2015) A Neural Mechanism for Sensing and Reproducing a Time Interval. *Curr Biol* 25:2599–2609.

Jin DZ, Fujii N, Graybiel AM (2009) Neural representation of time in cortico-basal ganglia circuits. *Proc Natl Acad Sci U S A* 106:19156–19161.

Johnson KO, Hsiao SS (1992) Neural mechanisms of tactual form and texture perception. *Annu Rev Neurosci* 15:227–250.

Jones CRG, Rosenkranz K, Rothwell JC, Jahanshahi M (2004) The right dorsolateral prefrontal cortex is essential in time reproduction: an investigation with repetitive transcranial magnetic stimulation. *Experimental Brain Research* 158:366–372.

Jones FN, Woskow MH (1962) On the relationship between estimates of magnitude of loudness and pitch. *The American journal of psychology* 75:669–671.

Jones M, Curran T, Mozer MC, Wilder MH (2013) Sequential effects in response time reveal learning mechanisms and event representations. *Psychol Rev* 120:628–666.

Kandler K, Clause A, Noh J (2009) Tonotopic reorganization of developing auditory brainstem circuits. *nature neuroscience* 12:711–717.

Kaneko S, Murakami I (2009) Perceived duration of visual motion increases with speed. *J Vis* 9:14.

Karmarkar UR, Buonomano DV (2007a) Timing in the absence of clocks: encoding time in neural network states. *Neuron* 53:427–438.

Karmarkar UR, Buonomano DV (2007b) Timing in the absence of clocks: encoding time in neural network states. *Neuron* 53:427–438.

Kautzky M, Thurley K (2016) Estimation of self-motion duration and distance in rodents. *Royal Society Open Science* 3:160118.

Keller GB, Bonhoeffer T, Hübener M (2012) Sensorimotor mismatch signals in primary visual cortex of the behaving mouse. *Neuron* 74:809–815.

Kelley AE, Berridge KC (2002) The neuroscience of natural rewards: Relevance to addictive drugs. *Journal of Neuroscience* 22:3306–3311.

Kim J, Ghim JW, Lee JH, Jung MW (2013) Neural correlates of interval timing in rodent prefrontal cortex. *J Neurosci* 33:13834–13847.

Kim J, Jung AH, Byun J, Jo S, Jung MW (2009) Inactivation of medial prefrontal cortex impairs time interval discrimination in rats. *Front Behav Neurosci* 3:38.

Kim J, Kim D, Jung MW (2018) Distinct Dynamics of Striatal and Prefrontal Neural Activity During Temporal Discrimination. *Frontiers in integrative neuroscience* 12:153.

King BM (1986) Odor intensity measured by an audio method. *Journal of Food Science* .

Kobayashi S, de Carvalho OP, Schultz W (2010) Adaptation of reward sensitivity in orbitofrontal neurons. *Journal of Neuroscience* 30:534–544.

Koch G, Oliveri M, Torriero S, Caltagirone C (2003) Underestimation of time perception after repetitive transcranial magnetic stimulation. *Neurology* 60:1844–1846.

Kornbrot DE, Msetfi RM, Grimwood MJ (2013) Time perception and depressive realism: judgment type, psychophysical functions and bias. *PLoS One* 8:e71585.

Kornerup Hansen A (1990) Zucht und Haltung des Mongolischen Gerbils im Hinblick auf die Verwendung als Modell in einem biomedizinischen Versuch. *Hamster und Gerbil. Zucht, Haltung, Ernährung, Versuchsmodelle. Altromin Tier-Labor-Service, Lage, Deutschland* pp. 119–130.

Kotz SA, Schwartze M, Schmidt-Kassow M (2009) Non-motor basal ganglia functions: a review and proposal for a model of sensory predictability in auditory language perception. *Cortex; a journal devoted to the study of the nervous system and behavior* 45:982–990.

Kraus BJ, Robinson nRJ, White JA, Eichenbaum H, Hasselmo ME (2013) Hippocampal "Time Cells": Time versus Path Integration. *Neuron* 78:1090–1101.

Kraus N, Smith DI, McGee T, Stein L, Cartee C (1987) Development of the middle latency response in an animal model and its relation to the human response. *Hearing research* 27:165–176.

Kuffler SW (1953) Discharge patterns and functional organization of mammalian retina. *J Neurophysiol* 16:37–68.

Kumar UA, Sangamanatha AV, Vikas J (2013) Effects of Meditation on Temporal Processing and Speech Perceptual

Skills in Younger and Older Adults. *Asian Journal of Neuroscience* 2013:8.

Lachau-Durand S, Lammens L, van der Leede BJ, Van Gompel J, Bailey G, Engelen M, Lampo A (2019) Preclinical toxicity and pharmacokinetics of a new orally bioavailable flubendazole formulation and the impact for clinical trials and risk/benefit to patients. *PLoS neglected tropical diseases* 13:e0007026.

Lappe M, Jenkin M, Harris LR (2007) Travel distance estimation from visual motion by leaky path integration. *Exp Brain Res* 180:35–48.

Lebedev MA, O'Doherty JE, Nicolelis MAL (2008) Decoding of temporal intervals from cortical ensemble activity. *Journal of neurophysiology* 99:166–186.

Legg CR, Lambert S (1990) Distance estimation in the hooded rat: experimental evidence for the role of motion cues. *Behav Brain Res* 41:11–20.

Leon MI, Shadlen MN (2003) Representation of time by neurons in the posterior parietal cortex of the macaque. *Neuron* 38:317–327.

Lepage M, Richer F (1996) Inter-response interference contributes to the sequencing deficit in frontal lobe lesions. *Brain : a journal of neurology* 119 (Pt 4):1289–1295.

Lewis PA, Miall RC (2003a) Brain activation patterns during measurement of sub- and supra-second intervals. *Neuropsychologia* 41:1583–1592.

Lewis PA, Miall RC (2003b) Distinct systems for automatic and cognitively controlled time measurement: evidence from neuroimaging. *Curr Opin Neurobiol* 13:250–255.

Lewis PA, Miall RC (2006) A right hemispheric prefrontal system for cognitive time measurement. *Behavioural processes* 71:226–234.

Lingner A, Wiegrebe L, Grothe B (2012) Sound localization in noise by gerbils and humans. *Journal of the Association for Research in Otolaryngology : JARO* 13:237–248.

Liu LN, Ding SG, Shi YY, Zhang HJ, Zhang J, Zhang C (2016) Helicobacter pylori with high thioredoxin-1 expression promotes stomach carcinogenesis in Mongolian gerbils. *Clinics and research in hepatology and gastroenterology* 40:480–486.

Livesey AC, Wall MB, Smith AT (2007) Time perception: manipulation of task difficulty dissociates clock functions from other cognitive demands. *Neuropsychologia* 45:321–331.

Loskota WJ, Lomax P, Verity MA (1974) *A stereotaxic atlas of the Mongolian gerbil brain (Meriones unguiculatus)* Ann Arbor Science.

Lucchetti C, Bon L (2001) Time-modulated neuronal activity in the premotor cortex of macaque monkeys. *Exp Brain Res* 141:254–260.

Luria AR (1962) *The Higher Cortical Functions in Man*.

Macar F, Lejeune H, Bonnet M, Ferrara A, Pouthas V, Vidal F, Maquet P (2002) Activation of the supplementary motor area and of attentional networks during temporal processing. *Experimental brain research* 142:475–485.

Macar F, Pouthas V, Friedman WJ (2013) *Time, action and cognition: Towards bridging the gap*, Vol. 66 Springer Science & Business Media.

Macdonald CJ, Lepage KQ, Eden UT, Eichenbaum H (2011) Hippocampal "time cells" bridge the gap in memory for discontiguous events. *Neuron* 71:737–749.

Machado A, Arantes J (2006) Further tests of the Scalar Expectancy Theory (SET) and the Learning-to-Time (LeT) model in a temporal bisection task. *Behav Processes* 72:195–206.

Mainen ZF, Kepecs A (2009) Neural representation of behavioral outcomes in the orbitofrontal cortex. *Current opinion in neurobiology* 19:84–91.

Mangels JA, Ivry RB, Shimizu N (1998) Dissociable contributions of the prefrontal and neocerebellar cortex to time perception. *Cognitive Brain Research* 7:15 – 39.

Mankin EA, Thurley K, Chenani A, Haas OV, Debs L, Henke J, Galinato M, Leutgeb JK, Leutgeb S, Leibold C (2019) The hippocampal code for space in Mongolian gerbils. *Hippocampus* 164:197.

Marks LE, Algom D (1998) Chapter 2 - psychophysical scaling In Birnbaum MH, editor, *Measurement, Judgment and Decision Making*, Handbook of Perception and Cognition (Second Edition), pp. 81 – 178. Academic Press, San Diego.

Marks LE, Gescheider GA (2002) *Psychophysical Scaling* American Cancer Society.

Matell MS, Meck WH (2000) Neuropsychological mechanisms of interval timing behavior. *BioEssays : news and reviews in molecular, cellular and developmental biology* 22:94–103.

Matell MS, Meck WH (2004) Cortico-striatal circuits and interval timing: coincidence detection of oscillatory processes. *Cognitive brain research* 21:139–170.

Matell MS, Meck WH, Nicolelis MAL (2003) Interval timing and the encoding of signal duration by ensembles of cortical and striatal neurons. *Behav Neurosci* 117:760–773.

Matell MS, Shea-Brown E, Gooch C, Wilson AG, Rinzel J (2011) A heterogeneous population code for elapsed time in rat medial agranular cortex. *Behav Neurosci* 125:54–73.

Matsumiya LC, Sorge RE, Sotocinal SG, Tabaka JM, Wieskopf JS, Zaloum A, King OD, Mogil JS (2012) Using the Mouse Grimace Scale to reevaluate the efficacy of postoperative analgesics in laboratory mice. *J Am Assoc Lab Anim Sci* 51:42–49.

Matthews AR, He OH, Buhusi M, Buhusi CV (2012) Dissociation of the role of the prelimbic cortex in interval timing and resource allocation: beneficial effect of norepinephrine and dopamine reuptake inhibitor nomifensine on anxiety-inducing distraction. *Frontiers in integrative neuroscience* 6:111.

Mauk MD, Buonomano DV (2004) The neural basis of temporal processing. *Annu Rev Neurosci* 27:307–340.

McFie J, Thompson JA (1972) Picture arrangement: a measure of frontal lobe function? *The British journal of psychiatry : the journal of mental science* 121:547–552.

McNaughton BL, O'Keefe J, Barnes CA (1983) The stereotrode: a new technique for simultaneous isolation of several single units in the central nervous system from multiple unit records. *Journal of neuroscience methods* 8:391–397.

Meck WH (2005) Neuropsychology of timing and time perception. *Brain and Cognition* 58:1–8.

Meck WH, Penney TB, Pouthas V (2008) Cortico-striatal representation of time in animals and humans. *Curr Opin Neurobiol* 18:145–152.

Mello GBM, Soares S, Paton JJ (2015) A scalable population code for time in the striatum. *Curr Biol* 25:1113–1122.

Miall C (1989) The storage of time intervals using oscillating neurons. *Neural Computation* 1:359–371.

Miller EK, Freedman DJ, Wallis JD (2002) The prefrontal cortex: categories, concepts and cognition. *Philosophical transactions of the Royal Society of London. Series B, Biological sciences* 357:1123–1136.

Mita A, Mushiake H, Shima K, Matsuzaka Y, Tanji J (2009) Interval time coding by neurons in the presupplementary and supplementary motor areas. *Nat Neurosci* 12:502–507.

Miyazaki M, Nozaki D, Nakajima Y (2005) Testing Bayesian models of human coincidence timing. *Journal of neurophysiology* 94:395–399.

Miyazaki M, Yamamoto S, Uchida S, Kitazawa S (2006) Bayesian calibration of simultaneity in tactile temporal order judgment. *Nat Neurosci* 9:875–877.

Moorman DE, Aston-Jones G (2015) Prefrontal neurons encode context-based response execution and inhibition in reward seeking and extinction. *Proceedings of the National Academy of Sciences* 112:9472–9477.

Narayanan NS, Cavanagh JF, Frank MJ, Laubach M (2013) Common medial frontal mechanisms of adaptive control in humans and rodents. *Nature neuroscience* 16:1888.

Narayanan NS, Laubach M (2006) Top-down control of motor cortex ensembles by dorsomedial prefrontal cortex. *Neuron* 52:921–931.

Narayanan NS, Laubach M (2009) Delay activity in rodent frontal cortex during a simple reaction time task. *Journal of neurophysiology* 101:2859–2871.

Nee DE, Jahn A, Brown JW (2014) Prefrontal cortex organization: dissociating effects of temporal abstraction, relational abstraction, and integration with FMRI. *Cereb Cortex* 24:2377–2387.

Nieder A, Freedman DJ, Miller EK (2002) Representation of the quantity of visual items in the primate prefrontal cortex. *Science* 297:1708–1711.

Niki H, Watanabe M (1979) Prefrontal and cingulate unit activity during timing behavior in the monkey. *Brain Res* 171:213–224.

Niki H, Watanabe M (1976) Cingulate unit activity and delayed response. *Brain research* .

Nobre K, Nobre A, Coull J (2010) *Attention and Time* Oxford University Press.

Nolde SF, Johnson MK, Raye CL (1998) The role of prefrontal cortex during tests of episodic memory. *Trends in cognitive sciences* 2:399–406.

Noulhiane M, Pouthas V, Hasboun D, Baulac M, Samson S (2007) Role of the medial temporal lobe in time estimation in the range of minutes. *Neuroreport* 18:1035–1038.

Nussbaum S, Liberman N, Trope Y (2006) Predicting the near and distant future. *J Exp Psychol Gen* 135:152–161.

O'Keefe J, Dostrovsky J (1971) The hippocampus as a spatial map. Preliminary evidence from unit activity in the freely-moving rat. *Brain Res* 34:171–175.

Ongur D, Price JL (2000) The organization of networks within the orbital and medial prefrontal cortex of rats, monkeys and humans. *Cerebral Cortex* 10:206–219.

Onoe H, Komori M, Onoe K, Takechi H, Tsukada H, Watanabe Y (2001) Cortical networks recruited for time perception: a monkey positron emission tomography (pet) study. *Neuroimage* 13:37–45.

O'Reilly RC, Noelle DC, Braver TS, Cohen JD (2002) Prefrontal cortex and dynamic categorization tasks: representational organization and neuromodulatory control. *Cerebral cortex (New York, N.Y. : 1991)* 12:246–257.

Ornstein R (1997) *On the Experience of Time* WestviewPress.

Oshio Ki, Chiba A, Inase M (2006) Delay period activity of monkey prefrontal neurones during duration-discrimination task. *Eur J Neurosci* 23:2779–2790.

Padoa-Schioppa C, Conen KE (2017) Orbitofrontal Cortex: A Neural Circuit for Economic Decisions. *Neuron* 96:736–754.

Palomero-Gallagher N, Zilles K (2015) Chapter 22 - isocortex In Paxinos G, editor, *The Rat Nervous System (Fourth Edition)*, pp. 601 – 625. Academic Press, San Diego, fourth edition edition.

Paneri S, Gregoriou GG (2017) Top-Down Control of Visual Attention by the Prefrontal Cortex. Functional Specialization and Long-Range Interactions. *Frontiers in neuroscience* 11:545.

Parker KL, Chen KH, Kingyon JR, Cavanagh JF, Narayanan NS (2014) D1-dependent 4 hz oscillations and ramping activity in rodent medial frontal cortex during interval timing. *Journal of Neuroscience* 34:16774–16783.

Parker KL, Chen KH, Kingyon JR, Cavanagh JF, Narayanan NS (2015) Medial frontal 4-hz activity in humans and rodents is attenuated in pd patients and in rodents with cortical dopamine depletion. *Journal of neurophysiology* 114:1310–1320.

Pastalkova E, Itskov V, Amarasingham A, ki GorBa (2008) Internally generated cell assembly sequences in the rat hippocampus. *Science* 321:1322–1327.

Paton JJ, Buonomano DV (2018) The neural basis of timing: Distributed mechanisms for diverse functions. *Neuron* 98:687–705.

Pecka M, Brand A, Behrend O, Grothe B (2008) Interaural time difference processing in the mammalian medial superior olive: the role of glycinergic inhibition. *The Journal of neuroscience : the official journal of the Society for Neuroscience* 28:6914–6925.

Perbal-Hatif S (2012) A neuropsychological approach to time estimation. *Dialogues in clinical neuroscience* 14:425–432.

Petersen CC (2014) Cell-type specific function of GABAergic neurons in layers 2 and 3 of mouse barrel cortex. *Current opinion in neurobiology* 26:1–6.

Petrides M, Pandya DN (1984) Projections to the frontal cortex from the posterior parietal region in the rhesus monkey. *The Journal of comparative neurology* 228:105–116.

Petrides M, Pandya DN (1999) Dorsolateral prefrontal cortex: comparative cytoarchitectonic analysis in the human and the macaque brain and corticocortical connection patterns. *The European journal of neuroscience* 11:1011–1036.

Petrides M, Pandya DN (2006) Efferent association pathways originating in the caudal prefrontal cortex in the macaque monkey. *The Journal of comparative neurology* 498:227–251.

Petruso EJ, Fuchs T, Bingman VP (2007) Time-space learning in homing pigeons (Columba livia): orientation to an artificial light source. *Anim Cogn* 10:181–188.

Petzschner FH, Glasauer S (2011) Iterative Bayesian estimation as an explanation for range and regression effects: a study on human path integration. *J Neurosci* 31:17220–17229.

Petzschner FH, Glasauer S, Stephan KE (2015) A Bayesian perspective on magnitude estimation. *Trends Cogn Sci* 19:285–293.

Petzschner FH, Maier P, Glasauer S (2012) Combining symbolic cues with sensory input and prior experience in an iterative bayesian framework. *Front Integr Neurosci* 6:58.

Pietrewicz AT, Hoff MP, Higgins SA (1982) Activity rhythms in the Mongolian gerbil under natural light conditions. *Physiology & behavior* 29:377–380.

Poulton EC (1968) The new psychophysics: Six models for magnitude estimation. psychol bull 69: 1-19. *Psychological Bulletin* 69:1–19.

Pouthas V, Perbal S (2004) Time perception depends on accurate clock mechanisms as well as unimpaired attention and memory processes. *Acta neurobiologiae experimentalis* 64:367–385.

Preuss TM (1995) Do rats have prefrontal cortex? The rose-woolsey-akert program reconsidered. *Journal of cognitive neuroscience* 7:1–24.

Quintana J, Yajeya J, Fuster JM (1988) Prefrontal representation of stimulus attributes during delay tasks. I. Unit activity in cross-temporal integration of sensory and sensory-motor information. *Brain Res* 474:211–221.

Radtke-Schuller S, Schuller G, Angenstein F, Grosser OS, Goldschmidt J, Budinger E (2016) Brain atlas of the Mongolian gerbil (Meriones unguiculatus) in CT/MRI-aided stereotaxic coordinates. *Brain structure & function* 221 Suppl 1:1–272.

Ramachandran V (2002) Encyclopedia of the human brain.

Ramnani N, Owen AM (2004) Anterior prefrontal cortex: insights into function from anatomy and neuroimaging. *Nature reviews. Neuroscience* 5:184–194.

Rangel A, Hare T (2010) Neural computations associated with goal-directed choice. *Curr Opin Neurobiol* 20:262–270.

Rao SM, Mayer AR, Harrington DL (2001) The evolution of brain activation during temporal processing. *Nat Neurosci* 4:317–323.

Refinetti R, Kenagy GJ (2018) Diurnally active rodents for laboratory research. *Laboratory animals* 52:577–587.

Reichenbach N, Herrmann U, Kähne T, Schicknick H, Pielot R, Naumann M, Dieterich DC, Gundelfinger ED, Smalla KH, Tischmeyer W (2015) Differential effects of dopamine

signalling on long-term memory formation and consolidation in rodent brain. *Proteome science* 13:13.

Renoult L, Roux S, Riehle A (2006) Time is a rubberband: neuronal activity in monkey motor cortex in relation to time estimation. *Eur J Neurosci* 23:3098–3108.

Reppert SM, Weaver DR (2001) Molecular analysis of mammalian circadian rhythms. *Annual review of physiology* 63:647–676.

Reppert SM, Weaver DR (2002) Coordination of circadian timing in mammals. *Nature* 418:935–941.

Reutimann J, Yakovlev V, Fusi S, Senn W (2004) Climbing neuronal activity as an event-based cortical representation of time. *J Neurosci* 24:3295–3303.

Rey HG, Pedreira C, Quiroga RQ (2015) Past, present and future of spike sorting techniques. *Brain Research Bulletin* 119:106 – 117 Advances in electrophysiological data analysis.

Reynolds JR, McDermott KB, Braver TS (2006) A direct comparison of anterior prefrontal cortex involvement in episodic retrieval and integration. *Cerebral cortex (New York, N.Y. : 1991)* 16:519–528.

Ridderinkhof KR, van den Wildenberg WPM, Segalowitz SJ, Carter CS (2004) Neurocognitive mechanisms of cognitive control: the role of prefrontal cortex in action selection, response inhibition, performance monitoring, and reward-based learning. *Brain Cogn* 56:129–140.

Roach NW, McGraw PV, Whitaker DJ, Heron J (2017) Generalization of prior information for rapid Bayesian time estimation. *Proc Natl Acad Sci U S A* 114:412–417.

Roberts S (1981) Isolation of an internal clock. *Journal of Experimental Psychology: Animal Behavior Processes* 7:242.

Romine CB, Reynolds CR (2004) Sequential memory: a developmental perspective on its relation to frontal lobe functioning. *Neuropsychology review* 14:43–64.

Rosenkilde CE, Divac I (1976) Time-discrimination performance in cats with lesions in prefrontal cortex and caudate nucleus. *Journal of comparative and physiological psychology* 90:343.

Rubia K, Overmeyer S, Taylor E, Brammer M, Williams S, Simmons A, Andrew C, Bullmore E (1998) Prefrontal involvement in "temporal bridging" and timing movement. *Neuropsychologia* 36:1283–1293.

Rudebeck PH, Ripple JA, Mitz AR, Averbeck BB, Murray EA (2017) Amygdala contributions to stimulus–reward encoding in the macaque medial and orbital frontal cortex during learning. *Journal of Neuroscience* 37:2186–2202.

Ryan A (1976) Hearing sensitivity of the mongolian gerbil, Meriones unguiculatis. *The Journal of the Acoustical Society of America* 59:1222–1226.

Sakurai Y, Takahashi S, Inoue M (2004) Stimulus duration in working memory is represented by neuronal activity in the monkey prefrontal cortex. *Eur J Neurosci* 20:1069–1080.

Salz DM, Tiganj Z, Khasnabish S, Kohley A, Sheehan D, Howard MW, Eichenbaum H (2016) Time Cells in Hippocampal Area CA3. *J Neurosci* 36:7476–7484.

Sambraus HH, Steiger A (1997) Das Buch vom Tierschutz. *Enke Verlag, Stuttgart* .

Samejima K, Ueda Y, Doya K, Kimura M (2005) Representation of action-specific reward values in the striatum. *Science* 310:1337–1340.

Schmidt H (1996) Rennmäuse und andere tropische Nager. *4. Auflage, Landbuch Verlag, Hannover* .

Schmitzer-Torbert N, Jackson J, Henze D, Harris K, Redish A (2005) Quantitative measures of cluster quality for use in extracellular recordings. *Neuroscience* 131:1–11.

Schneider E (2000) The anaesthesia in gerbils (Meriones unguiculatus) with midazolam, medetomidine and fentanyl and its complete reversal by atipamezole, flumazenil and naloxone in comparison to the anaesthesia with ketamine and medetomidine Ph.D. diss., Munich.

Schnyer DM, Nicholls L, Verfaellie M (2005) The role of VMPC in metamemorial judgments of content retrievability. *Journal of cognitive neuroscience* 17:832–846.

Schoenbaum G, Roesch MR, Stalnaker TA, Takahashi YK (2009) A new perspective on the role of the orbitofrontal cortex in adaptive behaviour. *Nat Rev Neurosci* 10:885–892.

Schweimer J, Hauber W (2005) Involvement of the rat anterior cingulate cortex in control of instrumental responses guided by reward expectancy. *Learn Mem* 12:334–342.

Setogawa T, Mizuhiki T, Matsumoto N, Akizawa F, Kuboki R, Richmond BJ, Shidara M (2019) Neurons in the monkey orbitofrontal cortex mediate reward value computation and decision-making. *Communications Biology* 2:126.

Sharp PE, Blair HT, Etkin D, Tzanetos DB (1995) Influences of vestibular and visual motion information on the spatial firing patterns of hippocampal place cells. *J Neurosci* 15:173–189.

Shi Z, Church RM, Meck WH (2013) Bayesian optimization of time perception. *Trends Cogn Sci* .

Shimamura AP, Janowsky JS, Squire LR (1990) Memory for the temporal order of events in patients with frontal lobe lesions and amnesic patients. *Neuropsychologia* 28:803–813.

Simen P, Balci F, de Souza L, Cohen JD, Holmes P (2011) A model of interval timing by neural integration. *J Neurosci* 31:9238–9253.

Sotocinal SG, Sorge RE, Zaloum A, Tuttle AH, Martin LJ, Wieskopf JS, Mapplebeck JCS, Wei P, Zhan S, Zhang S, McDougall JJ, King OD, Mogil JS (2011) The Rat Grimace Scale: a partially automated method for quantifying pain in the laboratory rat via facial expressions. *Mol Pain* 7:55.

Spaak E, Watanabe K, Funahashi S, Stokes MG (2017) Stable and Dynamic Coding for Working Memory in Primate Prefrontal Cortex. *J Neurosci* 37:6503–6516.

Spinella M, Yang B, Lester D (2004) Prefrontal system dysfunction and credit card debt. *The International journal of neuroscience* 114:1323–1332.

Steketee JD (2003) Neurotransmitter systems of the medial prefrontal cortex: potential role in sensitization to psychostimulants. *Brain research. Brain research reviews* 41:203–228.

Stevens JR, Rosati AG, Ross KR, Hauser MD (2005) Will travel for food: spatial discounting in two new world monkeys. *Curr Biol* 15:1855–1860.

Stevens S (1960) The psychophysics of sensory function. *American Scientist* 48:226–253.

Stevens S (1957) On the psychophysical law. *Psychol Rev* 64:153–181.

Stevens S, Greenbaum B (1966) Regression effect in psychophysical judgment. *Attention Perception Psychophysics* 1:439–446.

Stuermer IW, Tittmann C, Schilling C, Blottner S (2006) Reproduction of wild mongolian gerbils bred in the laboratory with respect to generation and season 1. morphological changes and fertility lifespan. *Animal Science* 82:377–387.

Stuermer IW, Plotz K, Leybold A, Zinke O, Kalberlah O, Samjaa R, Scheich H (2003) Intraspecific allometric comparison of laboratory gerbils with mongolian gerbils trapped in the wild indicates domestication in meriones unguiculatus (milne-edwards, 1867) (rodentia: Gerbillinae). *Zoologischer Anzeiger - A Journal of Comparative Zoology* 242:249 – 266.

Stuermer IW, Wetzel W (2006) Early experience and domestication affect auditory discrimination learning, open field behaviour and brain size in wild Mongolian gerbils and domesticated laboratory gerbils (Meriones unguiculatus forma domestica). *Behavioural brain research* 173:11–21.

Stuss DT (1992) Biological and psychological development of executive functions. *Brain and cognition* 20:8–23.

Stuss DT, Knight RT (2013) *Principles of Frontal Lobe Function* Oxford, UK.

Sun T, Hevner RF (2014) Growth and folding of the mammalian cerebral cortex: from molecules to malformations. *Nat Rev Neurosci* 15:217–232.

Taatgen NA, Van Rijn H, Anderson J (2007) An integrated theory of prospective time interval estimation: The role of cognition, attention, and learning. *Psychological Review* 114:577.

Taylor TE, Lupker SJ (2007) Sequential effects in time perception. *Psychonomic bulletin & review* 14:70–74.

Teghtsoonian M, Teghtsoonian R (1971) How repeatable are stevens's power law exponents for individual subjects? *Perception & Psychophysics* 10:147–149.

Teghtsoonian R, Teghtsoonian M (1978) Range and regression effects in magnitude scaling. *Percept Psychophys* 24:305–314.

Terrazas A, Krause M, Lipa P, Gothard KM, Barnes CA, McNaughton BL (2005) Self-motion and the hippocampal spatial metric. *J Neurosci* 25:8085–8096.

Thomas EAC, Weaver WB (1975) Cognitive processing and time perception. *Perception & Psychophysics* 17:363–367.

Thurley K (2016) Magnitude Estimation with Noisy Integrators Linked by an Adaptive Reference. *Front Integr Neurosci* 10:6.

Thurley K, Henke J, Hermann J, Ludwig B, Tatarau C, W a tzig A, Herz AVM, Grothe B, Leibold C (2014) Mongolian gerbils learn to navigate in complex virtual spaces. *Behav Brain Res* 266:161–168.

Thurley K, Schild U (2018) Time and distance estimation in children using an egocentric navigation task. *Scientific Reports* 8:18001.

Tobin S, Bisson N, Grondin S (2010) An ecological approach to prospective and retrospective timing of long durations: a study involving gamers. *PloS one* 5:e9271.

Tregellas JR, Davalos DB, Rojas DC (2006) Effect of task difficulty on the functional anatomy of temporal processing. *Neuroimage* 32:307–315.

Treisman M (1963) Temporal discrimination and the indifference interval. Implications for a model of the "internal clock". *Psychological monographs* 77:1–31.

Treisman M, Faulkner A, Naish PL, Brogan D (1990) The internal clock: evidence for a temporal oscillator underlying time perception with some estimates of its characteristic frequency. *Perception* 19:705–743.

Tsujimoto S, Sawaguchi T (2005a) Context-dependent representation of response-outcome in monkey prefrontal neurons. *Cereb Cortex* 15:888–898.

Tsujimoto S, Sawaguchi T (2005b) Neuronal activity representing temporal prediction of reward in the primate prefrontal cortex. *J Neurophysiol* 93:3687–3692.

Tsujimoto S, Yamamoto T, Kawaguchi H, Koizumi H, Sawaguchi T (2004) Prefrontal Cortical Activation Associated with Working Memory in Adults and Preschool Children: An Event-related Optical Topography Study. *Cerebral Cortex* 14:703–712.

Tzschentke TM (2001) Pharmacology and behavioral pharmacology of the mesocortical dopamine system. *Progress in neurobiology* 63:241–320.

Uylings HB, van Eden CG (1990) Qualitative and quantitative comparison of the prefrontal cortex in rat and in primates, including humans. *Progress in brain research* 85:31–62.

Uylings HBM, Groenewegen HJ, Kolb B (2003) Do rats have a prefrontal cortex? *Behav Brain Res* 146:3–17.

Varty GB, Morgan CA, Cohen-Williams ME, Coffin VL, Carey GJ (2002) The gerbil elevated plus-maze I: behavioral characterization and pharmacological validation. *Neuropsychopharmacology : official publication of the American College of Neuropsychopharmacology* 27:357–370.

Vilares I, Kording K (2011) Bayesian models: the structure of the world, uncertainty, behavior, and the brain. *Annals of the New York Academy of Sciences* 1224:22–39.

Vogt BA (2015) Chapter 21 - cingulate cortex and pain architecture In Paxinos G, editor, *The Rat Nervous System (Fourth Edition)*, pp. 575 – 599. Academic Press, San Diego, fourth edition edition.

Wagner R (1844) *Handwörterbuch der Physiologie mit Rücksicht auf physiologische Pathologie*, Vol. 2 Vieweg.

Wallis JD, Anderson KC, Miller EK (2001) Single neurons in prefrontal cortex encode abstract rules. *Nature* 411:953–956.

Walton ME, Kennerley SW, Bannerman DM, Phillips PEM, Rushworth MFS (2006) Weighing up the benefits of work: behavioral and neural analyses of effort-related decision making. *Neural networks : the official journal of the International Neural Network Society* 19:1302–1314.

Walton ME, Bannerman DM, Rushworth MFS (2002) The role of rat medial frontal cortex in effort-based decision making. *J Neurosci* 22:10996–11003.

Wang S, Feng D, Li Y, Wang Y, Sun X, Li X, Li C, Chen Z, Du X (2018) The different baseline characteristics of cognitive behavior test between Mongolian gerbils and rats. *Behav Brain Res* 352:28–34.

Ward LM (1979) Stimulus information and sequential dependencies in magnitude estimation and cross-modality matching. *Journal of experimental psychology. Human perception and performance* 5:444–449.

Watanabe M, Lee BJ, Kamitani W, Kobayashi T, Taniyama H, Tomonaga K, Ikuta K (2001) Neurological diseases and viral dynamics in the brains of neonatally borna disease virus-infected gerbils. *Virology* 282:65–76.

Wearden JH (1999) "beyond the fields we know...": Exploring and developing scalar timing theory. *Behavioural Processes* 45:3–21.

Wiener M, Turkeltaub P, Coslett HB (2010) The image of time: a voxel-wise meta-analysis. *Neuroimage* 49:1728–1740.

Wilson D, Reeder DM (1993) Mammals species of the world. A taxonomic and geographic reference. *2nd edition, Smithsonian Institution Press, Washington, D.C.* .

Wilson MA, McNaughton BL (1993) Dynamics of the hippocampal ensemble code for space. *Science (New York, N.Y.)* 261:1055–1058.

Winckler J (1974) Vitalfärbung von Lysosomen und anderen Zellorganellen der Ratte mit Neutralrot Vital Staining of Lysosomes and Other Cell Organelles of the Rat with Neutral Red. *Progress in Histochemistry and Cytochemistry* 6:III–89.

Wittmann M, Lehnhoff S (2005) Age effects in perception of time. *Psychological reports* 97:921–935.

Wong KF, Wang XJ (2006) A recurrent network mechanism of time integration in perceptual decisions. *Journal of Neuroscience* 26:1314–1328.

Wyttenbach RA, May ML, Hoy RR (1996) Categorical perception of sound frequency by crickets. *Science (New York, N.Y.)* 273:1542–1544.

Xu M, Zhang SY, Dan Y, Poo MM (2014) Representation of interval timing by temporally scalable firing patterns in rat prefrontal cortex. *Proc Natl Acad Sci U S A* 111:480–485.

Yamamoto S, Miyazaki M, Iwano T, Kitazawa S (2012) Bayesian calibration of simultaneity in audiovisual temporal order judgments. *PLoS One* 7:e40379.

Yeterian EH, Pandya DN, Tomaiuolo F, Petrides M (2012) The cortical connectivity of the prefrontal cortex in the monkey brain. *Cortex; a journal devoted to the study of the nervous system and behavior* 48:58–81.

Zakay D, Block RA (1995) An attentional-gate model of prospective time estimation. *Time and the dynamic control of behavior* pp. 167–178.

Zakay D, Block RA (1996) The role of attention in time estimation processes In Pastor MA, Artieda J, editors, *Time, Internal Clocks and Movement*, Vol. 115 of *Advances in Psychology*, pp. 143 – 164. North-Holland.

Zakay D, Block RA (2004) Prospective and retrospective duration judgments: an executive-control perspective. *Acta neurobiologiae experimentalis* 64:319–328.

Zeiler MD, Hoyert MS (1989) Temporal reproduction. *J Exp Anal Behav* 52:81–95.

Zhang H, Zhou X (2017) Supramodal representation of temporal priors calibrates interval timing. *Journal of Neurophysiology* 118:1244–1256.

6

APPENDIX

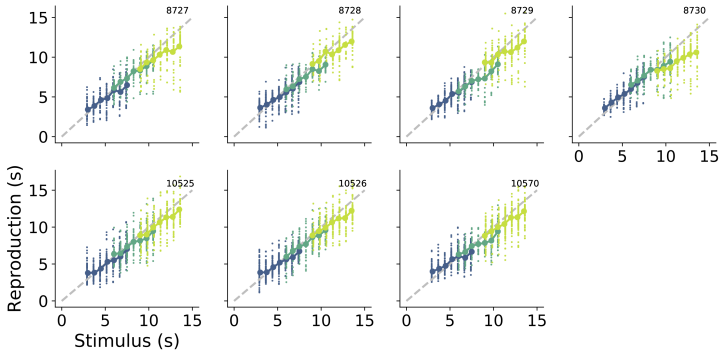

Figure 6.1: Time reproductions of all gerbil subjects. Individual reproduced values for the tested stimulus intervals are given as small dots and averages for each stimulus are depicted as large dots connected by a solid line. Colors identify stimulus distributions (cf. Figure 2.2c). Gray dashed lines mark bisecting lines.

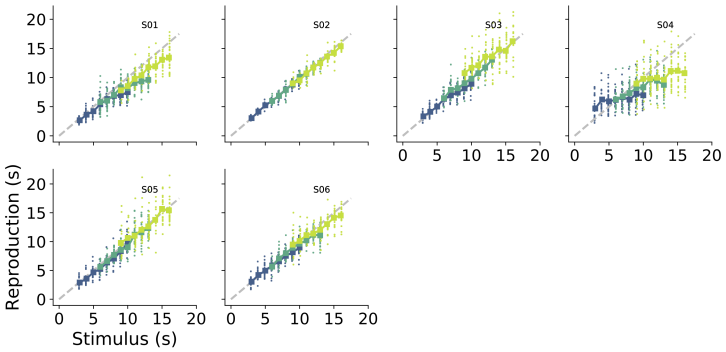

Figure 6.2: Time reproductions of all participants (humans). Individual reproduced values for the tested stimulus intervals are given as small dots and averages for each stimulus are depicted as large squares connected by a solid line. Colors identify stimulus distributions (cf. Figure 2.2c). Gray dashed lines mark bisecting lines.

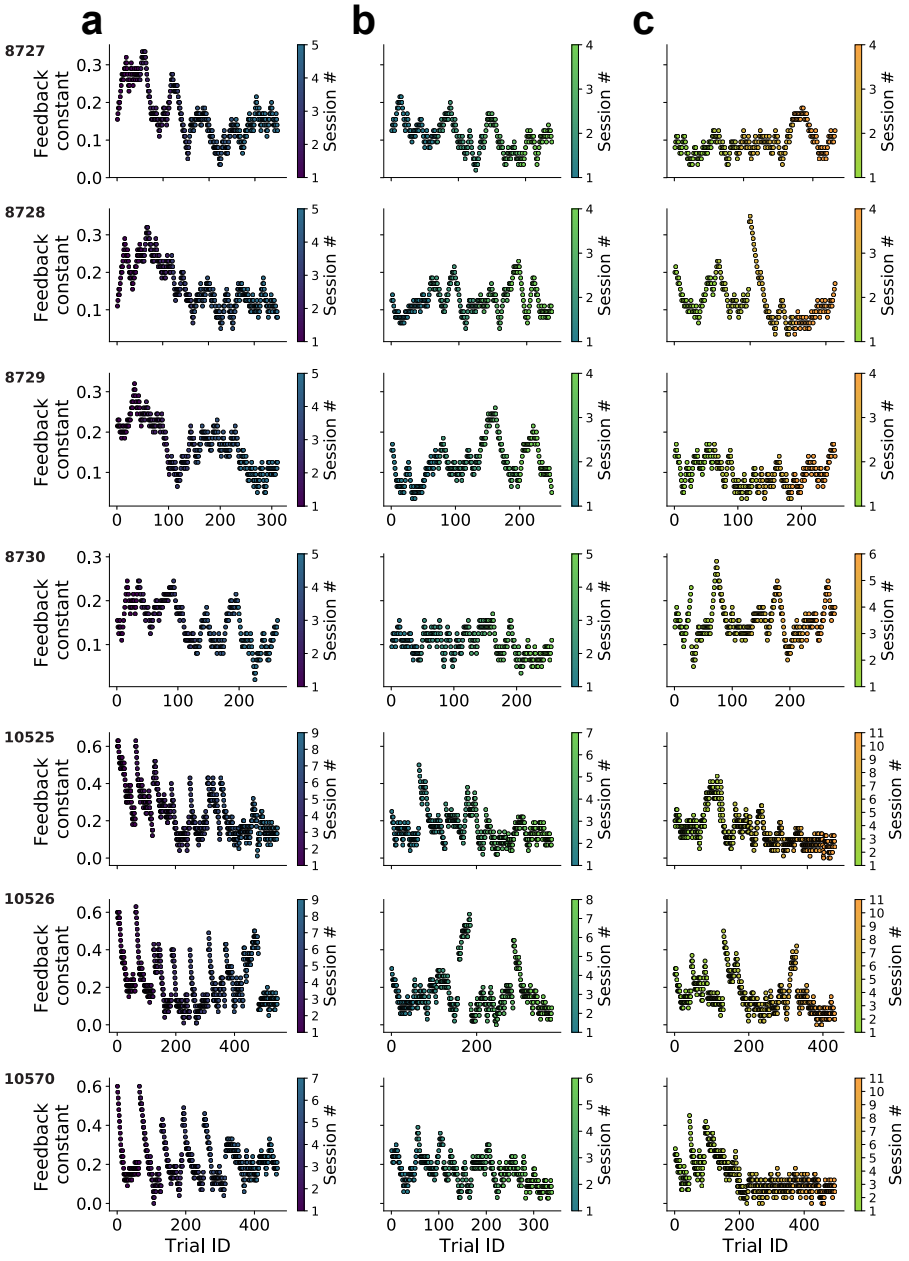

Figure 6.3: Performance quality of all animals progressing over time of test sessions. Each row shows the development of the feedback constants over sessions of the stimulus distributions A (a), B (b) and C (c) for individual animal subjects. Colorbars indicate the increasing session number. Color conventions derived from those used in Figure 3.1.

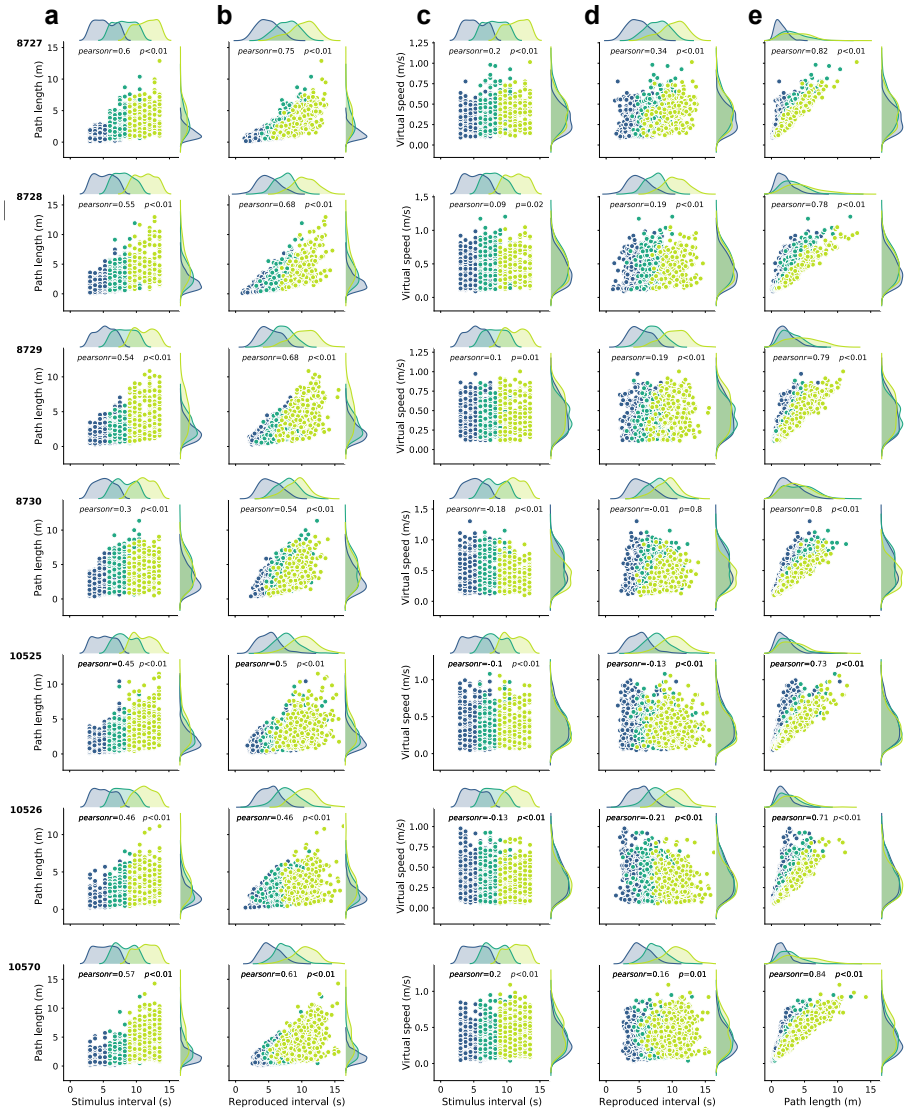

Figure 6.4: Trajectory parameters of temporal reproduction for all animal subjects individually – part I. Correlation of stimulus intervals and reproduced intervals with path length (a + b) and correlation of stimulus intervals and reproduced intervals with virtual running speed (c + d). (e) Correlation of path length with virtual running speed. Kernel density estimates on the marginal plots show the distribution of values on the respective axis. Pearson's correlation coefficient r and corresponding p-values are provided. Each row represents one individual animal. Same color conventions as in Figure 6.1.

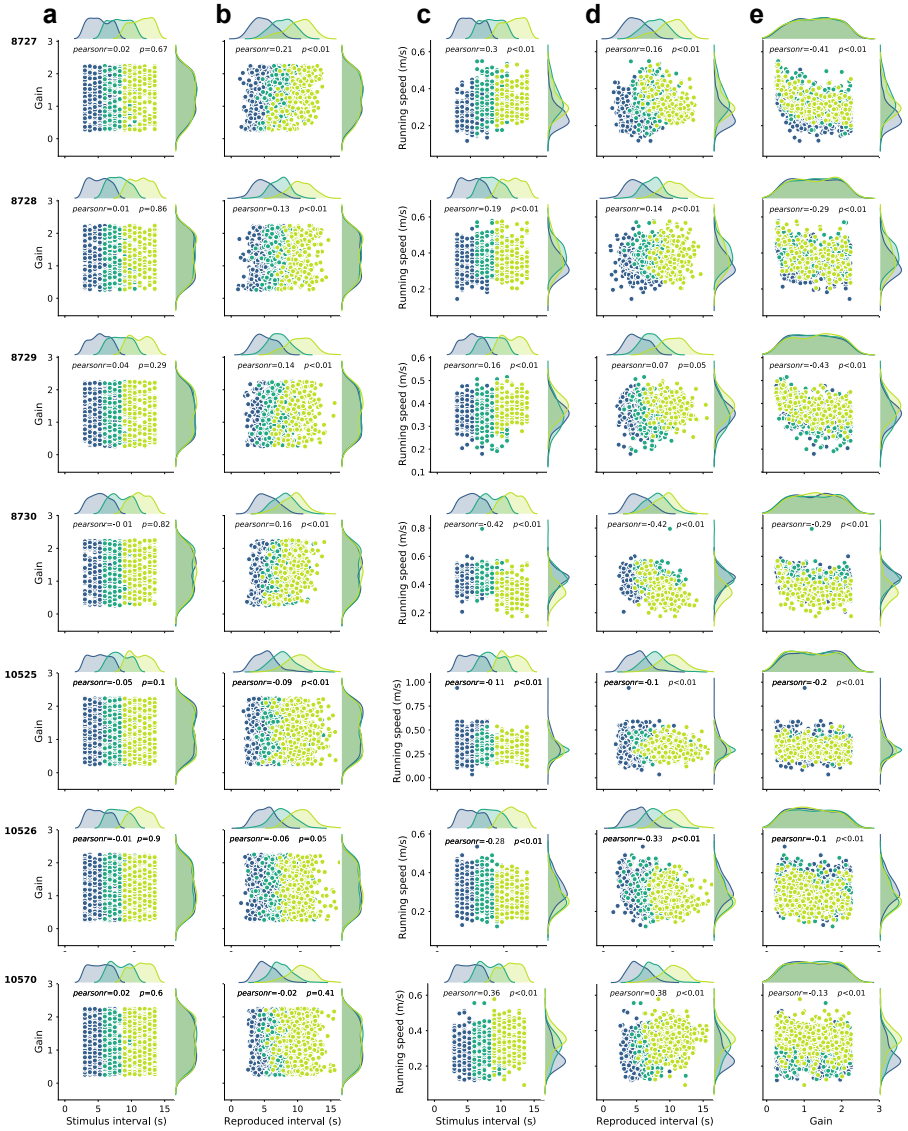

Figure 6.5: Trajectory parameters of temporal reproduction for all animal subjects individually – part II. Correlation of stimulus intervals and reproduced intervals with path length (a + b) and correlation of stimulus intervals and reproduced intervals with virtual running speed (c + d). (e) Correlation of applied gain factors with virtual running speed. Kernel density estimates on the marginal plots show the distribution of values on the respective axis. Pearson's correlation coefficient r and corresponding p-values are provided. Each row represents one individual animal. Same color conventions as in Figure 6.1.

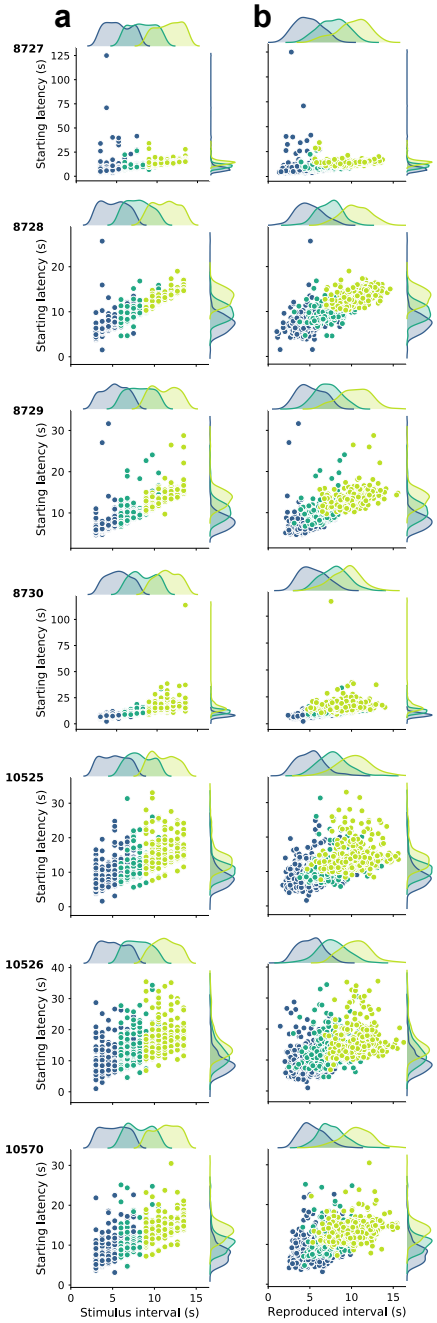

Figure 6.6: Trajectory parameters of temporal reproduction for all animal subjects individually – part III. Correlation of stimulus intervals and reproduced intervals with starting latencies (a + b). Kernel density estimates on the marginal plots show the distribution of values on the respective axis. Each row represents one individual animal. Same color conventions as in Figure 6.1.

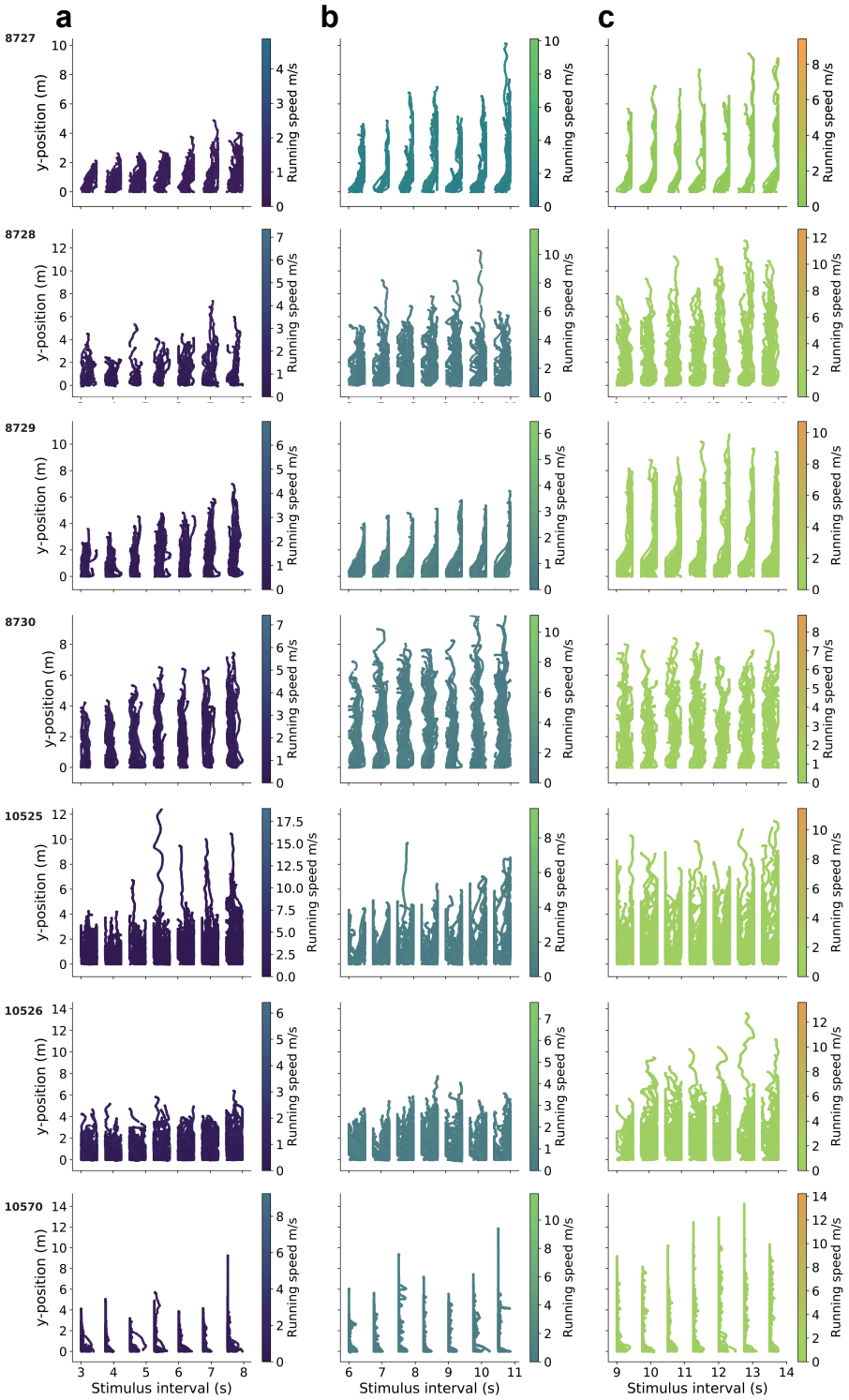

Figure 6.7: Y-position trajectories of all animals. Y-position of the running path is shown for tested stimulus sizes of stimulus distribution A (a), B (b) and C (c) for individual trials. The colorbars indicate running speed during distance travelled. Data is shown for each subject individually, pooled across sessions. Color conventions derived from those used in Figure 3.1.

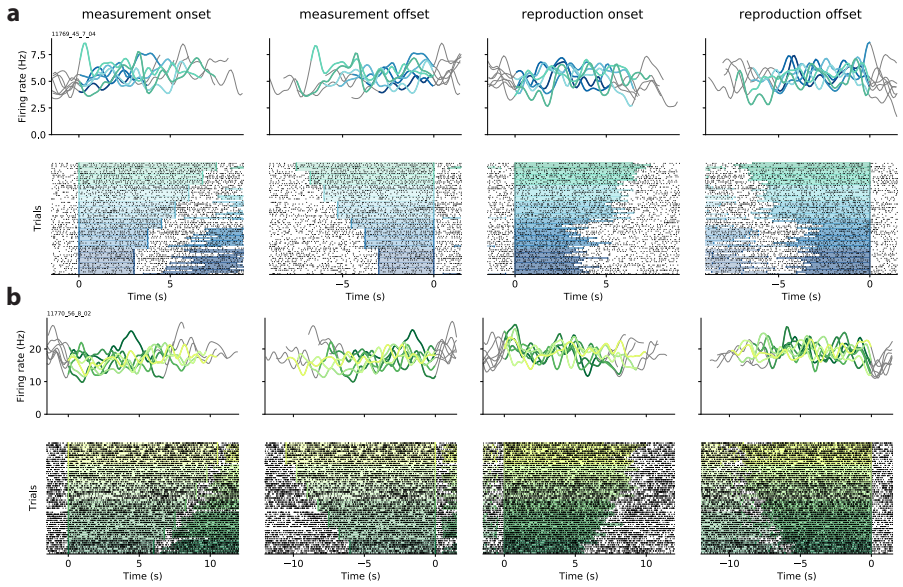

Figure 6.8: Examples neurons responding with sustained firing. Spike raster plots and spike density functions (σ = 100 ms) are shown for mPFC example neurons recorded during interval timing. These example neurons exhibited sustained firing in measurement phase as well as in reproduction phase when tested on stimulus distribution A (a) and B (b). Colors identify stimulus size within the distribution (cf. Figure 3.14a and Figure 3.14b). Trials were grouped according to the length of the sample interval and aligned to measurement onset, measurement offset, reproduction onset and reproduction offset. Color shaded areas in raster plots mark the respective phase in each trial.

Filter		Exposure time	Gain
	Slide #01		
DAPI (B)		1s	1.4
Nissl (G)		4s	2.0
DiI (R)		1s	0.5
	Slide #02		
DAPI (B)		1s	1.4
Nissl (G)		4s	2.0
DiI (R)		0.33s	1.0
	Slide #03		
DAPI (B)		1s	1.4
Nissl (G)		4s	2.0
DiI (R)		0.33s	1.0
	Slide #04		
DAPI (B)		1.5s	1.2
Nissl (G)		6s	2.4
DiI (R)		0.33s	1.0
	Slide #05		
DAPI (B)		1s	1.4
Nissl (G)		6s	2.4
DiI (R)		0.33s	1.0

Table 6.1 continued on next page

Filter	Exposure time	Gain
Slide #06		
DAPI (B)	1s	1.4
Nissl (G)	6s	2.4
DiI (R)	0.33s	1.0
Slide #07		
DAPI (B)	1s	1.4
Nissl (G)	6s	2.4
DiI (R)	0.33s	1.0

Table 6.1: Software settings of Lucia Image program for taking images of immunohistological stained coronal slices of animal #11769. The exposure time and gain was adjusted for each slice and fluorochrome for the corresponding filter: DAPI - Blue (B), Nissl - green (G), DiI - Red (R).

Filter		Exposure time	Gain
	Slide #01		
DAPI (B)		1.5s	1.4
Nissl (G)		46s	2.4
DiI (R)		0.5s	1.2
	Slide #02		
DAPI (B)		1.5s	1.4
Nissl (G)		6s	2.4
DiI (R)		0.5s	1.2
	Slide #03		
DAPI (B)		1.5s	1.4
Nissl (G)		6s	2.8
DiI (R)		0.5s	1.2
	Slide #04		
DAPI (B)		1.5s	1.4
Nissl (G)		6s	2.8
DiI (R)		0.5s	1.2

Table 6.2: Software settings of Lucia Image program for taking images of immunohistological stained coronal slices of animal #11770. The exposure time and gain was adjusted for each slice and fluorochrome for the corresponding filter: DAPI - Blue (B), Nissl - green (G), DiI - Red (R).

ACKNOWLEDGEMENTS

Undertaking this Ph.D. has been a truly life-changing experience for me, and it would not have been possible to do without the support and guidance that I received from many people.

Firstly, I would like to express my sincere gratitude to my advisor Dr. Kay Thurley for continuous support during my Ph.D. study, for his patience, motivation, and immense knowledge. His guidance helped me in all the time of research and writing of this thesis. Without his guidance and constant feedback, this Ph.D. would not have been achievable. Besides my advisor, I would like to thank the members of my thesis committee: Dr. Virginia Flanagin, Prof. Dr. Christian Leibold and Prof. Dr. Anton Sirota, for their insightful comments and encouragement, but also for the constructive criticism which incented me to widen my research from various perspectives.

I gratefully acknowledge the funding received towards my PhD from the "Bernstein Center for Computational Neuroscience" (BCCN) and the Graduate School of Systemic Neurosciences (GSN). Many thanks to the administration of the GSN, who were supportive and helpful on all regulatory and organizational concerns, in particular. Additionally, I would like to say a heartfelt thank you to the Graduate School of Systemic Neurosciences and particularly Prof. Dr. Benedikt Grothe to provide such an enlightening scientific environment and the opportunity to connect with other scientists in a social framework.

I am grateful to all of those I have had the pleasure of working with during this period. Thanks to my fellow labmates, Olivia Lewis (neé Haas), Franziska Hellmundt, Sebastian Groß, and Magdalena Kautzky, for the stimulating atmosphere and discussions, the support and inspiration over the years, during fruitful conversations in our coffee breaks.

I am indebted to all my friends and family: My Dad, Martina, and Julian for their unconditioned patience and support. In particular, I want to express my deepest appreciation and many heartfelt thanks to my best friend, Stella Freund who accompanied me on this long journey all way down, my family – especially to my Mom, Anette Henke and Rochus Möller, for always believing in me, supporting and encouraging me to pursue my goals. And finally to my love Mikesh (Micheal) Neugebauer, who has been by my side throughout the most demanding time of this Ph.D., helping in whatever way he could, during this challenging period, and without whom, it would not have been possible for me to complete what I started.

PUBLICATION LIST

ARTICLES

Garbers C, **Henke J**, Leibold C, Wachtler T, Thurley K (2015) Contextual processing of brightness and color in Mongolian gerbils. *Journal of Vision* 15:15.1.13–13.

Haas OV, **Henke J**, Leibold C, Thurley K (2019) Modality-specific Subpopulations of Place Fields Coexist in the Hippocampus. *Cerebral Cortex* 29:1109–1120.

Mankin EA, Thurley K, Chenani A, Haas OV, Debs L, **Henke J**, Galinato M, Leutgeb JK, Leutgeb S, Leibold C (2019) The hippocampal code for space in Mongolian gerbils. *Hippocampus* 164:197.

Thurley K, **Henke J**, Hermann J, Ludwig B, Tatarau C, Wätzig A, Herz AVM, Grothe B, Leibold C (2014) Mongolian gerbils learn to navigate in complex virtual spaces. *Behavioural Brain Research* 266:161–168.

EIDESSTATTLICHE VERSICHERUNG / AFFIDAVIT

Hiermit versichere ich an Eides statt, dass ich die vorliegende Dissertation *Processing of prospective and retrospective duration estimates in medial prefrontal cortex* selbstständig angefertigt habe, mich außer der angegebenen keiner weiteren Hilfsmittel bedient und alle Erkenntnisse, die aus dem Schrifttum ganz oder annähernd übernommen sind, als solche kenntlich gemacht und nach ihrer Herkunft unter Bezeichnung der Fundstelle einzeln nachgewiesen habe.

I hereby confirm that the dissertation *Processing of prospective and retrospective duration estimates in medial prefrontal cortex* is the result of my own work and that I have only used sources or materials listed and specified in the dissertation.

München, im November 11, 2019
Munich, November 11, 2019

Josephine Henke

AUTHOR CONTRIBUTIONS

The contributions of the authors Josephine Henke (JH), Kay Thurley (KT), Virginia Flanagin (FL) and Magdalena Kautzky (MK) to the studies conducted during my PhD are as follows: KT and VL conceived the study. KT, VL, and JH designed the experiments. KT created the virtual reality paradigm and JH performed the experiments with help of MK. Spike data preparation was done by JH and MK. JH analysed the data with help of KT. JH created all figures. We assert that aforementioned author contributions are correct and accurate:

Josephine Henke

Dr. Virginia Flanagin